Coherent and incoherent radiation processes in pulsars

Dissertation der Fakultät für Physik
der
Ludwig-Maximilians-Universität München

vorgelegt von Thomas Kunzl
aus München

München, den 18. 6. 01

1. Gutachter: Prof. Dr. Harald Lesch
2. Gutachter: Prof. Dr. Joachim Trümper

Tag der mündlichen Prüfung: 23. 11. 01

Coherent and incoherent radiation processes in pulsars

Dissertation der Fakultät für Physik
der
Ludwig-Maximilians-Universität München

vorgelegt von Thomas Kunzl
aus München

München, den 18. 6. 01

Zusammenfassung

In dieser Arbeit wird ein neuartiges Modell zur Radioemission von Pulsaren vorgestellt. Dazu werden die Standardmodelle für die kohärente Radiostrahlung kritisch diskutiert und die Bedingungen für ihre Gültigkeit untersucht. Es zeigt sich, daß zahlreiche theoretische und Beobachtungsergebnisse mit dem Standardmodell für die Pulsar-Radioemission nicht oder nur schwer vereinbar sind.

Allgemein akzeptiert ist, daß in dem rotierenden magnetischen Dipol hohe Spannungen induziert werden, die geladene Teilchen aus der Oberfläche ziehen können. üblicherweise wird nun angenommen, daß nahe am Neutronenstern Teilchen auf hochrelativistische Energien beschleunigt werden und durch exotische Prozesse ein dichtes Elektron-Positron-Plasma erzeugen. Durch Instabilitäten kann dieses dieses dann die kohärente Radiostrahlung erzeugen.

Es konnte gezeigt werden, daß insbesondere kohärente Krümmungsstrahlung als Mechanismus für die niederfrequente Radioemission ausgeschlossen werden kann. Für den meistdiskutierten Alternativprozeß sind dagegen - im Widerspruch zum Standardmodell - geringe Teilchendichten und -energien erforderlich, wie in dieser Arbeit dargestellt. Das hier entwickelte Modell nimmt ein mäßig relativistisches reines Elektronenplasma an, in dem die dissipierte Energie für die Radiostrahlung nicht aus der Teilchenenergie, sondern der Potentialdifferenz an der Oberfläche gezogen wird. Die gemittelte Energie der Stromträger bleibt unverändert. Das beschriebene Szenario ähnelt dem Stromfluß in einem Stromkreis an einer Batterie, wo an Widerständen nur Spannung abfällt, aber die stromtragenden Teilchen nicht abgebremst werden.

Dieses Modell kann unter anderem die Energetik, den Frequenzbereich, die Polarisationseigenschaften und kurze heftige Ausbrüche mit stark erhöhtem Fluß reproduzieren.

In einem weiteren Abschnitt wird skizziert, wie sich das Modell in ein Gesamtbild der Magnetosphäre einfügt, indem ein globales Strombild entworfen wird. Dazu wird gezeigt, daß es für die Strombildbeschreibung im Pulsarsystem eine natürliche Grenze gibt und daß sich an dieser Stelle eine Raumladung aufbaut. Im allgemeinen Fall nichtparalleler Rotations- und Dipolachse ermöglicht dann $\vec{E} \times \vec{B}$-Drift einen Abfluß der Teilchen und effektive Beschleunigung in den Außengebieten.

Im Rahmen eines solchen Modells läßt sich auch die hochenergetische Strahlung quantitativ erklären.

Contents

Massive stars end their lives in spectacular explosions (so-called *supernovae*), leaving behind them neutron stars - objects having the highest recorded gravity and the highest magnetic field strengths (a trillion times the Earth's) ever found in the Universe - that we can detect as pulsars. These objects are predestined to fascinate us, spinning as they do at up to 650 times a second; they are the densest objects which do not collapse into black holes yet (the Schwarzschild radius is some 40% of the pulsar radius), and are regarded as marking the edge of the visible universe.

But how are such objects detected at all, when the accepted theories give them a radius of only about 10 km? Astonishingly, more than a thousand pulsars have been found, mainly by ground radio telescopes; the emission can only be the result of a highly coherent process.

Radio observations have become so sensitive and precise that even single pulses can now be studied in detail. A highly inhomogenous radiation pattern has been revealed, in both space and time. Occasionally, some pulsars show sudden huge fluxes (so-called micropulses), or even interrupt their radio emission for a few periods (nulling).

Ever since radio pulsars were first detected, scientists have tried to understand the origin of the strong radiation. In this work some new ideas are introduced regarding the emission mechanism, and the conditions required to produce the main radiation features. Currently favoured models are also discussed.

In another part of this thesis, a rough sketch explains the more energetic radiation (X-rays, γ-rays) observed in a few rapidly spinning pulsars.

The main results of this thesis are:

- exclusion of coherent curvature radiation for low-frequency pulsar radio emission (Lesch *et al.*, 1998)
- requirements for particle energy and density for low-frequency radio emission by a plasma process which contradict the standard inner gap model (Kunzl *et al.*, 1998a)
- beaming of coherent emission by relativistic effects and the finite extension of the coherence cell (Kunzl *et al.*, 1998b)
- explanation of typical polarization features of coherent radio emission by propagation effects (von Hoensbroech *et al.*, 1998)
- exclusion of inner gaps because of heavy thermal and field emission from the pulsar surface (Jessner *et al.*, 2001)

- explanation of the observed radio luminosity in the framework of a current-circuit model with low densities and particle energies (chapter 5, Kunzl *et al.*, 2001)
- explanation of giant pulse brightness temperatures of up to 10^{31} K on a timescale of 10 ns
- sketch of a model for the global currents in a pulsar magnetosphere including drift on the neutral surface (chapter 6)
- explanation of the high-frequency spectrum of the Crab pulsar (IR to γ-rays) by synchrotron emission in an outer gap (Crusius *et al.*, 2001)

"Start at the beginning", the King said very, very gravely,
"and go on till you come to the end, then stop.
Lewis Carroll, *Alice in Wonderland*

1 Introduction

More than 30 years ago some strange new objects appeared on the astronomical stage. Up to then, neutron stars were only theoretical predictions of a new kind of matter, produced when a massive star can no longer maintain its nuclear burning but is too massive to become a stable white dwarf (Baade *et al.*, 1934, Oppenheimer & Volkoff, 1939). These stars were supposed to finish their lives in a huge explosion. Such a *supernova*, if occurring in our galaxy, could be seen even during day time for several weeks.

The remainders of these supernovae (of which four have been observed in our galaxy in the last 1000 years) were expected to be extremely compact objects surrounded by thin nebulae powered by the central source (fig. 1). In the Crab pulsar the outflowing wind can be observed directly by its X-ray emission - see fig. 2. Although their mass exceeds the solar mass, the radius of such a compact object should be in the order of only 10 km. At this small size they should be virtually undetectable even with large telescopes unless they have an extremely efficient radiation mechanism.

When, in 1967, Jocelyn Bell noted radio signals so regular that their period could be fixed with a precision of 1 in 100.000 (Hewish *et al.*, 1968), at first a terrestrial or instrumental origin was assumed. As it became clear that the source of the radiation was not in our solar system, there were even some speculations about an extraterrestial intelligence sending the pulses.

Pulses repeating at about once per second, excluded a source like a rotating main sequence star, or some source orbiting another star. Even a white dwarf seemed very unlikely. In the meantime, pulsars have been found whose periods are so small that the source must definitely be smaller than a white dwarf[1]. These are very old "recycled" pulsars ("millisecond pulsars") having recently been spun up by transfer of matter from a companion star, which are the fastest spinning objects known in space. The most likely

[1]This result comes from estimating the maximum size of the radiating source as the product of the variation time and the speed of light. So an object emitting pulsed radiation with a period of 10 ms has to be smaller than about $3 \cdot 10^6$ m which is marginally consistent with a "hot spot" on the surface of a white dwarf. For even smaller periods this solution is definitely excluded.

Figure 1: Supernova remnant of the Crab pulsar. 950 years ago the progenitor star ended its life in a huge explosion whose debris can still be seen as this expanding shell. The (invisible) neutron star in the centre is the only energy source that feeds and drives the nebula by strong low-frequency electromagnetic waves and a relativistic particle wind.

explanation for the pulses is that the radiation originates in the vicinity of a neutron star. There is little doubt about this hypothesis nowadays.

Today pulsars are generally accepted to be quickly-spinning neutron stars with a very strong magnetic field. Estimates of the magnetic field from observations of cyclotron line emission have been performed by Trümper *et al.* (1978). The authors found a cyclotron resonance at 55 keV in the binary system Her X-1 consistent with a surface magnetic field of $5 \cdot 10^8$ T. This was a first hint to the order of magnitude of the magnetic field stength. Such findings have led to B of up to 10^9 T. This agrees well with results obtained from the spindown rate of neutron stars (see below). Today it is generally accepted that normal pulsars are objects with B around 10^8 T.

The spindown rate of pulsars is extremely small (only 10^{-15} for normal pulsars and 10^{-20} for millisecond pulsars) but measurable (see Fig. 3).

Despite this period stability the neutron star must obviously lose enormous energy per second to suffer this spindown: with an estimated moment of inertia of $J = 10^{38}\,\mathrm{kg\,m^2}$ we find a numerical value of

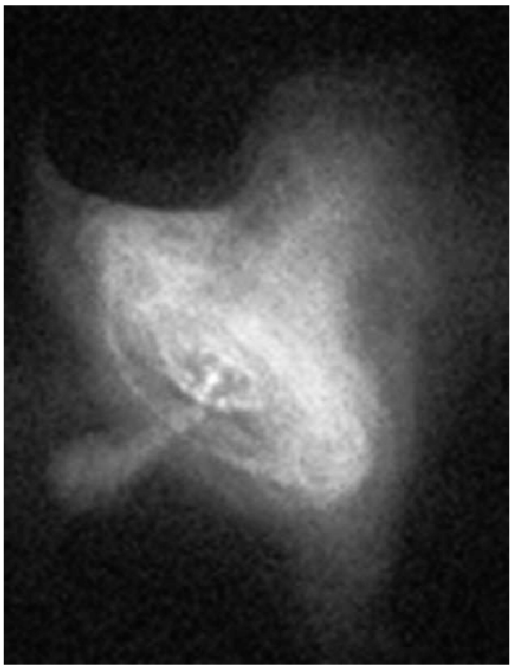

Figure 2: Inner part of the Crab nebula observed in X-rays by Chandra (Weisskopf *et al.*, 1999). The outflowing particle wind originating at the pulsar can clearly be seen. To emit X-rays by synchrotron radiation the particles must be highly relativistic.

$$\dot{E}_{\mathrm{rot}} = -J\Omega\dot{\Omega} = -3.85 \cdot 10^{24}\,\mathrm{W}\left(\frac{P}{\mathrm{s}}\right)^{-4} B_8^2 \tag{1}$$

where B_8 denotes the surface magnetic field in units of 10^8 T. In the second expression we inserted the connection between spindown and magnetic field for a braking due to dipole radiation in an orthogonal rotator, commonly used for determining the surface magnetic field as computed by Ostriker and Gunn (1969):

$$B_0 = 3.2 \cdot 10^{15}\,\mathrm{T}\sqrt{\left(\frac{P}{s}\right)\dot{P}}\,. \tag{2}$$

So although pulsars are rigorously stable clocks, they typically lose about

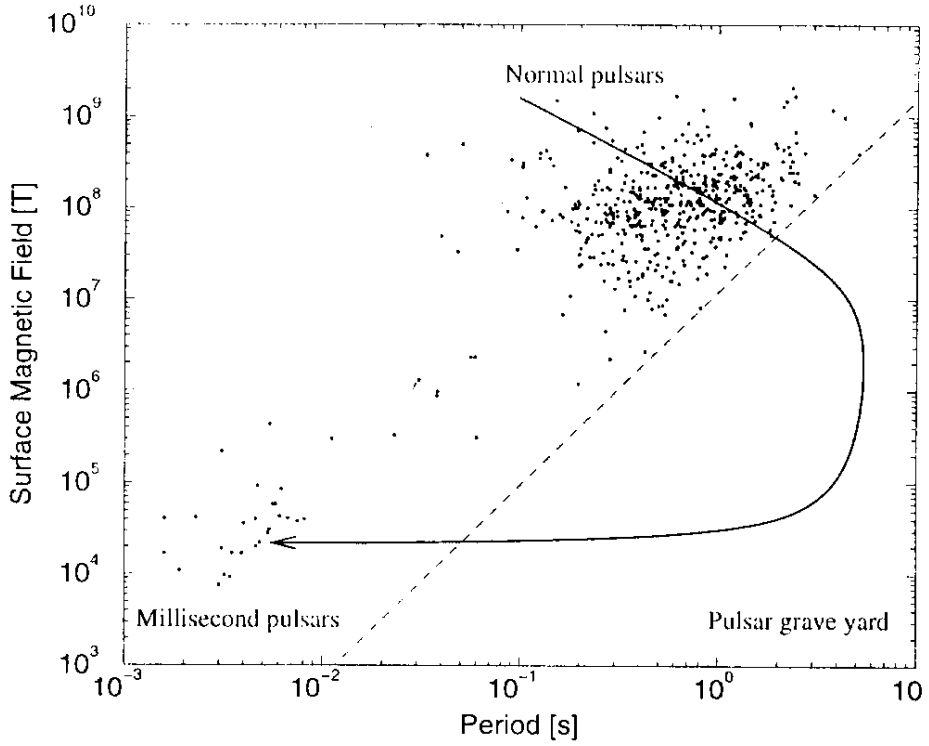

Figure 3: Period derivative of pulsars plotted against their periods. Two groups are clearly distinguishable. The left group are the so-called "recycled" or millisecond pulsars with very stable periods whereas the normal pulsars can be found at periods around one second. The straight line marks the so-called "death line" beyond which the standard model predicts that no radio pulsars exist.

10^{25} W of rotational energy, parts of which can be observed as electromagnetic radiation by terrestial and space telescopes.

In this framework, theory has to explain how a part of this spindown power is converted into radiation covering a wide band of the electromagnetic spectrum. A tiny fraction (about 10^{-5}) of the loss of rotational energy is converted into intense, highly coherent radio emission. Many details and features have been found in radio pulses so far, which provide strong tests for any theoretical model. Especially the high fluxes, the polarization features and the spectral behaviour (power law with a low-frequency cutoff at about 200 MHz where the maximum flux is found) need to be reproduced at least qualitatively. In this work we will mainly concentrate on radio emission models (which usually also sketch, how the harder radiation is produced). Most of the "classical" models were developed to explain radio emission.

X- and γ-ray observations have a lower spatial and temporal resolution due to the far lower fluxes but nevertheless give hints about dissipation processes in the magnetosphere. This is because the broad-band energy flux of the high-frequency emission is much larger than in the radio range.

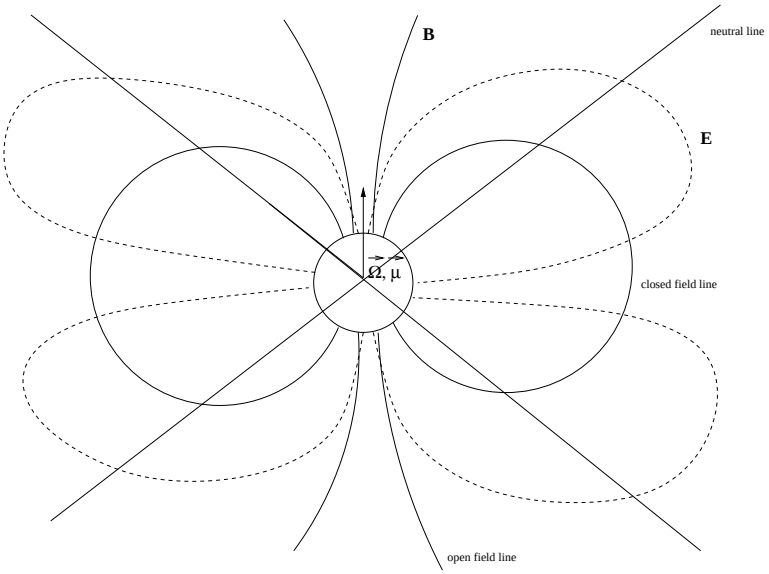

Figure 4: Vacuum fields of an aligned dipole rotator. Negative charges accumulate at both polar regions whereas the equatorial belt is charged positively. The "neutral line" (where $\vec{E} \cdot \vec{B}$ vanishes) appears under an angle of about 55 degrees to the rotation axis.

Soon after the discovery of pulsars, Goldreich & Julian (1969) showed that a rotating dipole cannot be surrounded by vacuum, as extremely strong electric fields are induced, which drag charged particles out of the neutron star surface. This is because a quadrupolar electric field results from a rotating dipole magnet (cf. fig. 4). In fact, such a field derives if we assume that the neutron star is almost superconducting. Therefore Ohm's law in its ideal form

$$\vec{E} + \vec{v} \times \vec{B} = 0 \tag{3}$$

is valid in the interior. But the tangential component of the electric field must be continuous at the surface whereas the radial component can show a jump, due to surface charges.

As we are considering a stationary problem, we require that the electric field outside is a potential field, meaning

$$\vec{E} = -\mathrm{grad}\,\Phi\,. \tag{4}$$

With these assumptions we obtain a unique solution for the potential

$$\Phi = -\frac{B_0 \Omega r_{\mathrm{NS}}^5}{3r^3} P_2(\cos\theta) + const. \tag{5}$$

with $P_2(y) = (3y^2 - 1)/2$ being the second Legendre polynom, and θ denoting the angle between magnetic field line and rotation axis. Evaluating the gradient, and taking only the component parallel to $\vec{B}$ yields

$$\vec{E} \cdot \vec{B} = \Omega r_{\mathrm{NS}} B_0^2 \left(\frac{r_{\mathrm{NS}}}{r}\right)^7 \cos^3\theta\,. \tag{6}$$

Therefore the electric field has a large parallel component to the magnetic field $\vec{B}$. This will allow charged particles to leave the neutron star (the electric force on an electron exceeds the gravitational force by a factor of 10^{12}!), and their accumulation compensates the parallel component of the field. The charge density necessary to fulfill $\vec{E} \times \vec{B} = 0$ everywhere in the magnetosphere reads

$$\rho_{\mathrm{GJ}} = -\frac{2\varepsilon_0}{x^3}\vec{\Omega} \cdot \vec{B_0} = \frac{\Omega B_0 \varepsilon_0 \left(1 - 3\cos^2\theta\right)}{x^3} \tag{7}$$

where B_0 means the (dipolar) surface magnetic field strength at the pole and x is the radial distance from the neutron star in units of pulsar radii. The angular dependence follows from the dipole parameter equation. There are additional corrections near the light cylinder by special relativistic effects

(the corotation speed approaches c, therefore the magnetic field is wound up and becomes stronger than in the non-rotating case) and very close to the surface by General Relativity (Muslimov & Tsygan, 1992). This is because the (negative) gravitational potential energy of a particle is comparable to its rest energy. In a distance of some pulsar radii the latter effect is negligible, as the gravitational binding is much weaker. Therefore we neglect these corrections in our discussion, as they do not play a significant role in the radio emission distance. This is supposed to be far off the neutron star surface but still well within the light cylinder so that both corrections should be of no importance.

This charge density, first computed in Goldreich & Julian (1969), $\rho_{\rm GJ}$ is called the *Goldreich-Julian density*. In the following we will also use this term for the corresponding particle density

$$n_{\rm GJ} := \left| \frac{\rho_{\rm GJ}}{e} \right| . \tag{8}$$

It is emphasized that this solution is only fully correct for a *static* magnetosphere in a parallel rotator. Nevertheless it is also useful for non-vanishing currents (the external dipolar field is hardly affected by induced magnetic fields), and for oblique rotators (replacing θ by $\theta - \phi$ where ϕ is the inclination angle).

Of course, the Goldreich-Julian density cannot be maintained all over the pulsar magnetosphere, because this solution is a static one, and there would be neither relativistic particles nor pulsed radiation in this case. Nevertheless it is a good approximation as long as the current-induced magnetic field is much smaller than the dipole field as in this case the dipolar structure is not modified significantly. However, this restriction is always fulfilled for pulsar magnetospheres.

Only two years after Goldreich and Julian's work, Sturrock (1971) proposed that the field lines which can corotate with the neutron star will keep the Goldreich-Julian (GJ-) density. Some field lines emanating near the dipolar axis extend so far into space that the corotation speed would, at some distance, exceed the speed of light. So the system cannot keep this static state everywhere as particles drifting outward through the so-called *light cylinder* cannot return directly. Therefore the GJ solution will be violated somewhere. The region where these "open field lines" penetrate the neutron star surface is called the "polar cap".

Sturrock assumed a gap that would develop if the entire region of open field lines were a vacuum. This idea was slightly modified in the model of Ruderman & Sutherland (1975). They considered an anti-aligned pulsar

($\vec{\Omega} \parallel -\vec{B}$, meaning a positive GJ-density above the polar cap) where the gap develops since ions are bound so tightly to the surface that they cannot leave the neutron star. So the gap above can only be closed by a pair cascade, initiated by stray γ- rays from outer regions. The primary particles will be accelerated to ultra-relativistic energies and therefore emit hard curvature radiation, producing a pair in the very strong magnetic field. These secondary particles will again be accelerated, producing another pair and so on until the gap is closed. In both cases, highly non-stationary pair formation is assumed (as the pair plasma will flow outwards and re-open the gap) with the resulting bunches being responsible for the observed radio emission by coherent curvature radiation.

In the following, Arons and his group proposed a similar *space charge limited flow* model (Scharlemann *et al.*, 1978, Arons & Scharlemann, 1979), where field line curvature, and the resulting nonlinear behaviour of the GJ-density, lead to acceleration on so-called *favourably curved field lines* in an inclined rotator, followed by an analogous pair cascade as in the Ruderman-Sutherland model. This idea extended the "gap" description also to almost parallel rotators. Shibata (1997), Shibata *et al.* (1998) assumed a stationary current causing acceleration on the "unfavourably" (in the Arons type) curved field lines.

Acceleration by particle inertia has been studied in detail by Michel (1974), Fawley, Arons & Scharlemann (1977), this is another space charge limited flow model assuming that particles are accelerated asymptotically to highly relativistic energies. However, no pair cascade would be possible in such a model.

A principally different type of acceleration model is the so-called outer gap model (Cheng *et al.*, 1986), where the acceleration region is located between the neutral surface and the light cylinder.

But no matter where the Goldreich-Julian solution is fulfilled; if particles somehow flow off the polar cap and return to the neutron star somewhere at a lower latitude, they cover a huge potential difference $\Delta\phi$. A typical value for $\Delta\phi$ is the voltage between the pole and the edge of the polar cap in the parallel case (Ruderman & Sutherland, 1975):

$$\Delta\phi = \frac{1}{2} B_0 \Omega R_{\rm cap}^2 = 6.58 \cdot 10^{12}\,{\rm V} \left(\frac{P}{\rm s}\right)^{-2} B_8\,. \tag{9}$$

Here we have used the expression for the polar cap radius

$$R_{\rm cap} = \sqrt{\frac{\Omega r_{\rm NS}^3}{c}} = 145\,{\rm m} \left(\frac{P}{\rm s}\right)^{1/2} \tag{10}$$

with the neutron star radius $r_{\rm NS}$ and the speed of light c.

As will be shown in this work the various pair production models all encounter severe difficulties, making further assumptions necessary, especially for slow pulsars. So it is doubtful whether the inner gap scenario is possible at all. Besides, there are a number of other arguments against this model. So, for several reasons, curvature radiation by bunches (needing a huge number of pairs) can be ruled out as a mechanism for the coherent radio emission (Lesch *et al.*, 1998). But, for the currently most favoured emission mechanism, some plasma process, low Lorentz factors (around 10) are required to make the process efficient enough (Melrose, 1978) or to reproduce the observed low frequencies (Kunzl *et al.*, 1998a). But as the highest fluxes are observed in the low radio frequencies, a convincing model must especially reproduce this frequency range. The above results are therefore incompatible with a pair cascade which would lead to average Lorentz factors of a few hundred (Daugherty & Harding, 1982).

So it is worthwhile to look for alternatives to the classical pair model to avoid the difficulties mentioned above. A mildly relativistic single-charge plasma needs a description without an inner gap in contrast to the RS scenario. We therefore adopt an entirely different approach, where no inner gap is assumed, and the inner part of the magnetosphere can be described as a current circuit with mildly relativistic particles. A dissipation region causes a voltage drop instead of deceleration. Of course in this framework pair production or even high energetic radiation from the inner region of the magnetosphere are excluded. The (non-thermal) emission above the radio frequencies is assumed to be produced in the outer magnetosphere (close to the light cylinder) where this model predicts an acceleration region similar to ideas first presented by Cheng & Ruderman (1977). The current circuit model is one main part of this work and is discussed in detail in chapter 5; a possibility for current closure, high energetic emission and the pair wind which flows out into the nebula, is sketched in chapter 6.

In the current circuit model deviations from ideality are caused by electrostatic density fluctuations which act as a resistance. The resistivity is limited by plasma effects, so that we can derive a minimum thickness of the radiation region necessary to match the observed luminosity. We find that typical low frequency fluxes can easily be reproduced with narrow radiation zones (Kunzl *et al.*, 2001).

To explain the so-called *micropulses*, we need to take several beaming effects into account. On the one hand there is the well-known relativistic light-house effect (*e.g.* Rybicki & Lightman, 1979), but additionally coherence itself causes anisotropy, even in the co-moving frame (Kunzl *et al.*,

1998b). These two mechanisms can explain even the highest brightness temperatures observed in burst-like substructures on time scales of only 10^{-8} s.

As in the outer gap models, the neutral surface (i.e. the conal area where n_{GJ} vanishes) plays a very important role in this work. This is because the current circuit picture certainly does not apply beyond the neutral surface, as charged particles cannot easily flow from the region of one space charge to the other. The neutral surface is therefore a natural border for the particles. This implies that charges accumulate there as soon as a non-vanishing (quasi-stationary) current flows along an appropriate field line.

For an inclined rotator, particles can drift across field lines and reach open field lines in the "correct" space charge region whence they can be accelerated outwards. Drift becomes possible as charges accumulate around the neutral surface. Thus the charge density deviates from the Goldreich-Julian value and perfect corotation is violated.

In the outer gap, particles can be accelerated very efficiently, as all field lines are "favourably curved" in the Arons sense. As almost all the potential difference drops in the outer magnetosphere, pair production can set in, with the positrons flowing back inwards to reach the neutral surface, and eventually drifting to field lines, on which they can flow further towards the neutron star. In Crusius *et al.* (2001) it is shown that, in principle, an outer gap scenario can explain the optical, UV and X-ray emission from the Crab pulsar.

Another advantage of an outer-gap model is that it can clarify the transfer of angular momentum. It is easy to show that the mean distance from the rotation axis where energy must be converted into radiation or highly relativistic particles, exactly matches the light cylinder radius. Hence, if there were an inner gap, where a significant part of the spindown power is dissipated, another dissipation or decoupling mechanism far beyond the light cylinder would be necessary.

Summarizing, the standard model is quite unsatisfactory in many ways and needs to be revised. This work introduces some new ideas which may help to give a better understanding of the processes in a pulsar magnetosphere.

[...] when she noted a curious appearance in the air;
it puzzled her very much at first,
but after watching it a minute or two
she made it out to be a grin[...].
Lewis Carroll, *Alice in Wonderland*

2 Observations

2.1 Radio observations

The most detailed information about pulsars are obtained from radio observations. It was with a radio telescope that Jocelyn Bell discovered the first of these objects (Hewish *et al.*, 1968). In the meantime several surveys have increased the number of known pulsars to more than a thousand. Only a few of them are radio-quiet, that means they do not emit radio pulses. The most prominent of this group is the X-ray pulsar Geminga, whose parameters suggest that it should be a radio pulsar as well. However, the non-detection of Geminga in radio frequencies might be due to geometric effects (the radio beam misses the Earth) or intrinsic (Malov (1994) proposes a model why Geminga's radio luminosity is so small).

A comprehensive catalogue of 558 pulsars detected in the radio band can be found in Taylor *et al.* (1993) which lists observational data such as rotation period and its derivative, pulse widths, radio fluxes at 408 and 1400 MHz, radio luminosity, magnetic field strength, spindown power and characteristic age. The gross features of the radio emission are virtually the same for all known pulsars. In particular these are the following:

2.1.1 Spectrum

A typical radio pulsar shows its highest flux at low radio frequencies, the maximum is usually reached between 60 and 400 MHz. For some pulsars, for which very low frequency data (below 400 MHz) are missing, it is not too accurately determined. But other cases suggest a mildly rising spectrum (probably a power law with a spectral index[2] of about $-1/3$) below the peak frequency, whereas above that maximum the flux drops in a power law with a spectral index of typically 1 - 3 (see figs. 5 and 6). In some cases the data

[2]Since most observed power law spectra fall towards higher frequencies, the usual convention is that a spectral index κ means $S_\nu \sim \nu^{-\kappa}$

more closely imply a broken power law, that means the spectrum becomes steeper at higher frequencies[3].

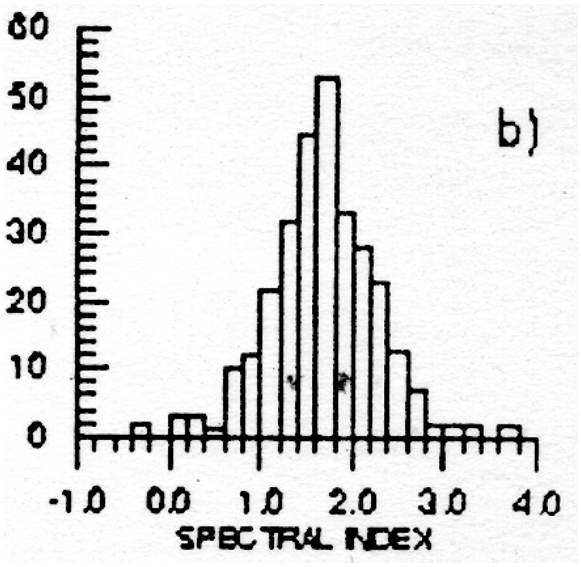

Figure 5: Distribution of spectral indices of radio pulsars (taken from Malofeev (1996))

Compared to the smallness of the source, pulsar radio fluxes are very high. A useful quantity for the intensity of a radio emitter is the brightness temperature T_{B}. This number denotes the temperature of a blackbody source required to emit the observed intensity at a certain frequency in the low-frequency limit:

$$T_{\mathrm{B}} = \frac{F_\nu c^2}{2\pi k_{\mathrm{B}} \nu^2} \left(\frac{R}{r}\right)^{-2} \tag{11}$$

where F_ν is the observed flux at the frequency ν, R stands for the transverse extension of the radiating source and r for the distance to the observer (see chapter 5 for a more detailed discussion).

Obviously, T_{B} strongly depends on the frequency. The brightness temperature is usually evaluated in the low-frequency limit (this approximation is applicable if the resulting $T_{\mathrm{B}}(\omega) \gg \hbar\omega/k_{\mathrm{B}}$ which is always true for pulsar radio emission). Pulsar radio emission shows typical brightness tempera-

[3]Some years ago, a pulsar with a negative spectral index up to several GHz, B1736-31, has been reported (Taylor *et al.*, 1993)

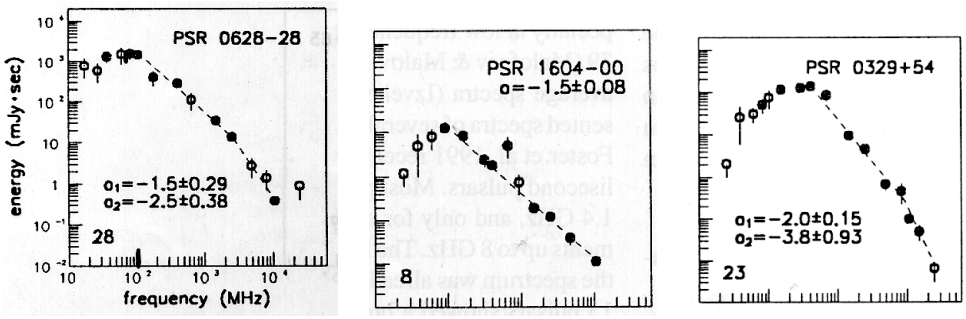

Figure 6: Radio spectra for three exemplary pulsars from the sample by Malofeev *et al.* (1994). The open circles are doubtful data points. Nevertheless in the second case there is a clear hint for a flattening of the spectrum below some 100 MHz which substantiates the assumption that all pulsars show a turnover in this frequency range.

tures of up to 10^{25} K which is a clear indicator of a highly coherent process (see next chapters).

For some pulsars, the spectral shape changes again for very high radio frequencies (above 10 GHz), where a flattening or even a turnover has been observed (Kramer *et al.*, 1996, 1997) (see fig. 7). Somewhere between the high frequency radio range and the X-rays such a turnup has to occur anyway as the radio emission power laws do not fit the X-ray spectra at all (the X-ray fluxes exceed the extension of the radio spectrum to keV energies by many orders of magnitude, cf. fig. 8).

2.1.2 Energetics

The observed radio fluxes allow a rough estimate of pulsar radio luminosity. The quantity "flux" has the dimension of a power per frequency interval per area. For simple luminosity estimates the following procedures are suggested:

First, the radiation is assumed to be broadband emission, that means the flux is taken to be constant over a frequency interval $\Delta\nu \approx \nu$. If the radiation were isotropic, the spatial angle would be 4π, which means the irradiated area would be the whole surface of a sphere, whose radius is the distance to the neutron star. From measurements of profile widths the actual spatial angle can be obtained. The corresponding fraction turns out to be in the range of $10^{-3} \ldots 0.1$, where the upper limit is reached for some millisecond

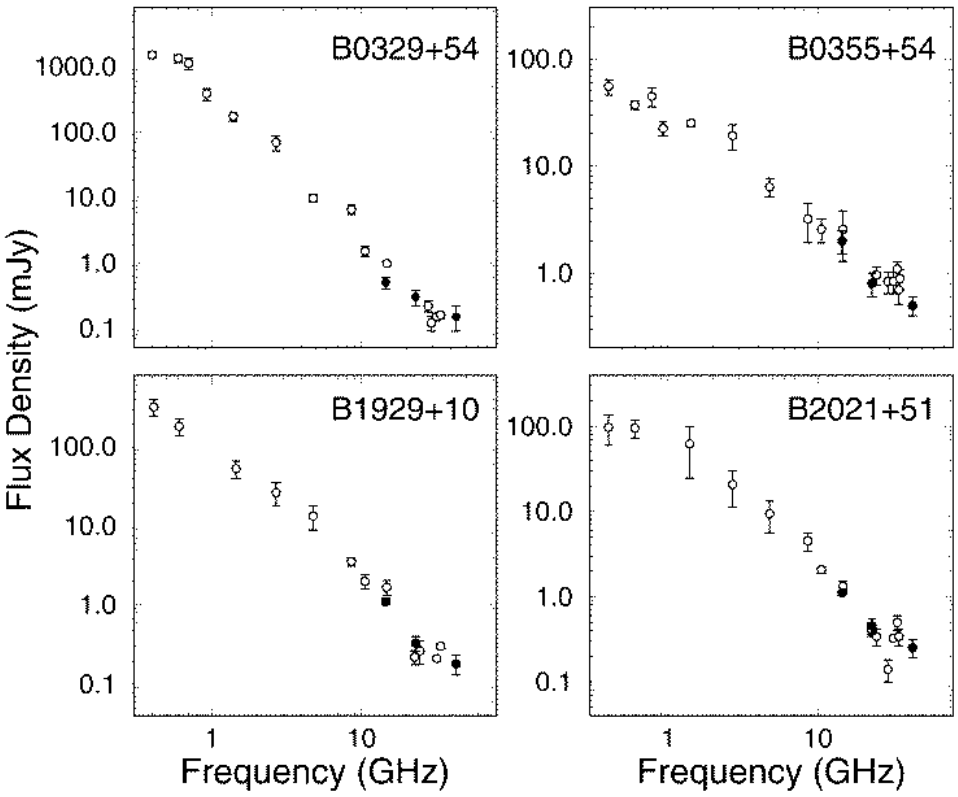

Figure 7: Flattening of the radio spectrum at high frequencies. This turnover is estimated to occur in all pulsars in the vicinity of $10 - 100$ GHz.

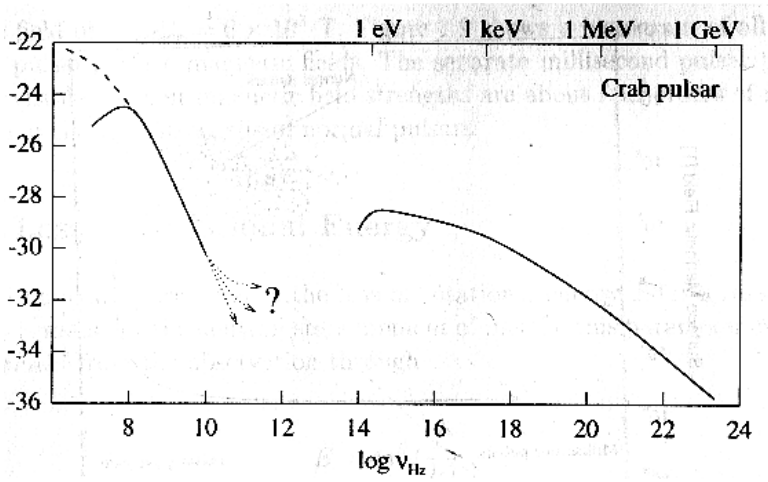

Figure 8: Spectrum of the Crab pulsar from radio to $\gamma-$ emission. On the ordinate, the flux is plotted against the frequency. So although the number of emitted photons drops towards higher frequencies, the total energy emitted in harder radiation nevertheless vastly exceeds the radio luminosity as the frequency band is much wider. In the microwave and far infrared band ($10^{12} \ldots 10^{14}$ Hz no pulsed emission has been found yet as the flux (and especially the broad-band power has a wide minimum there. So it remains unclear if there is non-thermal radiation in these frequencies or not.

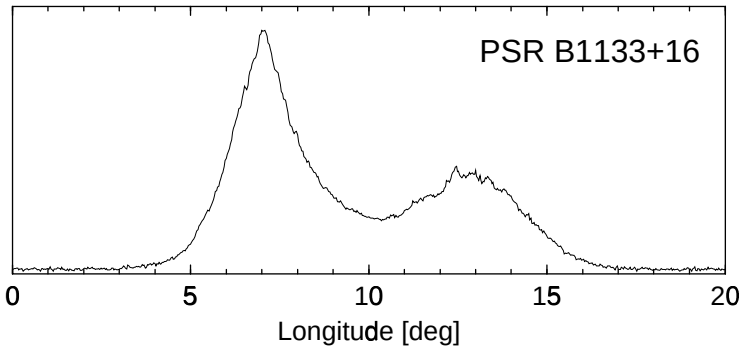

Figure 9: Mean pulse of PSR 1133+16. The averaged profile provides a "fingerprint" of the system, which develops when about 100 or more single pulses are added up (taken from Kramer).

pulsars whose profiles tend to be significantly broader than those of normal pulsars. Taking a typical profile width of 3% (usually the duration of one pulse is a few percent of the rotation period), Kramer (1995) gives a handy formula for the luminosity:

$$L = 3.8 \cdot 10^{18}\,\mathrm{W} \left(\frac{S_{400}}{\mathrm{mJy}}\right) \left(\frac{d}{\mathrm{kpc}}\right)^2 . \tag{12}$$

Here S_{400} means the flux measured at 400 MHz, and d is the distance to the neutron star. From (12) we find that the typical radio luminosities of pulsars are between 10^{19} and 10^{22} W, which transforms into a radio efficiency (i.e. the ratio of radio and spindown luminosity) of $10^{-9} \ldots 10^{-4}$ (cf. (1)).

Therefore the radio emission does not greatly affect the global energetics of the pulsar system as only this tiny fraction of the total energy loss is caused by radio emission. In other words, the global pulsar structure is definitely dominated by other dissipation processes (see chapter 6).

2.1.3 Mean and single pulses

If the radio emission of one pulsar is integrated over many periods, the normalized profile converges to some unique stable shape that can be seen as a "fingerprint" of the system (fig. 9). These profiles show quite a variety, and are usually classified by the number of peaks. Apart from a few cases where two peaks at a phase shift of nearly 180 degrees are observed the emission pattern is narrow, and shows some central peak and/or two or more symmetric peaks. Rankin (1983) referred to these different features of the pulse as 'core' and 'cone' components respectively. The flux ratio of these components can take almost any value; slow pulsars tend to have a dominating 'cone' component whereas young, energetic pulsars like the Crab are 'core' emitters. Nevertheless, the single pulses are highly stochastic and do not only vary in intensity but can also have a completely different profile, em e. g. only one component of a two-humped profile may appear (fig. 10). In some pulsars even so-called *nulling* has been observed, which means that for some periods the emission almost stops completely only to begin again suddenly later.

Looking at the substructures of the single pulses one can also find sharp peaks where the flux exceeds its mean value by up to a factor of several thousands (Boriakoff, 1992) (fig. 11). The Crab pulsar shows such outbursts on a timescale of less than 100 nanoseconds. Any radio emission model must be able to produce fluxes as high as that from such small regions in the magnetosphere.

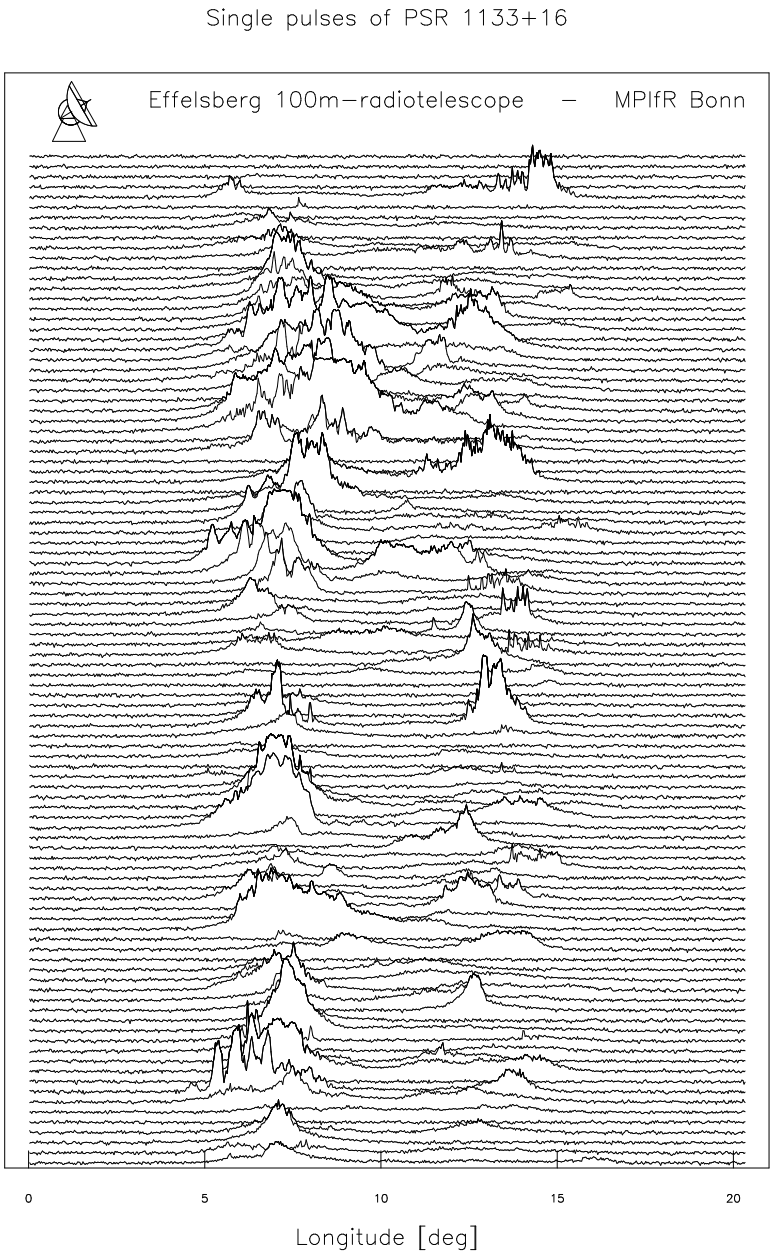

Figure 10: Single pulses of PSR 1133+16. It can clearly be seen that the individual pulses are highly irregular. In the upper part nulling occurs, meaning no radio emission is detected for some periods. The data are taken from Kramer (1995).

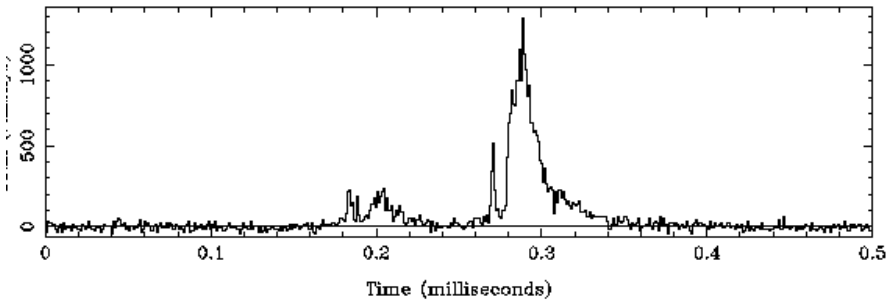

Figure 11: Giant pulse radio eruption in the Crab pulsar (Boriakoff, 1992). The flux enhancement is a factor of several thousands; the brightness temperature goes up to 10^{31} K.

Apart from these giant pulses, the typical 'core' emitter shows smoother single pulses than a 'cone'. The reason may be a stronger variation in the particle flow as the surface cools and the vacuum fields drop. Therefore, in this case, one should expect a spiky structure caused by highly coherent single pulses, strongly variable in space and time. As a variable particle outflow provides optimal conditions for wave growth and coherent emission (see chapter 4), higher coherence can be expected for old pulsars.

Alone the chaotic behaviour of the single pulses is a clear hint that the mechanism producing the radio emission is a highly non-stationary one.

2.1.4 Emission heights

Based on the generally accepted idea that radio emission can occur only on open field lines, pulse profile analyses can be used to estimate the distance to the neutron star where the radio emission is produced- the *emission height*. The first of these calculations was done by Blaskiewicz *et al.* (1991), who predicted emission heights between 30 and 100 pulsar radii. These results have been confirmed independently by another method using timing measurements (von Hoensbroech, 1995).

Furthermore, observations hint that the high frequencies seem to be produced closer to the neutron star than low frequencies. This so-called *radius to frequency mapping* (RFM) is found to be small, the values are even marginally consistent with no RFM at all. Mostly the RFM is fitted by a simple power law

$$x_{\rm em}(\nu) = C\nu^{-\eta} \tag{13}$$

where C is a constant of the appropriate dimension and η is in the range of 0.1 ± 0.1 Gil & Kijak (1992), Kramer (1994). In some cases the data can be explained better if a (positive) offset x_0 is added (that means the emission height saturates even for very high frequencies, Kramer (1995)). But since the effect is small anyway there is not much difference.

At least the study of RFM can definitely rule out coherent curvature radiation in its widely accepted form since it would predict a RFM of $\kappa = 10/17$ (Lesch *et al.*, 1998). This value results from the assumption that plasma bunches with the extension of one Debye length ($\lambda_{\rm D} \approx c/\omega_{\rm pe}$) emit at a distance where the CR frequency equals the local plasma frequency. As the emitted frequency is determined by the particle energy and the local curvature radius we obtain a unique solution for the distance where a certain frequency is emitted. The only free parameter - the pair density - does not affect the overall scaling and the RFM exponent. We argue that apart from energetic problems (see the detailed discussion in chapter 4) this is a strong argument against coherent curvature radiation as a source for radio emission.

2.1.5 Polarization

Another interesting feature of pulsar radio emission is its linear and circular polarization. Linear polarized emission is found in all pulsars and in most cases the polarization angle follows a characteristic S-shape suggesting that it is determined by the plane of a specific magnetic field line that crosses the line of sight at the moment. Therefore it supports the idea that the emission has its origin in the region of the open field lines since this geometry would exactly predict an S-shape such as shown in fig. 12.

Especially the low frequency radiation is sometimes almost fully linearly polarized. This polarization is another hint that some kind of maser process is responsible for the radio emission, as only a phase coupled radiator can produce linearly polarized emission.

Towards higher radio frequencies the linear polarized fraction typically decreases. In many cases some circular polarized component comes up at some GHz. We were able to show that in the framework of a Goldreich-Julian magnetosphere with low energetic particles this circular component and its properties can qualitatively be explained by propagation effects (von Hoensbroech, Lesch & Kunzl, 1998). Particularly the model reproduces the tendency that young, energetic pulsars emit polarized emission up to higher frequencies than slow pulsars. The principal idea of the model is as follows:

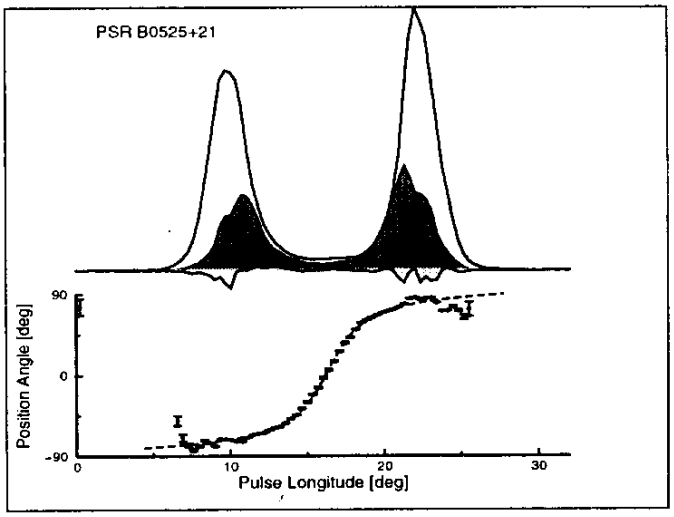

Figure 12: S-shape of the linear polarization (the linear polarized part is shown in black in the profile at the upper part of the figure). Such a behaviour agrees with a mechanism that emits radiation polarized in the plane of the magnetic field line (so-called rotating vector model).

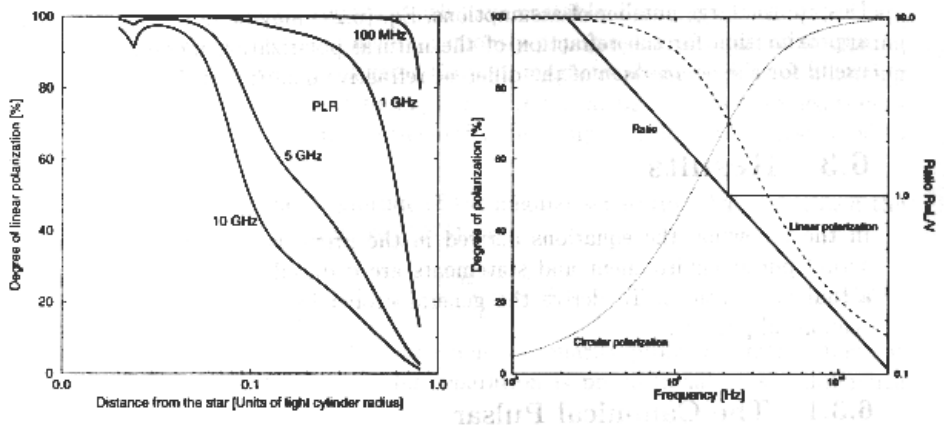

Figure 13: degree of linear polarization versus the distance from the neutron star (left) and frequency (right) for a "standard pulsar" with $P = 0.6$ s, $\dot{P} = 10^{-14.6}$ and an inclination angle of 45° for only one natural mode at a time (case 1). If the decoupling distance is *e. g.* 0.3 of the light cylinder radius (as assumed in the right plot), high frequencies already show circular polarization whereas the low-frequency radiation is still linearly polarized.

Radio emission of all frequencies is produced at a distance of typically a few percent of the light cylinder radius. As it is highly coherent, it can be taken to be polarized in the same way as the natural modes in the plasma. These are, however, elliptical, due to the magnetic field. To observe a net polarization at all, we cannot have both modes at the same time, as this would give unpolarized emission. Polarized radiation can be observed in two situations:
(1) Only one natural mode is emitted at a time;
(2) Both natural modes are produced at the same place and time, but become separated by birefringence.

As a simple approximation, we can compute the polarization for a cold single-charge plasma with GJ-density. The angle of the emitted wave to the magnetic field line is given roughly by $1/\gamma_{\rm beam}$, where $\gamma_{\rm beam}$ denotes the Lorentz-factor of the radiating beam plasma. As the wave propagates outwards it is surrounded by background plasma that may have a different Lorentz factor $\gamma_{\rm bg}$. Now the natural modes are given by the dielectric tensor for the magnetized electron plasma (see Melrose & Stoneham, 1977, Melrose, 1979). Calculations show that the model allows a wide range for the parameters $\gamma_{\rm beam}$, $\gamma_{\rm bg}$ and the *polarization limiting distance* (i.e. the distance at which the wave decouples from the plasma and does not change its polarization any more) without affecting the qualitative picture.

For the calculations the effects have to be integrated in the actual pulsar geometry along the magnetic field line starting at the emission distance and integrating up to the decoupling distance. This means, a dipolar structure modified by aberration (Phillips, 1992) and magnetic sweepback (Shitov, 1983) (as the magnetic field cannot keep corotation at the light cylinder) has to be used.

In case 1 we find that the radiation is almost linearly polarized at the emission region, but soon acquires a growing circular component as it travels outwards. Especially there is a strong frequency dependence, in the sense that the low frequencies still remain linearly polarized, whereas the high frequencies already have considerable circular polarization (see fig. 13). If the decoupling distance is chosen appropriately (*e.g.* 20% of the light cylinder radius) the mechanism produces linearly polarized low-frequency and circularly polarized high-frequency emission.

In cases where the ratio of circular and linear polarization is known for different frequencies, the background Lorentz-factor and the decoupling distance are connected (von Hoensbroech *et al.*, 1998), as the transition frequency depends on the particle energies and the polarization-limiting radius. Three pulsars , PSRs 0144+59, 1737-30 and 1913+10, can be used for

detailed parameter studies (von Hoensbroech & Lesch, 1999). It turns out that, for a fixed $\gamma_{\rm bg}$, the relative polarization limiting region is the same for all three examples (cf. fig. 14). Moreover, the data are consistent with a mildly relativistic plasma and a large decoupling distance (see von Hoensbroech & Lesch, 1999).

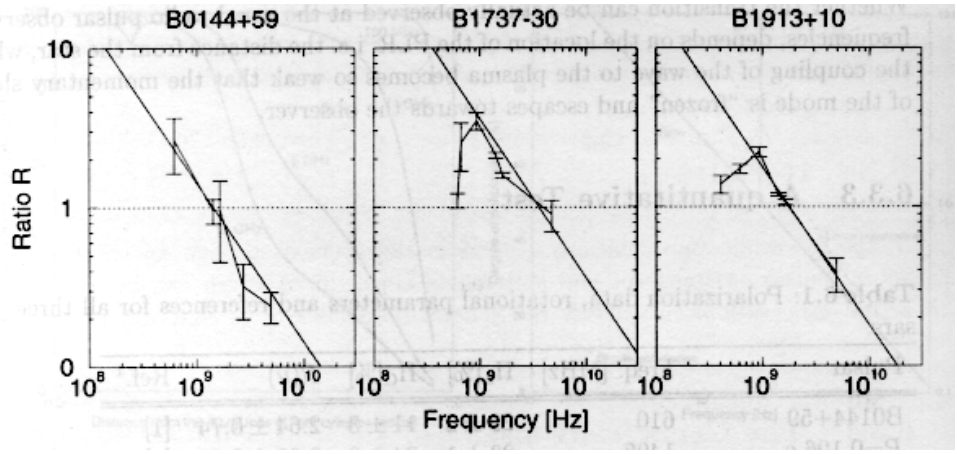

Figure 14: ratio of linear and circular polarization for the three pulsars PSR 0144+59, 1737-30 and 1913+10. The theoretical prediction fits the observed data strikingly well. Note that the model predicts a power law scaling with $R \sim \nu^{-1}$ but not the prefactor. This proportional constant, however, varies only by a factor of 2 for the three pulsars (which have entirely different characteristic ages and periods) and may be a complicated function of P, $\dot{P}$ and other parameters.

Case (2) could be used to investigate the depolarization observed at high frequencies. We compute the difference of the refractive indices of both modes, giving a hint about where the two modes become separated. This difference decreases strongly towards higher frequencies implying that if both modes are excited simultaneously they will separate for low frequencies, but are still superimposed for higher ν. Therefore, in the low frequency range, only one (polarized) mode at a time is observed, whereas above some GHz the two modes still overlap and cause depolarization. Furthermore, the model predicts that for pulsars with a large spindown, depolarization sets in at higher frequencies than for slow pulsars, as the difference of refraction indices grows with $\dot{E}$. Such a behaviour is in fact observed (Gould & Lyne, 1998).

In some cases the swing of the polarization angle does not show the

characteristic S-shape, but jumps by 90 degrees. These so-called *orthogonal polarization modes, OPM* (shown in fig. 15), are believed to occur when one wave mode (usually the dominant one) is replaced by the other, which is orthogonal to the first. Why this happens, is unknown. In cases of circular polarization, these OPMs normally show a sense reversal of the circular component. The phenomenon of OPM seems to be quite common, as almost all pulsars where polarization can be analyzed show this effect.

2.2 High frequency emission

All observations of pulsars above the radio band are much more difficult than low frequency observations, as the fluxes are far lower. This is because the emission, though non-thermal, appears to be incoherent (typical X-ray temperatures are only about 10^6 K if the radiation is taken to be thermal). Together with the small spatial extension of the radiating source, this limits the flux to values far below the low frequency radio fluxes. From the optical to the γ-emission the power rises, but the flux still declines, which affects the resolution of observations. The Crab pulsar can be detected from radio to γ- frequencies. The corresponding pulse profiles are plotted in fig. 16.

2.2.1 Infrared, optical and UV emission

Only few pulsars can be detected in the band between radio frequencies and X-rays. For most of them, only upper limits of the fluxes can be given and no spectral information or pulses can be resolved. So it is likely that this class of objects are cooling neutron stars emitting blackbody radiation. Pulsed emission has been found for the middle-aged pulsar PSR 0656+14 (Pavlov *et al.*, 1997) and for the three young pulsars PSRs 0531+21 (Crab), 0833-45 (Vela) and 0540-69. Nasuti *et al.* (1997) find almost flat spectra for all three of these objects though the spectral resolution of the Vela optical pulses is fairly poor (see fig. 17). At least the results strongly hint towards a non-thermal optical spectrum that cannot be fitted properly by assuming a blackbody source.

Optical pulses from the Crab pulsar were found soon after the discovery of pulsars (Cocke *et al.*, 1969). Recently even single optical pulses have been resolved (Mantel (2001), see fig. 18). For PSR 1706-44 there are upper limits from a non-detection (Mignani *et al.*, 1999), for PSR 1509-58 it is only known that the optical luminosity cannot be fitted simply by extending a thermal spectrum with its peak in the X-rays (Nasuti *et al.*, 1997, Caraveo *et al.*, 1994) to lower frequencies. Other optically detected pulsars are PSRs

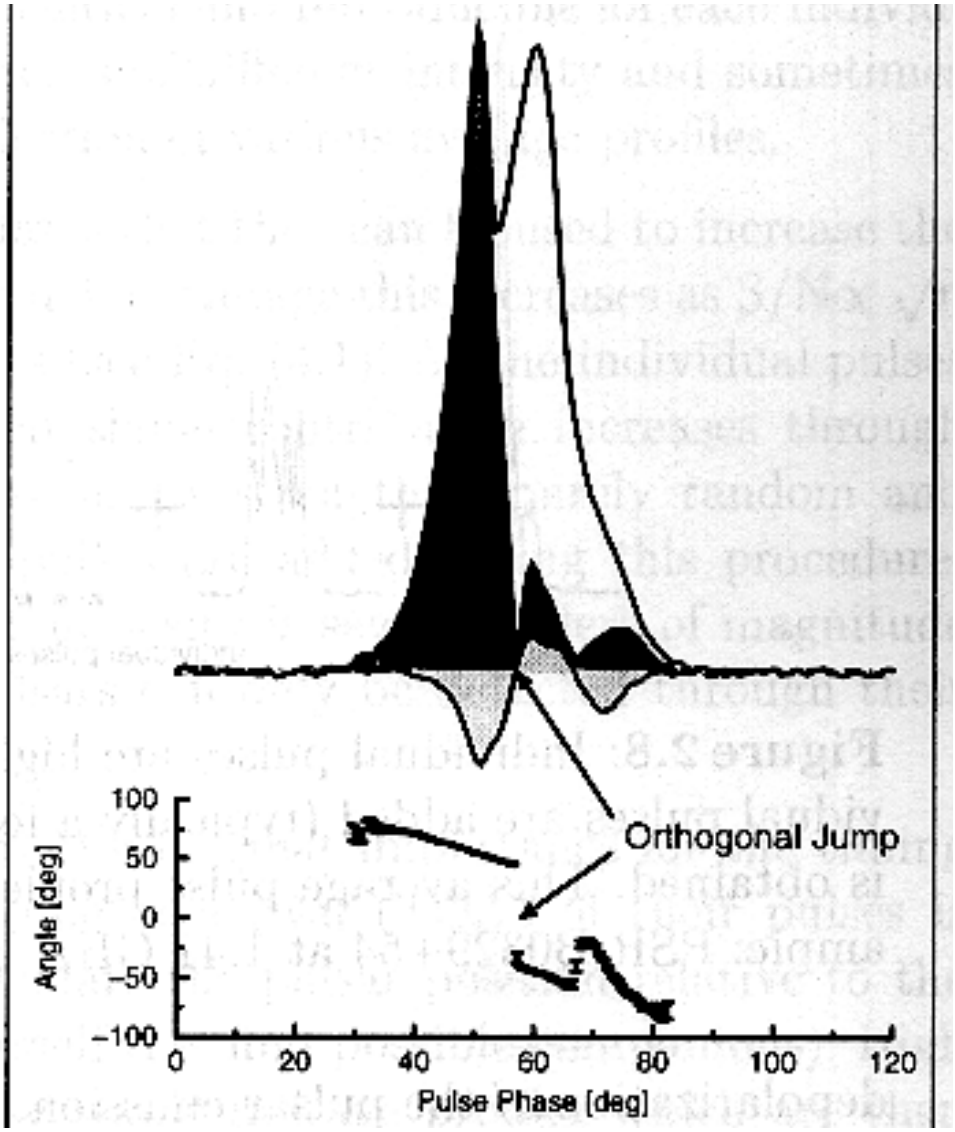

Figure 15: Orthogonal polarization mode (OPM). The reversal in the circular polarization aligns with such a phase jump.

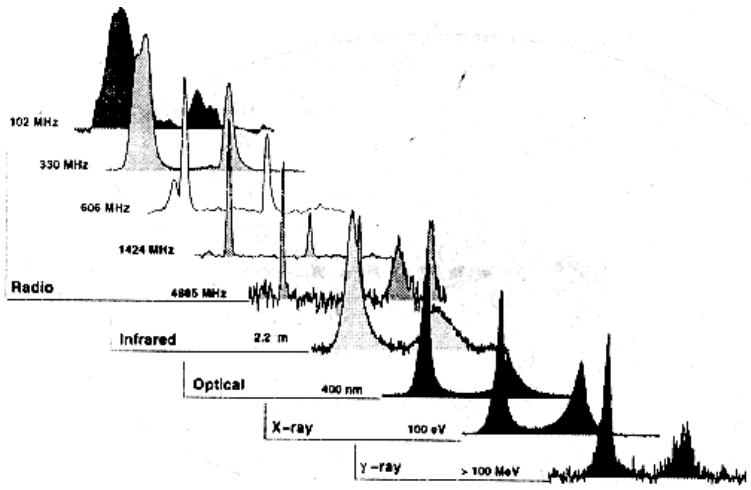

Figure 16: Pulse profiles of the Crab pulsar from low frequency radio emission to γ-rays. It can be seen that the profile width does not change significantly from radio to high-frequency emission.

0633+17 (Geminga), 1929+10 and 1055-52 (Becker & Trümper, 1997) but no pulsed emission has been resolved yet. The Crab pulsar has an optical efficiency of about 10^{-5} of the spindown luminosity, for the other examples mentioned, this fraction is considerably lower. We could show recently (Crusius *et al.*, 2001) that an outer gap model with copious pair production could explain the non-thermal emission from the optical to the X-rays via synchrotron emission. Details of our high-frequency emission model are described in chapter 6.

For obtaining more precise information on emission processes and other general features of pulsars' optical emission too few well-observed optical pulsars are known.

2.2.2 X-ray emission

X-ray pulsars are, of course, not observable from terrestial telescopes, as the high energetic radiation is absorbed by the Earth's atmosphere. So the first X-ray source, was traced by a detector launched in a rocket. Later the object was found to coincide with Sco X-1. Subsequent flights led to the discovery of the Crab pulsar or the corresponding supernova remnant as the brightest object on the X-ray sky (Bowyer *et al.*, 1964). Also many accreting neutron stars are visible in X-rays.

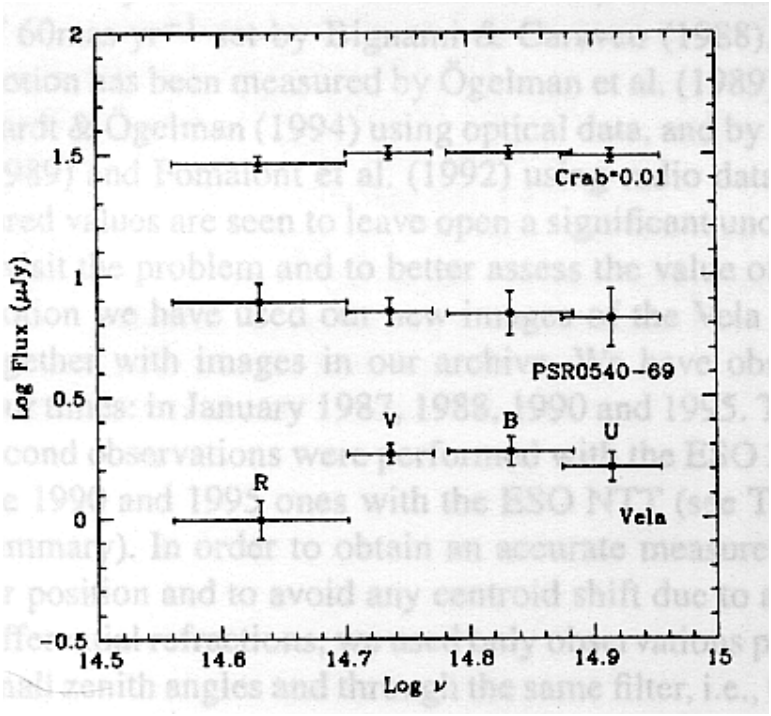

Figure 17: optical spectra of three pulsars (Nasuti *et al.*, 1997). For all examples (Crab, Vela and PSR 0540-69) the spectra appear to be almost flat.

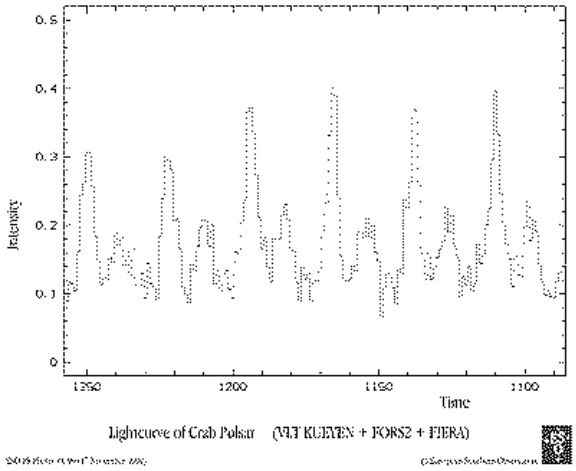

Figure 18: Individual optical pulses observed from the Crab pulsar by Mantel (2001)

Despite a number of subsequent missions of various satellites and atmospheric balloons, most of what we know about X-ray pulsars has been detected by ROSAT (Trümper, 1983), which was active between 1990 and 1998 and covered an energy range from 0.1 to 2.4 keV. The satellite ASCA, launched in 1993, allows observations up to 12 keV and thus provides a valuable extension of the ROSAT spectra towards higher energies (see fig. 19).

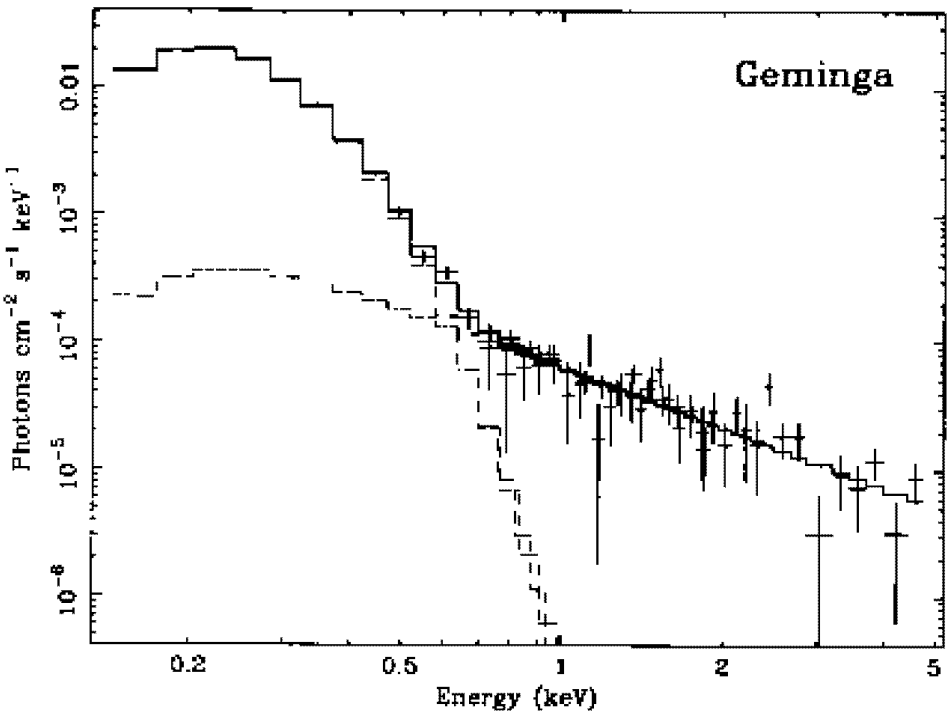

Figure 19: X-ray spectrum of Geminga taken from ROSAT and ASCA observations. The shape of the spectrum suggests a power law with a spectral index of around 1-2 for the high energies (above 1 keV) and a soft thermal component with a temperature of some $3 \cdot 10^6$ K.

Up to now, almost 40 X-ray pulsars have been identified, amongst them the youngest and most energetic, some middle-aged, and a number of millisecond pulsars (Becker & Trümper, 1997). Most of them are also radio emitters but there are a couple of radio quiet objects, emitting pulsed X-rays. Only three of them have been identified as neutron stars by fixing the pulse period and by positional coincidence with a supernova remnant.

These are Geminga (P = 295 ms), 1E 1207-5209 (P = 424 ms, Zavlin *et al.*, 2000) and the point source RX J0822-4300 in Puppis A (P = 75 ms, Pavlov *et al.*, 1999). Several other sources near supernova remnants have been detected but no pulsed emission has been found yet. These objects should also be visible in the radio band as their parameters are probably comparable to those of radio pulsars.

Another group of radio-quiet X-ray sources that are supposed to be neutron stars are the so-called anomalous X-ray pulsars. Their periods are in the range between 5 and 12 s whereas the spindown rate is as high as 10^{-11} typically. If the braking was only due to magnetic dipole braking this would imply field strengths of 10^{10} to 10^{12} T (so-called magnetars). This assumption is, however, not generally accepted.

Some very weak compact X-ray sources that do not coincide with a supernova remnant have been found. These objects are likely to be cooling neutron stars with a temperature of typically $7 \cdot 10^5$ K. The radiation of these objects is probably of thermal origin.

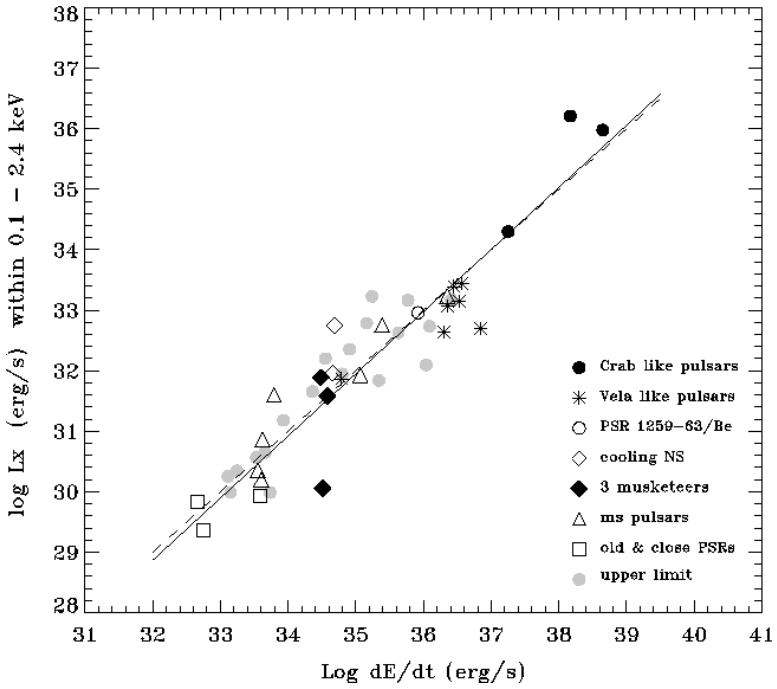

Figure 20: Pulsed X-ray luminosity (ROSAT band) vs. spindown power (Becker & Trümper, 1997). The data show a clear, almost linear correlation (the formal power law fit yields $L_{\rm X} \sim (-\dot{E}_{\rm rot})^{1.04}$).

Radio-loud X-ray pulsars can be classified as follows:

The young X-ray pulsars as Crab and 0540-69 typically show a strong power-law component with no detectable thermal contribution apart from the (unpulsed) cooling emission. A thermal component cannot be traced, maybe because the non-thermal X-ray flux is dominating even for soft X-rays. Moreover, the profiles of the radio and the X-ray pulses appear to be aligned.

The X-ray spectrum of a bit older ("Vela-like") pulsars, however, can usually be fitted by a pulsed soft thermal component (e.g. from a *hot spot*, maybe modified by the magnetic field and the pulsar's atmosphere (Zavlin *et al.*, 1995)) with a temperature of around 10^6 K (Page & Sarmiento, 1996) and a power law spectrum at the higher energies. As a consequence of the smaller spindown and the lower X-ray luminosity than for Crab-like pulsars the thermal component appears in the soft X-rays whereas the temperature is far too low to produce significant powers of harder thermal emission.

The X-ray spectrum of middle-aged pulsars is already dominated by thermal emission in the soft X-rays. This thermal component is still modified by the pulsar's hydrogen atmosphere and the strong magnetic field (Zavlin *et al.*, 1995). However, this group still shows a hard, non-thermal power law component (see fig. 19 for the prominent example Geminga[4]). The surface temperatures appear to be a little below those of Vela-like objects ($3 \cdot 10^5 \ldots 1.2 \cdot 10^6$ K) which is in accordance with the cooling models.

Also a few old nearby pulsars can be detected in X-rays. ROSAT and ASCA found high-energy emission from PSRs 1929+10, 0950+08 and 0823+26. The spectral and temporal resolution of these objects is still too poor to determine whether the emission is thermal or pulsed. Only PSR 1929+10, broad X-ray pulses have been found (Yancopoulos *et al.*, 1994). Becker & Trümper (1997) found that the spectrum could be reproduced both by a thermal as well as by a power-law fit.

For most millisecond X-ray pulsars only soft emission (around 1 keV) has been found apart from PSR 1821-24 which has been detected up to 17 keV.

Among the pulsed X-ray sources there is an almost linear correlation between X-ray and spindown luminosity (Becker & Trümper, 1997) as the X-ray efficiency is close to 10^{-3} for all known examples (see fig. 20). This correlation is a clear hint to a strong connection between X-ray emission and loss of rotational energy.

[4]Of course, Geminga is radio-quiet but its parameters very alike those of radio pulsars, so it is sorted into this group.

The new missions Chandra and XMM Newton will provide us with better data, and maybe give some new insight on the processes responsible for the X-ray emission.

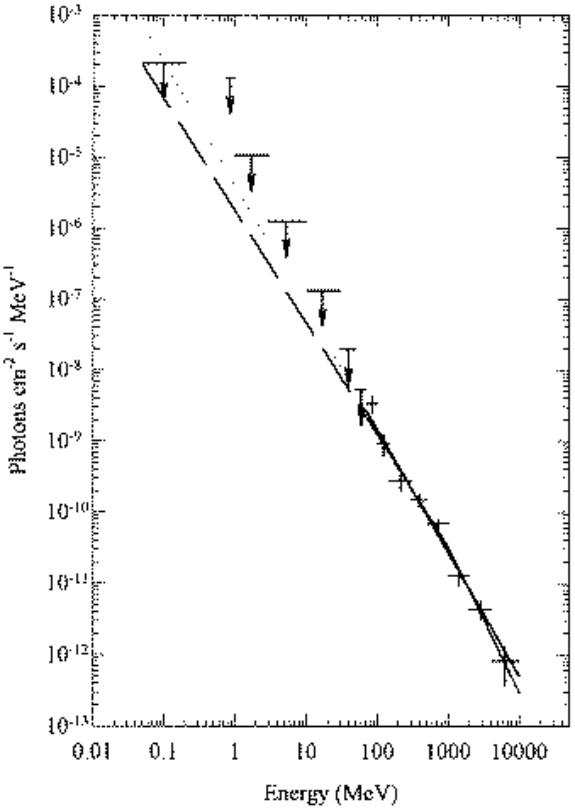

Figure 21: Observation in γ-rays from PSR 1055-52 (from Thompson *et al.* (1999))

2.2.3 γ- emission

Even very high energy emission has been detected in pulsars. For various reasons, however, the data are not very detailed. Only seven pulsars show γ- emission and some of them are only "detected" by positional coincidence as the low fluxes allow only a poor spatial and temporal resolution. At least the rather flat power law seems to extend to the GeV range (see fig. 21) leading to a considerable efficiency of γ-emission which can be up to about 10% of the spindown luminosity. The γ-emitters are exclusively young and

middle-aged pulsars whose efficiency even seems to increase with age (the data suggest a correlation $L_\gamma \sim \dot{E}^{1/2}$). But this might be a selection effect as the spindown luminosity declines with increasing age, so less efficient older γ- emitters cannot be detected any more.

γ- pulsars can typically be observed up to GeV energies, from the Crab pulsar even TeV emission has been detected. For the very high energies, however, it is not sure whether the emission is magnetospheric (pulsed) or created in the wind and therefore unpulsed, or at least not fluctuating with the rotation period. Nevertheless it is a clear indicator that, somewhere in the pulsar system, particles must be accelerated to TeV (corresponding to a Lorentz factor of more than 10^6 for electrons). This means that at least young pulsars can produce ultra-relativistic particles at a place where energy can be converted into escaping radiation. Thus the high frequency emission provides additional restrictions to models of the pulsar magnetosphere.

We next discuss widely accepted models for radio emission, as this frequency band allows the most detailed observations. Several theoretical models proposed mechanisms how the large rotation-induced voltage can be transferred into particle energy and subsequently into highly coherent low-frequency radiation. This is particularly interesting as it is not self-evident why a potential of 10^{13} V can produce particles which radiate coherently at photon energies of μeV. However, the GJ solution would prevent any acceleration and therefore must be violated somewhere to produce radiating particles at all. So candidates for acceleration regions had to be proposed. Additionally the models lead us to the first attempts of explaining pulsar radio emission in the framework of the GJ description. One of the early ideas subsists to this day and is the basis of most modern theoretical work on pulsars.

"How do you know, that I'm mad?", asked Alice.
"You must be mad", said the Cat,
"or you wouldn't have come here."
Lewis Carroll, *Alice in Wonderland*

3 Radio emission models

3.1 Inner gap models

In this section we discuss some widespread models of the magnetosphere which assume an acceleration region, close to the neutron star surface, that is shortened by copious pair production. There are four basically different types of inner gap/ pair cascade models.

3.1.1 Ruderman-Sutherland model ("starved magnetosphere")

The first (and most natural) model containing an inner gap was proposed by Sturrock (1971) and elaborated more precisely a few years later with a more likely boundary condition (Ruderman & Sutherland, 1975). Here the basic ideas of that model (henceforth RS model) are outlined, and a schematic view is given in fig. 22.

Radio pulsars are assumed to be almost antiparallel rotators meaning that $\vec{\Omega}$ and $\vec{B}$ make an angle of almost $180^{\,o}$. In this case the GJ charge density above the polar cap has a positive sign. Now, if the binding energy of ions is considerably higher that that of the electrons, it is possible that electrons may flow freely from the surface, whereas ions cannot. Therefore the neutron star cannot supply the magnetosphere with positively charged particles which means that, close to the polar cap, the density will be far below the GJ value. This is called a "starved magnetosphere".

In this region any charged particle would be quickly accelerated, in one or the other direction, by an almost unshielded vacuum field, and therefore reach highly relativistic energies. RS consider a mechanism called single photon pair production, a purely quantum mechanic effect that occurs only in very strong magnetic fields. The important quantities for this process are the perpendicular magnetic field (meaning the component normal to the photon's momentum) and the photon energy. The process only works effectively if the former is comparable to the critical magnetic field $B_{\rm crit}$ (see below), or the latter vastly exceeds the electron rest energy. Thus a high energetic photon that moves under a large angle to the magnetic field can

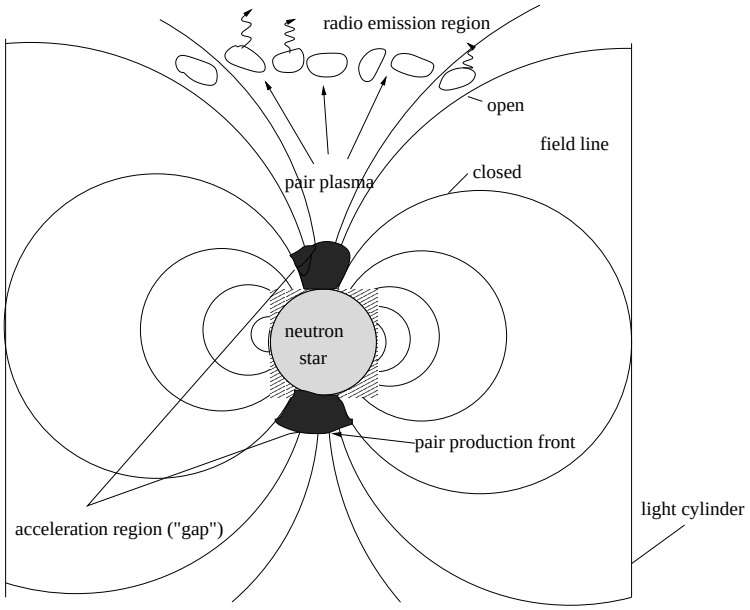

Figure 22: Schematic picture of the Ruderman/Sutherland model. In the inner gap just above the polar cap a significant fraction of the total voltage is dissipated and a dense pair plasma with about 10^4 secondaries per primary particle flows out. Energetic primary particles emit hard curvature radiation which is supposed to initiate the particle-production avalanche.

be absorbed by the latter, and materialize into an electron- positron pair, schematically:

$$\gamma + B \longrightarrow e^+ + e^- + B\,. \tag{14}$$

The magnetic field absorbs the momentum, which makes this process possible even in the absence of another particle (in vacuum the process is impossible, since it would violate momentum conservation).

Single photon pair production has been carefully studied theoretically. The crucial parameter for the efficiency is the product of the normalized magnetic field, perpendicular to the photon momentum, and the normalized photon energy. If its value is far below unity (which is the case in most inner gap models), the loss length can be expressed by an approximation given by Erber (1966):

$$l_{\rm loss} = \frac{4.4}{\alpha_{\rm FS}} \frac{\lambda_{\rm C}}{2\pi} \left(\frac{B_\perp}{B_{\rm crit}} \right)^{-1} {\rm e}^{4/(3\chi)} \tag{15}$$

where $\lambda_{\rm C} = \hbar/(m_{\rm e}c)$ is the Compton wavelength of the electron, $\alpha_{\rm FS} = 1/137.037$ denotes the fine structure constant and $B_{\rm crit} = (m_{\rm e}^2 c^2)/(e\hbar) = 4.414 \cdot 10^9$ T is the critical magnetic field.

$$\chi = \frac{B_\perp}{B_{\rm crit}} \frac{\hbar\omega}{m_{\rm e}c^2} \tag{16}$$

is the dimensionless strength parameter on which the efficiency of the process strongly depends.

The initiating process of the gap closure (producing a pair by converting a γ-photon coming from the outer regions of the magnetosphere) makes no difficulties, since the pitch angle is likely to be quite large (that means $B_\perp$ and B are comparable). Therefore a GeV photon will suffice.

RS argue further that these primary particles will be accelerated to ultrarelativistic energies by the parallel electric field, and emit energetic curvature radiation as they travel along the curved field lines. But due to the relativistic lighthouse effect, the initial pitch angle is close to zero. Since the path of the photon is unaffected by the magnetic field, however, the pitch angle increases as the photon travels outwards, due to the dipolar geometry. At some place the pitch angle becomes large enough to make another photon splitting possible. Ruderman & Sutherland (1975) assume that a value of about $\chi = 0.15$ is enough to initiate the pair avalanche. But since in most pulsars $B_0 \ll B_{\rm crit}$ and always $B_\perp \ll B_{\rm crit}$, especially in slow pulsars, maybe only $\chi = 0.05$ might be reached for a RS-type gap, which means no pair cascade at all.

The so-called *secondary particles* are now likely to have large pitch angles, meaning they can emit hard synchrotron emission almost perpendicular to the magnetic field, apart from being accelerated along $\vec{B}$ as well. So a cascade develops, until all accelerating fields are shortened by the affluence of charged particles. The density of this pair plasma is believed to exceed the GJ value by a factor of about 10^4. This plasma will flow outwards, and the whole process starts again.

A quantitative description of the RS model is as follows:

The potential difference available is taken to be the full voltage between the pole and the edge of the polar cap. For the (anti-)parallel rotator its value is

$$\Delta V = \frac{\Omega^2 r_{\rm NS}^3 B_0}{2c} = 6.6 \cdot 10^{12}{\rm V} \left(\frac{P}{\rm s}\right)^{-2} B_8 \tag{17}$$

where B_8 is the dipolar magnetic field at the pulsar surface in units of 10^8 T.

This potential difference allows particle Lorentz factors of about 10^7. Such particles emit curvature radiation with a characteristic frequency at

$$\nu = \frac{3}{4\pi}\frac{c}{R_{\rm C}}\gamma^3 \,. \tag{18}$$

The curvature radius $R_{\rm C}$ for a purely dipolar field can be approximated by

$$R_{\rm C} = \frac{4}{3}\frac{r_{\rm NS}x^{1/2}}{\sin\theta_{\rm cap}} \approx 6.5\cdot 10^5 {\rm m}\left(\frac{P}{\rm s}\right)^{-1/2} x^{1/2} \tag{19}$$

for a field line at the edge of the polar cap. The value taken in the RS model is much smaller than the dipole result (19). This is because the standard model assumes small-scale multipole components, close to the surface, that do not affect the gross structure of the magnetosphere, but significantly reduce the local radius of curvature. The multipoles (or an off-centered dipole, which would enhance the magnetic field strength on the surface) are necessary to obtain large enough values for χ. Having the purely dipolar magnetic field placed in the neutron star centre alone, most pulsars would not be able to initiate a pair avalanche as described in the RS model.

If the pair density exceeds the GJ density by a factor of M, or roughly $n_{\rm sec} = Mn_{\rm GJ} \approx Mn_{\rm prim}$ when the cascade terminates, the typical Lorentz factor can be roughly estimated by

$$\gamma_{\rm sec} = \frac{\gamma_{\rm prim}}{M} \tag{20}$$

as a function of the primary Lorentz factor. This handy formula is valid if the energy of primary particles is fully converted into secondary pairs, and the primary density is equal to $n_{\rm GJ}$. In reality, (20) is an overestimation because on the one hand a certain percentage of the energy will be lost into escaping radiation, furthermore the primary density must be smaller than the GJ value because otherwise there would be no acceleration, and thus the multiplication factor exceeds M as defined above.

The non-stationary discharge means a "sparking", i.e. dense plasma clouds separated by voids, which naturally provide the bunches needed for coherent radio emission. In this environment, curvature radiation hits the radio band if the emission height x in (19) is about 100 and γ is a few hundreds.

3.1.2 The Arons model (slot gaps)

Arons & Scharlemann (1979) proposed another idea of how particle acceleration close to the neutron star can be possible. The authors assume a nearly parallel rotator which can supply enough particles (here electrons) to reach the GJ density right above the surface. They then consider a slightly oblique rotator (see fig. 23). In (7) the (parallel) GJ density is modified by a cosine factor which depends on the azimuthal angle. For an oblique rotator there are two types of field lines: on one half the geometric correction factor rises when one moves outwards along the field line (in Arons & Scharlemann (1979) they are called "favourably curved"), whereas on the other type the situation is vice versa. On such "unfavourably curved" field lines no radio emission would be possible. A relativistic plasma element with GJ- density moving along a favourably curved field line becomes underdense further outwards. This means that the accelerating fields are not perfectly shielded any more, and acceleration is possible. A more detailed discussion of these effects can be found in section 6.

For a purely dipolar geometry Arons & Scharlemann (1979) find

$$\Delta V = 3.58 \cdot 10^{10}\mathrm{V} \left(\frac{P}{\mathrm{s}}\right)^{-5/2} B_8(x-1) \tag{21}$$

with $x - 1 \ll 1$ being the extension of the gap in units of pulsar radii.

Due to the strong dependence of the rotational period voltages sufficient to initiate a pair cascade (analog to the RS model) are reached only for periods well below one second or for high multipole components near the surface (Beskin (1999) gives a limit of about 0.1 to 0.3 s). Especially for the newly discovered 8.5 s pulsar J2144-3933 (Young *et al.*, 1999), dominating small scale multipole components or an extremely off-centered dipole (the dipolar centre must be only about 1 km below one polar cap) are required to make the model work (Arons, 2000).

The Arons model could still be valid even for slow, old pulsars, if one considers inverse Compton scattering (ICS) instead of curvature radiation, as the former can produce harder photons from the same particle energy. Additionally, effects of General Relativity (GR) (Muslimov & Tsygan, 1992), alter the GJ-density profile and make all field lines "favourably" curved close to the surface (Zhang *et al.*, 2000).

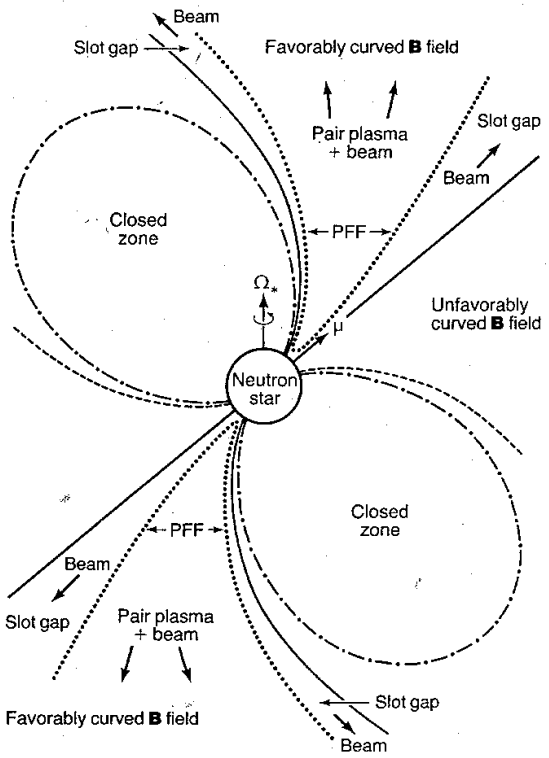

Figure 23: Slot gap model for an inclined rotator. In this model radio emission is expected only from "favourably curved" field lines, as only field lines curved towards the axis allow an underdensity of charges, and can therefore have accelerating fields. The model was proposed by Arons and his group (Arons & Scharlemann (1979)).

3.1.3 The Shibata model

In Shibata (1997), Shibata *et al.* (1998) a third inner gap idea is described. Similar to the Arons model it also uses the geometric effect of field line curvature in an oblique rotator. But in contrast to the former, Shibata assumes a fixed current flowing off the surface (which is necessarily a little below the relativistic GJ current $j_{\rm GJ} = n_{\rm GJ}ec$). Provided $j(r)r^3/n_{\rm GJ}(r_{\rm NS}) = const.$ on the field lines bending away from the rotation axis (the "unfavourably curved" ones in the Arons model), the density has to drop, which can only be achieved by accelerating the particles.

As the velocity of the electrons is limited by c, sooner or later the GJ

density has dropped so far that, even for particles moving with the speed of light there would still be an overdensity. That means the particle energy would grow exponentially until the pair cascade sets in and shields the accelerating fields. But even this requires a fairly high pair multiplicity of at least 10^6 or even more.

On the "towards" field lines the necessary density increase can easily be obtained by slowing down the particles to subrelativistic velocities. The simulations show that, on these field lines, damped oscillating solutions will occur (Shibata, 1997).

3.1.4 The model of Michel (inertia acceleration)

Michel (1974) and Fawley *et al.* (1977) have analyzed effects caused by the finite particle mass. This means that a particle gaining energy is accelerated or, in other words, its velocity is always below c. Neglecting field-line-curvature (i.e. the monopole case) one can find a self-consistent solution from the boundary condition that the particle energy rises asymptotically to a maximum value. Let the maximum Lorentz factor be γ_0, with the corresponding normalized velocity, $\beta_0 < 1$. The two boundary conditions that have to be fulfilled for large distances are $\mathrm{d}\gamma/\mathrm{d}r = \mathrm{d}^2\gamma/\mathrm{d}r^2 = 0$. The first means a vanishing parallel electric field for the maximum velocity, whereas the second guarantees the asymptotic solution.

The one-dimensional case has been studied by Michel (1974). In this case the transverse variation scales of the potential are assumed to be much larger than the parallel extension.

For a current density of j_0 the corresponding density of the surplus charge proves to be

$$\rho - \rho_{\mathrm{GJ}} = (\beta_1 - \beta)\, j_0 / (\beta\beta_0 c) \tag{22}$$

with $\beta_1 = j_0/(n_{\mathrm{GJ}} e c) < \beta_0$ being the velocity where the $\mathrm{d}^2\gamma/\mathrm{d}s^2$ changes sign. (There is an error in Michel (1974) as he sets $\beta_1 = \beta_0$ and uses the wrong form for the Laplacian in the expression after his eq. (3). The fact that $\beta_1 < \beta_0$ can easily be understood as the second dervative of γ has to change its sign twice. A correct discussion of the one-dimensional case can be found in Fawley *et al.* (1997)). This result can be inserted into the Poisson equation

$$\frac{1}{r^2}\frac{\mathrm{d}}{\mathrm{d}r}\left(r^2\frac{\mathrm{d}\phi}{\mathrm{d}r}\right) - \frac{2\phi}{r^2} = -g \tag{23}$$

where ϕ is the electric potential and

$$g(r) = \frac{\rho(r)}{\varepsilon_0 \cos\theta} \tag{24}$$

in spherical coordinates.

Solving the Poisson equation for the extreme relativistic limit and under the assumption that the region of most effective acceleration is narrow, Michel (1974) finds a maximum Lorentz factor of about

$$\gamma_0 = \sqrt{2\sigma} \tag{25}$$

where

$$\sigma = \frac{eB\Omega r_{\rm NS}^2}{m_{\rm e}c^2}. \tag{26}$$

The two-dimensional case is discussed in Fawley *et al.* (1977). It includes a finite perpendicular variation scale K^{-1} which adds one more term $\nabla_\perp^2 \Phi \approx -K^2\Phi$ to Poisson's equation. The main difference is that the current density must be slightly *higher* than the relativistic GJ-value in contrast to the one dimensional case where both the asymptotic values for β and $n/n_{\rm GJ}$ are below 1.

Inserting typical pulsar parameters, one finds that the resulting particle energies are around 10^4 for normal pulsars and some 10^5 even for the Crab pulsar. This means that in this scenario no pair cascade, like in the other inner gap models, is possible. But then the question is, what radio emission mechanism would apply in this model since neither the classical curvature radiation description nor a plasma instability is applicable.

3.2 Outer gap models

The first outer gap model was proposed soon after the inner gap idea by Cheng *et al.* (1976), Cheng & Ruderman (1977). However, the currently discussed idea is that the neutral line plays an important role for the acceleration. The basic principle was shown by Cheng *et al.* (1986) for an almost antiparallel rotator.

Within the framework of the RS model there are two types of open field lines. One type lies entirely in the positive region, whereas the other crosses the neutral surface to extend into the region of negative GJ charge. The latter is the one sort which is supposed to be responsible for the outer gap.

On the outside of the neutral surface (a negative region), the electrons can flow freely across the light cylinder and leave a partial void, which acts

like a positive space charge, as the shielding charge density is negative. This space charge repels positrons approaching the neutral surface from inside, so that the plasma density in the vicinity of this separation line will be very small. The basic principle of the outer gap model is depicted in figs. 24 and 25.

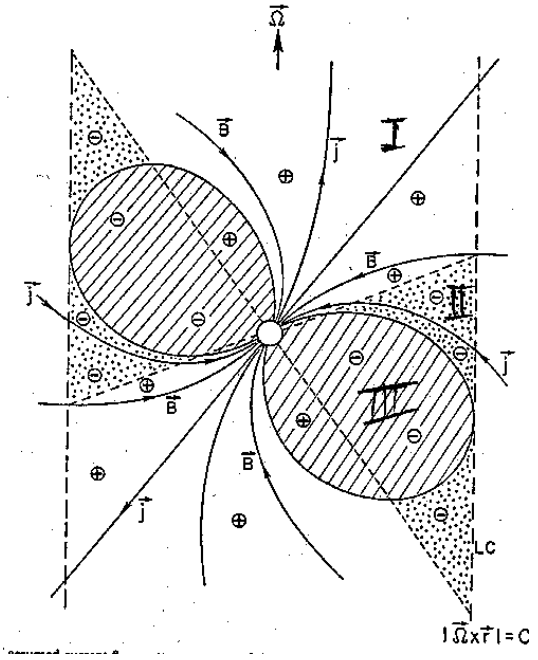

Figure 24: Sketch of the almost anti-aligned pulsar with the flowing currents and the development of the outer gap near the neutral line (taken from Cheng *et al.*, 1986). The three indicated regions are the open field lines that do not cross the neutral line (I), the proposed outer gap region (II) and the closed field lines (III).

The depletion zone will grow until it is large enough to allow a sparking as in the RS model, meaning the gap is closed by copious pair-production. Of course, in outer gaps, single photon pair-production is no longer possible as the magnetic field strength is much too small. But processes like $\gamma - \gamma$ interaction or $e - \gamma$ collisions - so-called *triple electron pair production* (Mastichiadis *et al.*, 1986) - could be sufficiently effective to start a pair cascade. To show this we roughly compute the energy loss of a highly relativistic particle due to the second effect using fig. 10 from Mastichiadis *et al.* (1986). The quantity

$$L := -\mathrm{d}E/(m_\mathrm{e}c^2\,\mathrm{d}t)\cdot 1/(n_\gamma c) \tag{27}$$

as defined in Mastichiadis *et al.* (1986) reaches about $10^{-21}\,\mathrm{cm}^2 = 10^{-25}\,\mathrm{m}^2$ for a Lorentz factor of 10^6 and does not depend strongly on the photon energy.

The thermal photon density can be roughly estimated by dividing the total blackbody radiation from the hot neutron star by the mean photon energy and considering the spatial angle at which the neutron star appears. This yields

$$cn_\gamma = \sigma_\mathrm{SB}T^4x^{-2}\,(k_\mathrm{B}T)^{-1} = 4.11\cdot 10^{33}\,\mathrm{m}^{-2}\mathrm{s}^{-1}\,T_6^3x^{-2} \tag{28}$$

where σ_SB is the Stefan-Boltzmann constant and T_6 denotes the neutron star surface temperature.

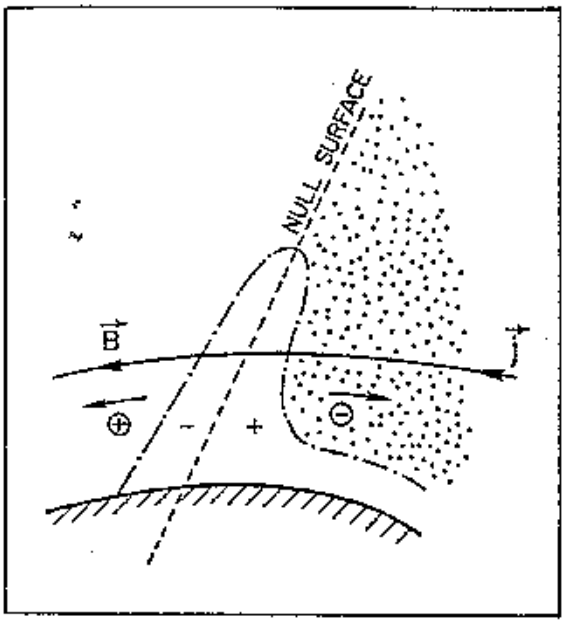

Figure 25: Detailed view of the vicinity of the neutral line (taken from Cheng *et al.*, 1986). The electrons drift out towards the light cylinder, whereas positrons from inside are repelled by the positive charge that builds up through the lack of electrons. So the gap grows until it is filled by the pair production sparking.

Inserting all numbers we find a loss rate of

$$\frac{\mathrm{d}\gamma}{\mathrm{d}t} = 1.10 \cdot 10^3 \,\mathrm{s}^{-1} \left(\frac{x}{1500}\right)^{-2} T_6^3 \tag{29}$$

for $\gamma = 10^6$.

This means that especially for quickly spinning (x small) or hot pulsars the process is quite efficient. The actual loss rate will be even higher, as the photon density increases, once the process is started, because of synchrotron and curvature radiation.

Cheng *et al.* (1986) find a typical maximum voltage of $2 \cdot 10^{15}$ V for a narrow gap (ratio of width and length of 0.1) and Crab-like parameters. This voltage is reached along the central field line of the gap and drops towards its boundaries in a parabolic shape for the rectilinear approximation (neglecting field line curvature), when the cylindrical boundary is taken to be an equipotential.

Hirotani & Shibata (1998a, 1998b) modelled a self-consistent outer gap with the current density as a free parameter. Balancing acceleration by the electric field with losses due to curvature radiation for currents between 0.01 and 0.2 of the GJ current $j_{\mathrm{GJ}} := n_{\mathrm{GJ}} ec$, they find terminal Lorentz factors of a few 10^7, which are sufficient to initiate a pair cascade by the processes mentioned above. This cascade is consistent with observations, since in the Crab nebula a plasma wind is observed whose density is much higher than a pure GJ flow would provide. Rough estimates of the wind density can be obtained via the X-ray luminosity of the wind as the magnetic field in the wind zone is known and therefore the particle energy and the single-particle synchrotron luminosity can be derived. If the nebula is fed only by particles the number of outflowing particles in the Crab pulsar must exceed the Goldreich-Julian flux by a factor of 10^4 (Arons, 1983). This number arises from the assumption that almost all of the pulsar's spindown power is fed into the nebula (even the γ- fluxes observed are only up to 10% of the loss of rotational energy) and an estimate on average particle energies. These can be fixed fairly well from synchrotron X-ray emission from the wind. The total particle flux into the wind in units of the GJ flux reads

$$\dot{N} = 2A_{\mathrm{cap}} n_{\mathrm{GJ}} cM = 2.7 \cdot 10^{30} \,\mathrm{s}^{-1} \, M \left(\frac{P}{\mathrm{s}}\right)^{-2} B_8 \,. \tag{30}$$

Together with the total spindown power given in eq. (1) we then find an energy per particle of

$$E_{\mathrm{wind}} = 1.4 \cdot 10^{-6} \,\mathrm{J} \left(\frac{P}{\mathrm{s}}\right)^{-2} B_8 M^{-1} \tag{31}$$

which corresponds to a Lorentz factor of

$$\gamma_{\rm wind} = \frac{E_{\rm wind}}{m_{\rm e}c^2} = 1.7 \cdot 10^7 \left(\frac{P}{\rm s}\right)^{-2} B_8 M^{-1} \,. \tag{32}$$

As the X-ray emission in the wind suggests only Lorentz factors of a few 1000, we need to have $M \gg 1$ in any case, especially for the young, energetic pulsars.

A clear advantage of outer gap models is that they explain in a natural way why the light curves of a pulsar look quite different in radio and high frequency ranges, in the sense that high energy profiles tend to be broader. There are a few exceptions such as the Crab pulsar, where this profile broadening does not show very clearly (see fig. 16). This might be a geometric effect, as the Crab is an almost orthogonal rotator. Additionally the phases at radio and high frequency emission are usually non-aligned as shown (fig. 16).

Chiang & Romani (1994), Yadigaroglu & Romani (1995), Romani (1996) have modelled the light curves and spectra in the γ-range in the framework of an outer gap model, and find them to be consistent with observational results. Concerning the mechanism responsible for the high frequency radiation, we could show that small and large pitch angle synchrotron radiation can explain the complete spectra, and the energetics of the emission above the infrared, for the Crab pulsar (Crusius *et al.*, 2001). For the calculations we used an outer gap model of the Cheng *et al.* (1986) type. To obtain the correct luminosities the idea requires an efficient pair cascade, with a density exceeding the GJ value by about 10^4 which is consistent with the observationally deduced wind density from Chandra X-ray observations (Weisskopf *et al.*, 1999).

3.3 A critical discussion of inner gap models

3.3.1 Surface particle emission and polar gaps

Though the original RS model was formulated for an antiparallel rotator, it could also be applied to the parallel case. For an almost *parallel* rotator, however, RS models can work only as long as the binding energy for electrons is high enough to prevent sufficient electron emission from the surface. Particles are drawn from the surface by several well-studied effects. We have shown that thermal and field emission of electrons can usually shield the field on the surface completely (Jessner *et al.*, 2001). Our arguments will be briefly discussed in the following:

The relevant fundamental surface emission processes are accepted to be field and thermal emission. Thermal emission was detected by Edison (1884) and studied quantitatively by Dushman (1930). Fowler & Northeim (1928) performed detailed calculations on field emission from metal surfaces. Their results have been confirmed by many experiments.

Both processes are strongly dependent on the binding energy E_{W}. Field emission furthermore depends on the Fermi energy E_{F}, which in turn can be estimated from the density on the pulsar surface:

$$E_{\mathrm{F}}(\rho) = \frac{2\pi^4\hbar^4c^2}{e^2B_0^2m_{\mathrm{e}}}\left(\frac{\rho Z}{Am_{\mathrm{p}}}\right)^2 . \tag{33}$$

Here Z and A denote the element number and the atomic mass number respectively. Using a Thomas-Fermi-Dirac-Weizsäcker approximation, Abrahams & Shapiro (1991) estimated the mass density for iron in the cold limit to be $2.9 \cdot 10^6 \mathrm{kg\,m^{-3}}$. Inserting the values for iron, $A = 56$, $Z = 26$ and a typical surface magnetic field $B = 10^8$ T, the Fermi energy evaluates to 417 eV. As a first approximation we can use $E_{\mathrm{W}} = E_{\mathrm{F}}$.

For a relativistic flow of electrons from a cold cathode, a number density of

$$n_{\mathrm{field}}(E_0) = \frac{e^2}{2\pi\hbar c}\sqrt{\frac{E_{\mathrm{W}}}{E_{\mathrm{F}}}}\frac{E_0^2}{E_{\mathrm{W}}+E_{\mathrm{F}}}\exp\left(-\frac{4\sqrt{2m_{\mathrm{e}}}E_{\mathrm{W}}^{3/2}}{3\hbar eE_0}\right) \tag{34}$$

is found in Fowler & Northeim (1928) where E_0 is the electric field.

The other effect, which is even more important, is a purely classical one. Thermal surface emission occurs because, due to the energy distribution function, there is always a fraction of particles whose energies exceed the binding energy.

The number density of electrons emitted from a hot metallic surface in the presence of an electric field is given by the Dushman equation (Dushman, 1930)

$$n_{\mathrm{DS}}(T, E_0) = \frac{m_{\mathrm{e}}k_{\mathrm{B}}^2}{2\pi^2c\hbar^3}T^2\exp\left(-\frac{E_{\mathrm{W}}}{k_{\mathrm{B}}T}+\frac{e}{k_{\mathrm{B}}T}\sqrt{\frac{eE_0}{4\pi\varepsilon_0}}\right) \tag{35}$$

with the Boltzmann constant k_{B}.

As can be seen from figure 26, both effects can easily supply the GJ density, apart from (unrealistic) cases where the binding energy is extremely high, and both temperature and electric field are very small.

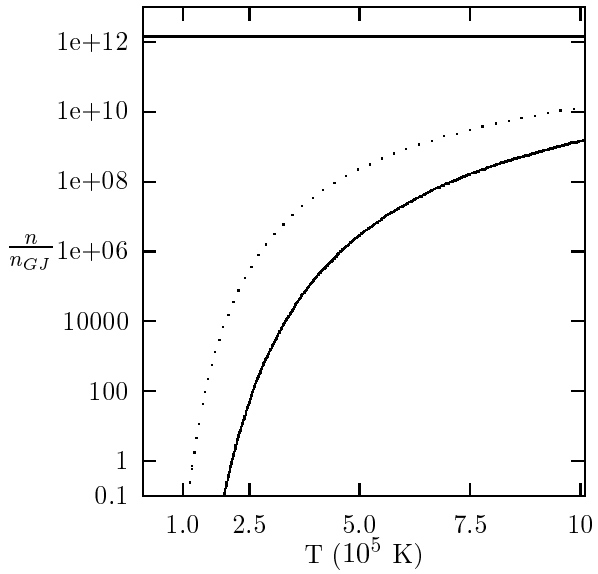

Figure 26: Electron densities by thermal and field emission compared to the GJ density for an electron binding energy of 417 eV. Thin solid line: thermal emission, dots: thermal emission with the Schottky effect, thick solid line: cold cathode emission.

The ion binding energy appears to be similar to those of the electrons Abrahams & Shapiro (1991). So we can conclude that the RS model is very unlikely to be applicable for pulsars in its present form, unless the estimates for $E_{\rm W}$ are significantly wrong.

3.3.2 Further criticisms on existing gap models

The three inner gap models with a pair cascade all suffer from various other difficulties. First of all, each of them uses some doubtful assumptions which are discussed in the following.

The classical RS model requires an antiparallel rotator. On the one hand in the meantime, pulsars with either positive or negative sign of $\vec{\Omega} \cdot \vec{B}$ have been found, so that the binding energy argument mentioned above applies. Furthermore, it is even doubtful if the binding energy of ions is large enough to maintain a RS gap in an antiparallel rotator.

Apart from that, the existence of sufficiently strong small-scale high multipoles is not sure, and in a purely dipolar geometry the pair cascade is only possible for very energetic pulsars. Multipoles are necessary to produce small

curvature radii and stronger magnetic fields, both allowing harder curvature photons and larger pitch angles between the photons and the magnetic field lines. As these multipoles do not contribute to the magnetic field in the emission region, they cannot be detected observationally. Therefore there is no independent strong argument for small scale multipole structures.

Even with the inclusion of GR effects (Muslimov & Tsygan, 1992), the death line would not be altered significantly. An alternative mechanism for the production of seed photons for the cascade would be inverse Compton scattering of thermal photons and ultrarelativistic particles, which would ease the constraints on the field topology. But this mechanism predicts "death lines" that run through the middle of the pulsar population in the $P - \dot{P}$ diagram, which would mean two different groups of pulsars that do not show an observable difference (Zhang *et al.*, 2000).

The Arons model can only work for rapidly rotating pulsars, due to the strong dependence of the voltage of the period. Beskin (2000) gives a maximum period of a few tenths of a second. The classical slot gap idea is also in contradiction to observations, finding radio emission from both "favourably" and "unfavourably" curved field lines (Lyne & Manchester, 1988). The latter problem is solved by including effects of General Relativity, which make every field line a "favourably curved" one close to the neutron star. Nevertheless the energetic problem remains, since the voltages in the Arons model are significantly below the RS values, apart from quick rotators, even with GR effects included.

The main weakness of the Shibata model is that the back reaction of overdense regions on the current flow is neglected. So it is more likely that on these field lines there will be no exponential rise of the particles' energy but a quenching which reduces the current density flowing off the surface. Thus it is doubtful if one can really set the conditions so that stationary acceleration in overdense regions becomes possible.

Besides these particular problems there are several further arguments making the pair cascade scenario in an inner gap unlikely. First of all, there are electrodynamic reasons. If there is copious pair-production at some time, why do the (low-energetic) particles flow out, and leave a gap with such high field strength? One would rather expect that, at most, a more or less stationary gap with a very low voltage would develop. Also in laboratory experiments vacuum gaps only occur on small spatial scales comparable to the Debye length so that they can be interpreted as strong plasma waves. Such waves, however, could only accelerate particles to ultra-relativistic energies in a resonant case. However, none of the existing inner gap models has treated the problem of backflowing positrons and their effect

self-consistently. Just assuming that the particles of the "wrong" charge flow back and hit the surface, leads to lots of problems with charge neutrality of the neutron star unless it is clear how this huge current is closed in the outer magnetosphere. Additionally, too many backflowing particles would heat the polar cap to a temperature exceeding the upper limits derived from the soft X-ray flux. Arons (1983) finds a polar cap temperature of 400 eV (around $4.5 \cdot 10^6$ K) for the Vela pulsar due to heating of backflowing positrons in a RS scenario (his eq. (16)). Also for slower pulsars the "hot spot" would not be significantly cooler (the temperature scales only with $T \sim P^{-2/7}$ for the RS case). But the thermal soft X-ray emission found from Vela suggests a temperature of only about $1 \cdot 10^6$ K (Page & Sarmiento, 1996). So either the backflow of secondaries must be considerably smaller, an additional cooling mechanism would be required or a pair cascade does not fit the observational results.

Another crucial point is the question of how the angular momentum transfer needed for the spindown of the neutron star is possible. The ratio of spindown power and loss of angular momentum is simply

$$\frac{\dot{E}_{\rm rot}}{\dot{L}} = \frac{I\Omega\dot{\Omega}}{I\dot{\Omega}} = \Omega \tag{36}$$

So the mean distance, where energy must be radiated away to fulfill both energy and momentum conservation, evaluates as:

$$\bar{R} = \frac{\dot{L}c}{\dot{E}_{\rm rot}\beta_\perp} = \frac{c}{\Omega\beta_\perp} = \frac{r_{\rm LC}}{\beta_\perp} \tag{37}$$

where $\beta_\perp$ is the velocity component of the particle in the direction of the rotation velocity. (37) shows that even massless particles (photons or ultrarelativistic electrons) must decouple from the pulsar system close to the light cylinder. So if there was an efficient dissipation region in the inner magnetosphere in compensation for it, significant losses must occur beyond the light cylinder. For outer gap models, this problem is eased considerably, since they predict the main losses to occur in the outer regions anyway.

Finally we have shown (Kunzl *et al.*, 1998a) that if some plasma process is responsible for the low frequency radio emission, especially for the fast pulsars, neither the Lorentz factors nor the multiplicity factor of a pair cascade are allowed to be high. The results of our caluculations have been fully confirmed by a more detailed analysis by Melrose & Gedalin (1999) using a relativistic thermal energy distribution function for the radiating particles and studying the wave modes precisely.

Kunzl *et al.* (1998a) argue that a relativistic plasma process produces emission of a frequency

$$\nu_{\rm em} = \frac{1}{2\pi}\omega_{\rm p}^{(0)}\gamma^{\alpha/2} \tag{38}$$

where α is an integer between 1 and 3 and $\omega_{\rm p}^{(0)}$ is the plasma frequency

$$\omega_{\rm p}^{(0)} = \sqrt{\frac{ne^2}{m_{\rm e}\varepsilon_0}} \tag{39}$$

without any Lorentz factors. As can be seen from the two previous equations, the plasma frequency scales with the square root of the particle density which means it grows as the multiplicity factor M rises.

Combining these two conditions we find the proportionality

$$\nu = CM^{1/2}\gamma^{\alpha/2} \tag{40}$$

where $C = \sqrt{(\Omega B_0 e)/(2\pi^2 m_{\rm e} x_{\rm em}^3)}$ depends only on pulsar parameters (magnetic field strength at the point of emission and period). The emission height, however, can be estimated from observations to be around 100 pulsar radii or less (Blaskiewicz *et al.*, 1991, von Hoensbroech, 1995) but it is definitely smaller than the light cylinder radius. As mentioned in Chapter 2, timing measurements and profile widths independently strongly suggest an inner magnetospheric process. So setting the $x_{\rm em} = x_{\rm LC}$, we find a minimum frequency that can be emitted by a particle with a Lorentz factor γ by a plasma process. Taking the Crab pulsar as a prominent example, the process must explain radio emission at 160 MHz (where the maximum radio flux is observed).

Therefore the fact that magnetospheric 160 MHz radio emission from the Crab is observed, provides an upper limit for the density and particle energy. For the Crab pulsar this yields:

$$M\gamma^{\alpha} \leq 163 \tag{41}$$

for an emitted frequency of $\nu = \gamma^{\alpha/2}\nu_{\rm pe}$ and a multiplicity factor of M. This important restriction is discussed in more detail in the next chapter.

Outer gap models have fewer difficulties with acceleration and the emission properties of neutron stars. On the one hand the development of an acceleration region beyond the neutral line is natural as particles can flow freely out towards the light cylinder. Moreover, pair production in this region does not affect radio photons any more, as the plasma frequency has

dropped to values far below typical radio frequencies. The outer gap can be seen as an umbrella with a hole in the middle where the radio emission can be observed. This is a natural explanation for the non-alignment of radio and X-ray pulses in most X-ray and radio-loud pulsars. Only two possible points of criticism shall be mentioned here, for which this work proposes solutions.

Since it is observationally shown that the radio emission originates in the inner magnetosphere, and there is little doubt that relativistic particles are responsible for it in some way, it has to be discussed how mildly relativistic particles can occur in the inner magnetosphere, when there is no inner gap.

A second item is that, in the literature, only outer gap models for RS type (i.e. anti-aligned) pulsars can be found. If the acceleration region near the light cylinder is a common feature, it should also be found in almost aligned or highly inclined rotators. Both types of rotating neutron stars can be observed as radio pulsars.

Last but not least, it has been ignored in the literature so far that an outer gap is incompatible with an inner gap. The reason for this is that for a dense pair plasma the neutral line has no effect at all, because the small space charge necessary can easily be obtained by a slight change in the velocities of the two plasma components. Both gap types in one pulsar would be possible only with an oscillating process, meaning that when the inner gap sparks, the outer gap grows, and sparks before the dense plasma from inside reaches the neutral surface and fills the void. But this would be a very unstable system; if the sparking is not extremely well synchronized, it will soon run out of phase and close at least one gap. As the particles cannot escape directly in the inner part of the magnetosphere, it is hard to find appropriate conditions that make the inner gap grow again.

Summarizing, it can be said that there is considerable observational and theoretical evidence that the current inner gap models face serious problems, and that the high-energetic radiation is likely to originate in the outer magnetosphere. Inner and outer gaps cannot be maintained simultaneously, but only the outer gap can develop directly, by plasma crossing the light cylinder. Besides, it is doubtful if a large inner gap can exist at all, as heavy thermal and field emission from the surface tend to close an inner gap anyway. Furthermore, even with a fully developed inner gap, there are severe problems in initiating the pair cascade, unless strong small-scale multipoles reduce the curvature radius, and enhance the magnetic field strength.

"Would you tell me please, which way I ought to go from here?"
"That depends a good deal on where you want to get to", said the Cat.
"I don't much care where – ", said Alice.
"Then it doesn't matter which way you go", said the Cat.
Lewis Carroll, *Alice in Wonderland*

4 Radio emission mechanisms

In astrophysics we have to distinguish between two fundamentally different kinds of electromagnetic radiation. So-called *incoherent* emission is the result of a stochastic superposition of elementary waves. Therefore the single sources have no phase correlation to each other. Consequently, the phases have to be averaged and the source can be seen as a number of N non-interacting elementary emitters. So if one single radiator emits the power $P_{\rm single}$, the total power is $NP_{\rm single}$ or less (as absorption might reduce the actual luminosity). So Ginzburg & Zheleznyakov (1970a, 1970b) define an incoherent process by the condition $P_{\rm total} \leq NP_{\rm single}$. A classical incoherent process is thermal emission (each atom radiates independent of all others). In analogy to blackbody radiation we can also identify an incoherent process if the brightness temperature of the radiation does not exceed the particle "temperature" $E_{\rm particle}/k_{\rm B}$ (see chapter 5).

On the other hand a process that produces a power $P > NP_{\rm single}$ requires a correlation between the phases of the elementary emitters. In the extreme case, the phases of all particles are coupled in such a manner that all waves show constructive interference in a certain direction. Then the wave field $E_{\rm wave}$ is comparable to $NE_{\rm single}$ (maximum coherence) and therefore $P_{\rm total} = N^2 P_{\rm single}$ as $P_{\rm total} \sim E_{\rm total}^2$.

Coherent emission has been observed from various astronomical objects and in laboratory experiments. Mechanisms for producing coherent emission that have been discussed so far are bunching of charges (particles in one bunch radiate in phase), relativistic plasma emission (instabilities excite waves on which particles can be scattered coherently) or maser emission (plasma waves with a negative absorption coefficient grow, accelerate charges and cause them to emit phase-coupled radiation). All of these mechanisms have been applied to pulsar radio emission. In the following we will discuss these ideas critically.

4.1 Coherent curvature radiation

A widely discussed process for pulsar radio emission is coherent curvature radiation by bunches (CCR). The assumption is quite natural, since the magnetic field of a neutron star is so strong that outflowing charged particles can hardly deviate from the path prescribed by the magnetic field line. But the polarization of curvature emission is fixed by the plain of a magnetic field line, which would reproduce the characteristic S-swing of the polarization angle. In such models the bunches are believed to develop from the curved path the beam has to follow along the strong magnetic guide field.

The idea of coherent curvature radiation has been prominent from the beginning of pulsar models. The mechanism has been examined by many authors since then (Gunn & Ostriker, 1971, Sturrock, 1971, Ruderman & Sutherland, 1975, Ginzburg & Zheleznyakov, 1975, Buschauer & Benford, 1976, Kirk, 1980, Benford & Buschauer, 1983) and even in some recent papers (Rankin, 1992, Gil ,1992, Gil & Sendyk, 2000, Khechinashvili *et al.*, 2000, Melikidze *et al.*, 2000, Gil & Mitra, 2001).

Despite this popularity, there are a number of severe difficulties.
Melrose (1992) argued that reactive instabilites (i.e. instabilities that are not due to an unstable velocity distribution) produce a small bunching effect, but are self-quenching, meaning they increase the velocity spread and make kinetic description necessary. But if the velocity spread is too large, the bunches will disperse more quickly than they can be built up. Additionally, the wave vector $\vec{k}$ of the emitted radiation must coincide with the maximum of the spatial Fourier transform of the bunch. Due to the relativistic lighthouse effect $\vec{k}$ is within a forward cone with an opening angle of $1/\gamma$ (Rybicki & Lightman, 1979). Therefore the bunch has to be pancake shaped, as $k_\perp \leq k_\parallel/\gamma$. As along the magnetic field line the "forward" direction changes, the bunch has to rotate in a similar manner as it travels along the curved field line, as otherwise the above condition would be violated somewhere. What may cause this rotation is unknown.

Moreover we have shown (Lesch *et al.*, 1998) that CCR is unable to fulfill basic energetic and RFM constraints from the observations, even for maximum coherence. In the following our argumentation is described.

A particle with energy $\gamma m_e c^2$ moving along a curved magnetic field line radiates at a characteristic frequency.

$$\nu_C = \frac{3c}{4\pi R_C}\gamma^3. \tag{42}$$

Taking the frequency to be given by the observations we therefore find

an expression for the particle Lorentz factor γ:

$$\gamma = \left(\frac{4\pi\nu_{\mathrm{C}} R_{\mathrm{C}}}{3c} \right)^{1/3} . \tag{43}$$

Far inside the light cylinder the curvature radius for a purely dipolar field line crossing the surface at a polar angle of θ_{s} is

$$R_{\mathrm{C}}(\theta, \theta_{\mathrm{s}}) = \frac{r_{\mathrm{NS}}}{3} \frac{\sin\theta}{\sin^2\theta_{\mathrm{s}}} \frac{(1+3\cos^2\theta)^{3/2}}{1+\cos^2\theta} \tag{44}$$

for a polar angle of θ (Smirnow, 1973). This expression can be well approximated by

$$R_{\mathrm{C}}(x) \approx R_{\mathrm{C}}(r_{\mathrm{NS}})\sqrt{x} \tag{45}$$

where x is the radial distance to the neutron star centre in units of r_{NS}.

The total power radiated by one particle with a Lorentz factor of γ is

$$P_{\mathrm{C}} = \frac{2}{3}\gamma^4 \frac{e^2 c}{4\pi\varepsilon_0 R_{\mathrm{C}}^2} . \tag{46}$$

Since we consider a coherent process, the single particle power is enhanced by a factor of N_{coh}, meaning the number of coherently radiating particles. So the power emitted by one coherence volume is

$$P_{\mathrm{N}} = P_{\mathrm{C}} N_{\mathrm{coh}}^2 . \tag{47}$$

Melrose (1992) calculates the coherence volume as

$$V_{\mathrm{C}} = \frac{c^3\gamma^2}{\pi\nu^3} \tag{48}$$

via

$$V_{\mathrm{C}} = \frac{\lambda^3}{\Delta\Omega \cdot (\Delta\omega/\omega)} \tag{49}$$

where $\Delta\Omega$ denotes the solid angle to which the radiation is confined, and $\Delta\omega/\omega$ is the bandwidth of the emission (for broadband emission this can be set equal to 1). Due to the relativistic lighthouse effect, the emission angle is approximately given by $\Delta\Omega = \pi/\gamma^2$.

This yields the coherence number by multiplying V_{C} by the density $n := Mn_{\mathrm{GJ}}$, where M again denotes the pair multiplicity factor.

To obtain the observed radio luminosity L, we need $N_\mathrm{V} = L/P_\mathrm{N}$ coherence cells. If these are arranged in a cube, we find a minimal size of the emission region

$$\Lambda = (N_\mathrm{V} V_\mathrm{C})^{1/3} \,. \tag{50}$$

Now we can calculate the energy loss of a coherently radiating particle crossing the emission region to find

$$W_\Lambda = \frac{\Lambda}{c} P_\mathrm{C} N_\mathrm{C} \tag{51}$$

which must not exceed the particle energy itself, as we do not consider reacceleration on the large scales comparable to the curvature radius R_C along the field line.

Apart from that, bunching of charges is a plasma process. Thus no freely propagating emission below the local plasma frequency ω_p can be produced in this way. So we can determine a minimum emission frequency from the condition $\nu \geq \omega_\mathrm{p}/(2\pi)$. It reads

$$\nu_\mathrm{min} = \frac{3^{2/5}}{4\pi c^{1/5}} \left(\frac{8eM\Omega B_0}{3m_\mathrm{e}} \right)^{3/5} x^{-9/5} R_\mathrm{C}^{1/5} \tag{52}$$

where we have again used $x = r/r_\mathrm{NS}$ as the dimensionless radial coordinate. This equation alone can be seen as an argument against CCR because $R_\mathrm{C} \sim x^{1/2}$, so that eq. (52) predicts a RFM exponent of 10/17 for this process. Such an exponent is clearly ruled out by the observations which predict a maximum exponent of around 0.2 (Gil & Kijak, 1992, Kramer, 1994).

Combining this restriction with the energetic constraint in (51), and inserting all the expressions from the above equations, we can even find a more principal energetic restriction. The maximum luminosity in the scenario just described is

$$L_\mathrm{curv} \leq \frac{243}{32} \frac{\pi \varepsilon_0 m_\mathrm{e}^3 c^4}{e^3 M \Omega B_0} \nu^3 x^3 R_\mathrm{C} \,. \tag{53}$$

Inserting numbers for some well-studied pulsars (fig. 27) we find that the observed luminosities, especially for the low frequencies cannot be produced by CCR. The situation improves slightly for a dense pair plasma, but even then curvature radiation can only provide enough power in frequencies above several GHz.

Therefore CCR does not play a significant role for the low-frequency radio emission of pulsars.

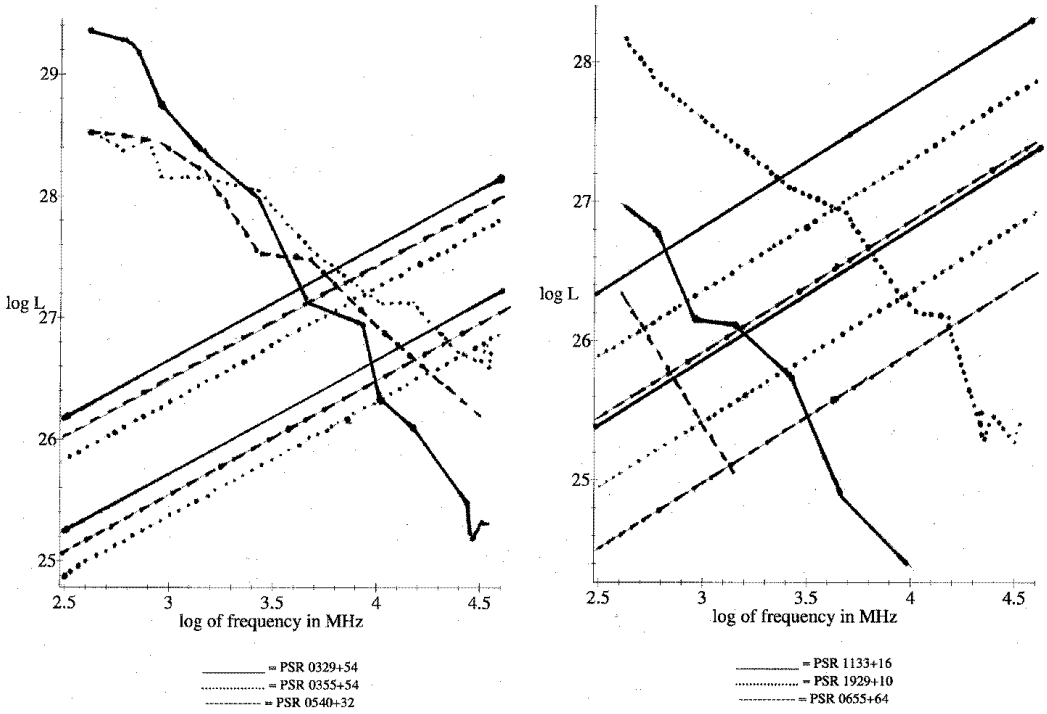

Figure 27: Luminosities of six radio pulsars, compared to the maximum possible luminosity that can be obtained by CCR (straight lines). The lower set of lines is for a GJ case, whereas the upper group assumes $n = 10^4 n_{\rm GJ}$. It can clearly be seen that in no case the low frequency fluxes are reached, not even for the weakest radio pulsar of Taylor *et al.* (1993), PSR 0655+64.

4.2 Relativistic plasma emission

As CCR can be ruled out as shown above, alternatives have to be discussed. Among those, plasma turbulence appears to be a more promising candidate for the production of coherent radio emission. A similar, non-relativistic kind of mechanism is observed in the solar corona and is a multi-stage process. A possible scenario involves longitudinal or Alfvén waves growing due to some instability. However, it is still unclear which instability is an acceptable source of plasma turbulence. The three mechanisms discussed in the literature are streaming, curvature-driven and cyclotron instabilities. The former seem to be a natural consequence of non-stationary discharges, which are required to obtain two-stream instabilities, that grow rapidly enough (Usov, 1987) to fully develop far inside the light cylinder. Usov's model

assumes a non-stationary discharge with a period of τ. The particles of one bunch have an energy distribution and therefore the bunches disperse as they travel out. The most energetic particles of the structure have a velocity very close to c, whereas the mildly relativistic ones move at a speed significantly below the speed of light. For $\gamma \gg 1$ we can compute the velocity as

$$\beta = 1 - \frac{1}{2\gamma^2}\,. \tag{54}$$

So, after some time, the fastest particles of one bunch catch up with the slowest of the one ahead. This is the case at a distance of

$$r = 2c\tau\gamma_{\mathrm{min}}^2 \tag{55}$$

if γ_{min} is the Lorentz factor of the slowest particles. At the point where the two bunches meet, there is suddenly an extreme two-stream instability, which has a growth rate comparable to the plasma frequency, and therefore develops almost instantly. So the appropriate parameters for τ and γ_{min} can easily explain an emission height of some 50 pulsar radii. A schematic view of the situation is shown in fig. 28.

Melrose & Gedalin (1999) have examined the conditions necessary to produce low frequency radio emission by a two-stream instability with a low relativistic background plasma being hit by an intrinsically relativistic beam. (Melrose & Gedalin (1999) assume a relativistic Maxwell or Jüttner distribution $f(\gamma) \sim \mathrm{e}^{-\rho\gamma}$, where $\rho \approx 1/\langle\gamma\rangle$ is some normalized inverse temperature). The authors have found that frequencies of a few 100 MHz require that the background, as well as the beam particles, are only mildly relativistic:

$$\omega_{\mathrm{obs}} = \omega_{\mathrm{pe}}^{(0)}\gamma^{1/2}\langle\gamma_{\mathrm{rel}}\rangle \tag{56}$$

where $\omega_{\mathrm{pe}}^{(0)}$ is the plasma frequency without any Lorentz factors, and γ_{rel} denotes the relative Lorentz factor between the beam and the background particles. Inserting typical values for the P, B_0 and x_{em}, one finds that even for no pair production, only $\gamma_{\mathrm{bg}} \approx \langle\gamma\rangle \approx 10$ is allowed for frequencies well below 1 GHz.

Wave propagation and dispersion in the framework of such a model has been extensively studied by Gedalin *et al.*, 1998, Melrose & Gedalin (1999), Melrose *et al.*, 2001). It is found that only the reactive version of growing Langmuir waves applies for the considered scenario. The kinetic description would be needed only for $\gamma_{\mathrm{rel}}^5/(\gamma_{\mathrm{bg}}^2\Delta\gamma^3) \leq 1$, which is never satisfied, as the beam energy is larger than either the intrinsic energy spread of the background particles, or the energy spread of the beam. In the reactive

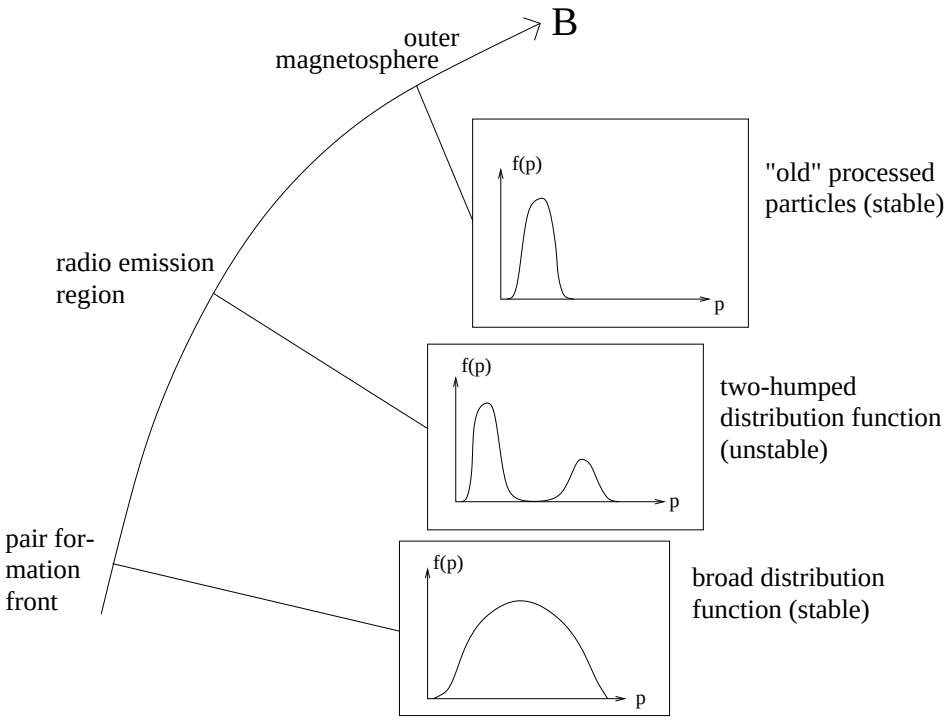

Figure 28: Evolution of particle energy distribution functions in a non-stationary discharge (Usov, 1987). The pair cascade close to the surface creates bunches of particles with a large energy spread (lower figure). As the bunch travels out, an unstable distribution function develops as the fastest particles of one bunch fetch up the slowest component of the previous bunch. This instability leads to coherent radio emission and decelerates the particles of the energetic component. So in the end, a stable distribution of low-energetic particles remains (upper figure).

case, and for a strong beam (meaning that the beam density is comparable to the background density) the approximate growth rate is given by

$$\Gamma = \frac{\omega}{\gamma_{\mathrm{bg}}\langle\gamma_{\mathrm{rel}}\rangle}\,. \tag{57}$$

Furthermore, Melrose & Gedalin (1999) show that Alfvén waves can grow only if the resonance condition, requiring that the phase velocity of the wave equals the beam velocity

$$v_{\mathrm{ph}} = v_{\mathrm{beam}} \Longrightarrow \gamma_{\mathrm{beam}} = 4\gamma_{\mathrm{bg}}^2\frac{\omega_{\mathrm{c}}}{\omega_1'} \tag{58}$$

is fulfilled, where $\omega_{\mathrm{c}} = eB/m_{\mathrm{e}}$ denotes the gyro frequency and ω_1' is the Lorentz transformed critical frequency, above which the parallel Langmuir mode becomes subluminal (equations (17) and (40) in Melrose & Gedalin (1999)). Since this is never the case inside the pulsar magnetosphere for reasonable parameters, an instability using the beam resonance with Alfvén waves can be ruled out.

4.3 Maser processes

Another widely favoured idea for pulsar radio emission is some plasma maser process. Melrose (1978) showed that a coherent process (maser) by bunches cannot work for various reasons. Since the efficiency of the process is limited by bunch dispersion and self suppression, the observed brightness temperatures cannot be reproduced.

Therefore a maser mechanism by some plasma instability is more likely. The simplest direct process of this type is emission due to acceleration of charges along the magnetic field. This mechanism in its maser form (amplified linear acceleration emission, ALAE) is a promising candidate for the radio emission.

For the ALAE we consider a plane monochromatic electrostatic wave. Its electric field accelerates charged particles crossing it:

$$\frac{\mathrm{d}^2\vec{r}(t)}{\mathrm{d}t^2} = \frac{q}{m\gamma^3(t)}\vec{E}\left[\vec{r}(t), t\right] \tag{59}$$

where q is the particle's charge and m its rest mass. Taking $\gamma(t)$ as a slowly varying quantity we can linearize eq. (59) to find

$$\frac{\mathrm{d}^2\vec{r}(t)}{\mathrm{d}t^2} = \frac{q}{m\gamma^3}\vec{E}(t)\,. \tag{60}$$

Together with the linearized expression for the Fourier transformed current density

$$\vec{j}\left(\vec{k},\omega\right) = q\mathrm{e}^{-i\vec{k}\cdot\vec{r}_0}\int\left[\frac{\mathrm{d}\vec{r}^{(1)}(t)}{\mathrm{d}t} - i\vec{v}t\vec{k}\cdot\vec{r}^{(1)}(t)\right]\mathrm{e}^{i\left(\omega-\vec{k}\cdot\vec{v}\right)t}\,\mathrm{d}t \tag{61}$$

and with

$$\vec{r}(t) := r^{\vec{(0)}}(t) + r^{\vec{(1)}}(t) \tag{62}$$

where the zero-order orbit is given by

$$\vec{r}^{\,0}(t) = \vec{r}_0 + \vec{v}t\,. \tag{63}$$

one finds

$$\vec{j}\left(\vec{k},\omega\right) = \frac{iq^2}{m\gamma^3\omega'}\mathrm{e}^{-i\vec{k}\cdot\vec{r}_0}\omega\tilde{E}\left(\omega'\right)\vec{b} \tag{64}$$

with the temporal Fourier transform of the electric field $\tilde{E}\left(\omega'\right)$, the unit vector in the direction of the magnetic field $\vec{b}$ and the Doppler shifted frequency

$$\omega' = \omega - \vec{k}\cdot\vec{v}\,. \tag{65}$$

From these results one can derive the power radiated at a certain time by integrating the energy flux over the spatial angle, and switching on and off the electric field adiabatically finally to find some generalized Larmor formula:

$$P(t) = \frac{q^2}{6\pi\varepsilon_0 c^2}\left|\frac{qE(t)}{m}\right|^2\,. \tag{66}$$

This result can be applied to a monochromatic plane electric wave, with a frequency ω_0 and an energy distribution function with a positive gradient at some energy. In the simplest case of a δ- distribution of the particle energies ($f(\gamma) = \delta(\gamma_0)$) and negligible plasma frequency, Melrose (1978) finds negative absorption (=growth) for

$$\omega < \frac{3}{2}\omega_0\gamma^2 \tag{67}$$

If the electric wave is considered to be a plasma wave (meaning $\omega_0 = \omega_\mathrm{p}$), it can be shown that a sufficient optical depth (which is limited by field line curvature) can be obtained only for Lorentz factors of the order of 10

and densities around the GJ value. So if the ALAE mechanism plays a significant role for pulsar radio emission a pair cascade is incompatible with its requirements and has to be ruled out.

4.4 Particle energies for radio emission

We have presented another very simple independent argument that a plasma process responsible for pulsar radio emission is only possible for low Lorentz factors and small densities (Kunzl *et al.*, 1998a). The calculations have been performed for the Crab pulsar as a prominent example but can be applied to other pulsars as well.

From the Crab pulsar we observe radio emission having a peak at a frequency of about 160 MHz. So the emission process must be able to produce this low frequency radiation. Since the emission is pulsed with the rotation period $P = 33.4$ ms, it must have its origin inside the light cylinder $r_{\rm LC} = c/\Omega$. For the Crab pulsar, this maximum distance is less than 1600 km or 160 pulsar radii.

The (peak) emission frequency of any relativistic plasma process must be coupled to the plasma frequency $\omega_{\rm p}$ (cf. (39)). Therefore we expect $\nu = \gamma^{\alpha/2}\nu_{\rm p}^{(0)}$ with $\nu_{\rm p}^{(0)}$ being the plasma frequency without any Lorentz factors and α some integer number (for CR emission by bunches $\alpha = 1$ whereas the ALAE mechanism corresponds to $\alpha = 3$).Using (39) and parameterizing the density as $n = Mn_{\rm GJ}$ we find

$$\nu_{\rm min} = \nu_{\rm p}^{(0)}\gamma^{\alpha}/2 = \frac{1}{2\pi}\sqrt{\frac{Mn_{\rm GJ}e^2\gamma^{\alpha}}{m_{\rm e}\varepsilon_0}}\,. \tag{68}$$

For a simple estimation we neglect all angular corrections and take only the "parallel" GJ density. Then we obtain

$$\nu_{\rm min} = \frac{1}{2\pi}\sqrt{\frac{2B_0\Omega e}{m_{\rm e}x^3}}M^{1/2}\gamma^{\alpha/2}\,. \tag{69}$$

This equation can be solved for a product containing the two interesting quantities pair multiplicity and particle Lorentz factor:

$$M\gamma^{2\alpha-1} = \frac{4\pi^2\nu_{\rm min}^2 m_{\rm e}}{2B_0\Omega e}x^3\,. \tag{70}$$

Inserting the peak frequency ($\nu_{\rm min} := 160$ MHz), light cylinder radius ($x := x_{\rm LC} = c/(r_{\rm NS}\Omega) = 159$) and the dipolar surface magnetic field $B_0 :=$

$3.8 \cdot 10^8$ T) of the Crab pulsar we find the *maximum* possible value of the product in the previous equation to be

$$(M\gamma^\alpha)_{\max} = \frac{2\pi^2 \nu_{\min}^2 m_e c^3}{B_0 \Omega^4 e r_{\rm NS}^3} = 163\,. \tag{71}$$

If we take $x < x_{\rm LC}$ (i.e. a purely magnetospheric process), this limit is even smaller. For the ALAE mechanism ($\alpha = 3$) we again find that very low Lorentz factors (below 10), and densities in the range of only $n_{\rm GJ}$ can be allowed. But even for a process with $\alpha = 1$, the low frequency radio emission of the Crab pulsar is incompatible with pair cascade models as it would require the production and propagation of coherent radiation below the plasma frequency.

Of course, the same type of argument can also be applied to other examples. However, for middle-aged pulsars the argumentation must be slightly different, as the restriction $x < x_{\rm LC}$ is quite a weak one in these cases. So for high-altitude emission and a process with $\alpha = 1$, the values are consistent with a pair cascade. But since observations strongly suggest that the emission heights in average pulsars are far below the light cylinder radius, one should rather estimate $x_{\rm em} \approx 50$, which yields a number of some thousands on the right-hand side of (71). Therefore the argument is still convincing, though not as strong as for the Crab pulsar.

Summarizing it should be emphasized once more that our argument did not use further assumptions about the details of the emission process. So we showed that **any** plasma process can only produce the low-frequency radio emission from the observationally deduced distances if the neither the plasma density nor the particle energy is large. Both restrictions make a plasma process incompatible with an inner gap pair cascade.

Melrose (2000) pointed out that there might still be a possibility to remove this incompatibility, namely, if there are voids (low-density regions with $n \approx n_{\rm GJ}$) in the magnetosphere which act as waveguides where the coherent radio emission is produced and propagates. In such a scenario the high energetic pair plasma could feed in energy and thus reproduce the luminosities. However, this model has not yet been elaborated quantitatively.

4.5 Alternative models

Several other emission processes have been proposed. Some authors have suggested mechanisms producing radio emission close to the light cylinder. This is because some observational results seem to hint that the radio emission comes perhaps from much larger distances than 1000 km from the

surface. For instance, Gwinn *et al.* (1997) find a transverse size of the radio emission region in Vela of about 500 km, which suggests emission close to the light cylinder.

As the plasma frequency in the outer magnetosphere is usually too small to account for the observed radio frequencies Lyutikov *et al.* (1999a, 1999b) consider two electromagnetic instabilities. These are the cyclotron Cherenkov instability, which is excited at the anomalous Doppler resonance

$$\omega(\vec{k}) - k_{\parallel} v_{\parallel} + \omega_{\rm c}/\gamma_{\rm res} = 0 \tag{72}$$

and the Cherenkov drift instability occurring at the Cherenkov drift resonance

$$\omega(\vec{k}) - k_{\parallel} v_{\parallel} - k_{\perp} u_{\rm d} = 0. \tag{73}$$

Here $u_{\rm d} = \gamma v_{\parallel} c/(\omega_{\rm c} R_{\rm C})$ denotes the drift velocity.

The first process is supposed to produce "Core" emission whereas the second mechanism should be responsible for the "Cone". The model requires a very efficient inner gap producing a dense pair plasma (multiplicity around 10^5) with only mildly relativistic particles (Lorentz factor of about 10). This is a somewhat doubtful assumption, as numerical simulations of an inner gap pair cascade predict mean Lorentz factors of at least 100 (Daugherty & Harding, 1982). However, the Cherenkov model works only for very large distances from the neutron star (1000 pulsar radii) which makes it inapplicable for ms-pulsars. But observational results give no hint of different emission mechanisms in normal and recycled pulsars (Kramer *et al.*,1998, Xilouris *et al.*, 1998). Moreover, no detailed calculations have yet been performed to find whether the process produces enough luminosity in the low frequency range, to reproduce the observed flux. Altogether radio emission from regions close to the light cylinder cannot definitely be ruled out, but is nevertheless based on a number of quite doubtful assumptions, and therefore it will not be considered further.

Another proposed radio emission mechanism is the so-called "electrosphere" type. In these models, the pulsar is supposed to have a net charge (Krause-Polstorff & Michel , 1985a, 1985b). In other words, a monopole electric field on the surface builds up, allowing a closed magnetospheric system where no charged particles cross the light cylinder. The magnetosphere in such a model is split up into a corotating region and several vacuum gaps, where charges can be accelerated and lose energy into radiation. The main disadvantage of these models is that they cannot explain the pulsar particle wind (as observed in the Crab pulsar) and no quantitative studies

of emission features have yet been performed. So a detailed discussion of an electrospheric model is beyond the scope of this work.

Summarizing, it can be said that, currently, the most likely process for radio emission is some concept similar to the ALAE described above. To summarize our findings, coherent curvature radiation faces many difficulties in fulfilling observational constraints. The ALAE mechanism requires low Lorentz factors and densities which make it incompatible with inner gap models. Nevertheless in the absence of other promising radio emission scenarios, the ALAE still has to be taken seriously. In the following, we will use this process as the only important radio emission mechanism, a view supported by recent numerical simulations (Schopper *et al.*, 2001) showing the growth of solitons in a mildly relativistic plasma by a two-stream instability. It was shown in the simulations that a full two-stream instability (generated by a non-stationary discharge or some propagation effect similar to the Usov model) can efficiently drive waves and produce highly coherent radio emission. In particular, the preliminary results suggest that some particles are reflected, and dragged on again by the next bunch of particles coming from inside. Such a reacceleration sketch will be elaborated in the next chapter.

"I didn't know that Cheshire-Cats always grinned;
in fact, I didn't know
that cats could grin at all", said Alice.
"They all can", said the Duchess, "and most of 'em do."
Lewis Carroll, *Alice in Wonderland*

5 The current-circuit picture

5.1 Motivation

The main problem with acceleration models in pulsar magnetospheres is that as soon as particles are accelerated or decelerated, either the current density or the number density changes. In particular, deceleration causes a jam of particles, meaning the density rises. As a consequence, this *virtual cathode* reduces the current density coming from inside, releasing the jam. Such a virtual cathode effect can in fact be observed in laboratory experiments (Woo, 1987). Increasing the current over a critical value builds up a space charge, which quenches the stream of following particles. In the time-averaged picture the number of inflowing particles must equal the number of outflowing charges (i. e., the current is divergence free).

However, a depletion region would show some kind of runaway effect: in an underdense region the parallel electric field is not fully shielded, accelerating particles reduces the number density of the electrons further and the gap grows. This effect is, of course, limited by the speed of light which is the maximum possible particle speed. Nevertheless, an underdense region can only be filled by a pair cascade, an increase of the current density, or another overdense region at a larger distance.

The latter scenario, however, describes nothing but an electrostatic wave superimposed on a GJ plasma. So, instead of speaking of an acceleration and deceleration region, we can just as well interpret this wave as a non-ideality (i.e. a region where an electric field parallel to $\vec{B}$ appears) in an otherwise perfectly shielded environment with $\vec{E} = -\vec{v} \times \vec{B}$.

The important point is now that such a structure can only be stable if $\mathrm{div}\vec{j} = 0$ is fulfilled. This means that the inflowing and outflowing currents must be equal, in other words, the velocities in the GJ region above and below the wave have to be identical (apart from curvature effects). But if the particles do not lose kinetic energy in a dissipation region, the radiated power must be supplied by the field itself. Of course, this condition will not hold for small-scale structures and short time scales such as a growing electrostatic wave; but a spatially and temporally averaged model cannot

contain global deceleration unless in a dense pair plasma, where the current is conserved by increasing the velocity difference between the two charge types.

Such a model is comparable to a resistance in a current-circuit, where electrons are not slowed down, but a fraction of the induced voltage drops in the wave region (see fig. 29). So plasma waves act only as a promoter transforming the rotationally induced field energy into radiation. **Especially the dissipated energy per particle is not limited by its own kinetic energy, so that even low relativistic particles may dissipate an effective energy, which vastly exceeds $\gamma m_e c^2$. Thus the incompatibility of low relativistic particles and high radio luminosity is removed (see below).**

The advantages of such a description are obvious: density fluctuations occur only as waves so that there are no global density changes. Moreover, there is no energetic problem as pointed out above. Such a difficulty occurs when the kinetic energy of the streaming particles is the only source for radiation and the Lorentz factors are below 10. The observed mean intensity of the radio emission requires either a higher energy density of the plasma in the inner magnetosphere (i.e. higher Lorentz factors or number densities), or some reacceleration in the radio emission region. In the latter case the current-circuit model provides the most natural explanation, since reacceleration exactly balances the losses. Furthermore, the similarity to a current-circuit would elucidate how mildly relativistic particles could be produced at all, without an acceleration region in the inner magnetosphere. There will, of course , exist a boundary layer just above the surface where the particles evaporate off the neutron star and are accelerated to their terminal energies. However, this layer is not a gap in the Ruderman/ Sutherland sense.

Last but not least, such a picture is reasonable, as the average current is determined globally (namely by having a system with a more or less fixed resistance – cf. sect. 6.3.), so that the current is driven through the resistive circuit by the potential difference. A purely local description, in turn, neglects back reactions of the losses on the system.

5.2 Radio luminosity and brightness temperature

In the following we derive a quantitative model for the radio emission of pulsars. The particular aim is to explain the energetics of the radiation, from observed or observationally derived pulsar parameters such as

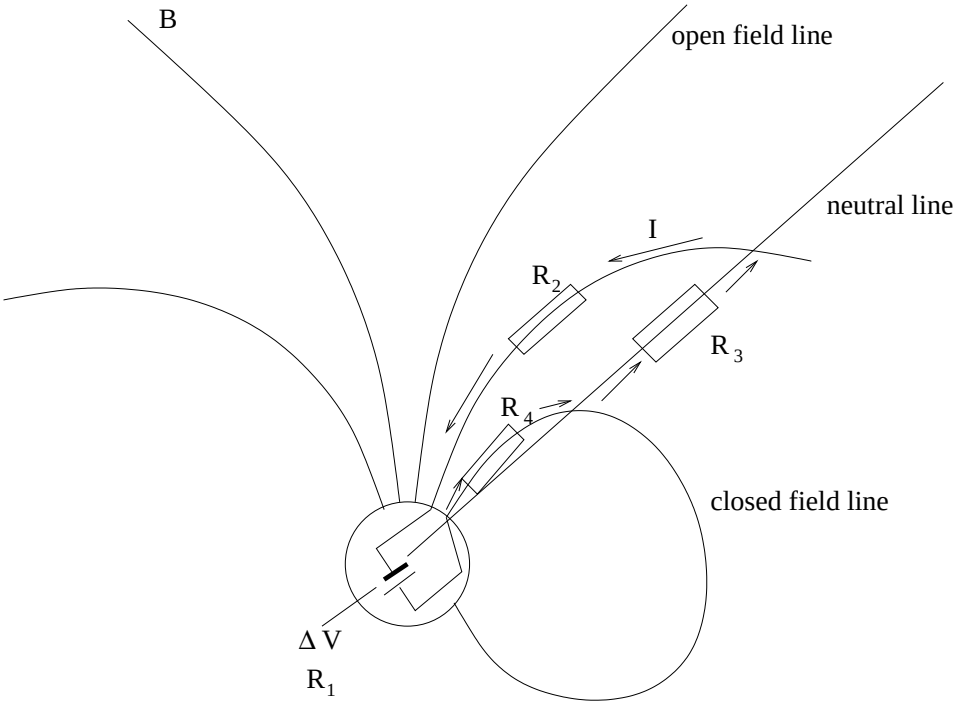

Figure 29: Schematic view of the current circuit model. There are four possible places of resistivity, where R_1 denotes the battery's own resistance, which is supposed to be very small. R_2 is the non-ideality in the radio emission region, R_3 is a system intrinsic resistance which vastly dominates the other three (cf. sect. 6), whereas R_4 combines the other inner magnetosphere losses, such as resonant ICS with thermal photons which only makes up a tiny fraction of the total spindown luminosity.

- the period P
- the dipolar surface magnetic field B
- the brightness temperature $T_{\rm B}$ of the low frequency emission
- the emission height $x_{\rm em}$
- the total luminosity in the radio band L

With these input parameters we derive a value for the radial width of the emission region, which must be small to be consistent with observations. A narrow radiation zone is suggested by both the highly structured emission in

space and time. If this region was fairly thick, many elementary discharges along a field line at the same time would be expected which would smoothen the profile.

As radiation mechanism we assume a plasma process similar to the ALAE Melrose (1978) in a GJ magnetosphere directly connecting particle energy, plasma frequency (which in this case depends only on emission height and particle energy) and the emitted frequency via

$$\nu = \frac{\omega_{\rm p}^{(0)}}{2\pi}\gamma^{\alpha/2}\,. \tag{74}$$

In this notation the values for α discussed in the literature are 1,2 or 3 accordingly (Ursov & Usov, 1988, Melrose & Gedalin, 1999, Lesch *et al.*, 2000, Melrose *et al.*, 2001). In the next chapter we will debate an argument why the description of the pulsar system as a resistive current circuit makes $\alpha = 1$ less likely than a higher value. Inserting (7) for the density and (39) we can solve this equation for γ:

$$\gamma = \left[\frac{\omega_{\rm p}(x_{\rm em})}{2\pi\nu}\right]^{-2/\alpha} = \left(\frac{B_0\Omega e}{2\pi^2\nu^2 m_{\rm e}x_{\rm em}^3}\right)^{-1/\alpha}\,. \tag{75}$$

For a random-phase process the brightness temperature of a radiating particle is limited to its own energy divided by the Boltzmann constant

$$T_{\rm B}^{\rm max} = \frac{\gamma m_{\rm e}c^2}{k_{\rm B}}\,. \tag{76}$$

This limit can be understood by taking the definition of the brightness temperature:

$$T_{\rm B} = \frac{c^2 F_\nu}{2\pi k_{\rm B}\nu^2}\left(\frac{R}{r}\right)^{-2} \tag{77}$$

where F_ν is the radiation flux at a frequency ν, R denotes the extension of the source and r its distance from the observer. Solving this equation for F_ν we find

$$F_\nu = \frac{2\pi\nu^2}{c^2}k_{\rm B}T_{\rm B}\left(\frac{R}{r}\right)^2\,. \tag{78}$$

Assuming broadband emission ($\Delta\nu \approx \nu$) and using the obvious condition that the minimum timescale for the radiation is about one period $\tau = 1/\nu$, together with the estimate that the minimum spatial extension of the radiating source is $R \leq c/\omega$ we find

$$E_{\rm rad} \approx \Delta\nu\, F_\nu r^2 \tau \int\limits_\Omega {\rm d}\Omega = 2k_{\rm B}T_{\rm B}\,. \tag{79}$$

So, apart from a factor of 2 (which can be dropped for our rough estimations) we find the restriction for the brightness temperature given above.

Therefore, an incoherent process from an electron with a Lorentz factor of γ cannot produce radiation with a brightness temperature exceeding $10^{10}{\rm K}\gamma$. However, in the case discussed here, this argument is not applicable. The reason for this is that we do not consider absorption. The power output of a radiation process is not limited any more if the radiation produced further inside is not absorbed. Consider a cylindrical plasma column of radius R, length l, particle density n and single particle power output $P_{\rm single}$ in forward direction. Then the total power adds up to

$$P_{\rm ges} = lR^2\pi n P_{\rm single}. \tag{80}$$

Thus the brightness temperature can reach arbitrarily high values on the condition that l is large enough no matter, whether the emission process is coherent or not.

Consequently we use a different estimate for the brightness temperature. The average flux is received from an area that can be well approximated by the projection of the polar cap to the emission height:

$$A = A_{\rm cap} x_{\rm em}^3\,. \tag{81}$$

The total radio luminosity over a frequency band of $\Delta\nu$ around the frequency ν can therefore be equated to the thermal flux of a blackbody with the appropriate brightness temperature. For broadband emission ($\nu = \Delta\nu$) and using eq. (78) we find

$$L = F_\nu \Delta\nu A_{\rm cap} x^3 \approx \frac{2\pi\nu^3}{c^2} k_{\rm B} T_{\rm B} A_{\rm cap} x_{\rm em}^3 \tag{82}$$

which yields a brightness temperature of

$$\begin{aligned} T_{\rm B} &= \frac{Lc^2}{2\pi\nu^3 k_{\rm B} A_{\rm cap} x_{\rm em}^3} = \\ &= 1.87\cdot 10^{23}\,{\rm K} \left(\frac{L}{10^{20}\,{\rm W}}\right) \left(\frac{\nu}{400\,{\rm MHz}}\right)^{-3} \left(\frac{P}{\rm s}\right) \left(\frac{x_{\rm em}}{50}\right)^{-3}\,. \end{aligned} \tag{83}$$

Note that there is no additional geometric factor as the estimate of the total radio luminosity already averages over some typical profile shape. The

values for the brightness temperature found in (83) are consistent with observationally deduced results (Sutherland, 1979, Kramer, 1995).

In the next step we show that our model is able to reproduce these fluxes under the assumption of a thin layer emitting coherent radiation. As already mentioned we propose a mechanism of the relativistic plasma emission type.

For the discussed process, particles are scattered by strong, nonlinear plasma waves (solitons) excited by the two-stream instability. So the radiation mechanism is equivalent to inverse Compton scattering (ICS) of solitons by relativistic electrons. As the particle approaches the wave with almost the speed of light we have to perform the same Lorentz transformations as for a relativistic electron scattering an electromagnetic wave.

For each particle coherent ICS radiates a power of

$$P_{\rm rad}^{\rm coh} = N\sigma_{\rm T}c\cdot\frac{E_{\rm wave}^2\varepsilon_0}{2}\gamma^2 \tag{84}$$

with the wave electric field $E_{\rm wave}$ if $\hbar\omega_{\rm wave} \ll m_{\rm e}c^2$, which is very well fulfilled for radio emission[5]. N is the coherence number, and γ^2 comes from the Lorentz transfomation of $E_{\rm wave}$. As long as the wave electric field is small, the wave can be treated linearly as a small density fluctuation. For an unstable situation the wave grows exponentially. Of course, growth saturates quickly for the wave will also accelerate particles as a back reaction. From that point on, wave growth has to be caluclated with the non-linear theory. The strongest possible wave has an electrostatic field energy comparable to the kinetic energy of the plasma. In the extreme, these two energy densities are equal

$$n_{\rm GJ}\gamma m_{\rm e}c^2 = \frac{1}{2}\varepsilon_0 E_{\rm wave}^2 \tag{85}$$

which means (84) can be rewritten as

$$P_{\rm rad}^{\rm coh} = N\sigma_{\rm T}cn\gamma^3 m_{\rm e}c^2\,. \tag{86}$$

Since particles are not assumed to be decelerated in the radio emission region, we can interpret the radiated power as an electric dissipation field (which is the field necessary to balance radiation losses). Its strength is

$$E_{\rm diss} = \frac{P_{\rm rad}^{\rm coh}}{ec} = \frac{2N\sigma_{\rm T}\Omega B_0\varepsilon_0 m_{\rm e}c^2}{e^2x_{\rm em}^3}\gamma^3\,. \tag{87}$$

[5]For higher wave energies the cross section is no longer described by $\sigma_{\rm T}$, so that the Klein-Nishina cross section ($\sigma_{\rm KN} \approx \sigma_{\rm T}(\ln\gamma)/\gamma$) must be used.

5.3 Extension of the radiation region and the maximum luminosity

Now we calculate the radial width of the radiation zone. This is an important test of the model, as the very small RFM taken from the observations requires a fairly narrow emission zone. Apart from that, the highly modulated radiation observed in the radio band would be hard to explain for too large a width.

In (87) the only the free parameter left is N. However, this number cannot directly be derived from the brightness temperature as mentioned before. Nevertheless there are upper limits for the coherence factor which serve to derive a minimum radial width of the emission region.

As we consider a plasma wave being the cause of coherence, the maximum volume of coherently radiating particles is a sphere of around one Debye volume. Taking into account relativistic effects, Melrose (1992) finds a maximum coherence volume of

$$V_{\mathrm{coh}} = \left(\frac{c}{\omega_{\mathrm{p}}}\right)^3 \frac{\gamma^2}{\pi} \tag{88}$$

and therefore

$$\begin{aligned} N_{\mathrm{max}} &= n_{\mathrm{GJ}} \left(\frac{c}{\omega_{\mathrm{p}}}\right)^3 \frac{\gamma^2}{\pi} = \sqrt{\frac{m_{\mathrm{e}}^3 c^6 \varepsilon_0 \gamma^7 x_{\mathrm{em}}^3}{2\Omega} B_0 e^5} = \\ &= 6.41 \cdot 10^{13} \gamma^{7/2} \left(\frac{P}{\mathrm{s}}\right)^{1/2} B_8^{-1/2} \left(\frac{x_{\mathrm{em}}}{50}\right)^{3/2} . \end{aligned} \tag{89}$$

Another hard limit for the dissipation field comes from plasma physics.

$$\sigma_{\mathrm{pl}} = \frac{\varepsilon_0 \omega_{\mathrm{p}}^2}{\nu_{\mathrm{coll}}} \geq \varepsilon_0 \omega_{\mathrm{p}} = \sqrt{\frac{n e^2 \varepsilon_0}{m_{\mathrm{e}} \gamma}} . \tag{90}$$

This restriction comes from the maximum collision frequency ν_{coll} (among particles or between particles and waves) for which ω_{p} is an upper limit. The conductivity of a plasma is given by

$$\sigma \approx \varepsilon_0 \frac{\omega_{\mathrm{p}}^2}{\nu_{\mathrm{coll}}} \tag{91}$$

(*e. g.* Krall & Trivelpiece, 1973) which leads to (90) when we set $\nu_{\mathrm{coll}} = \omega_{\mathrm{p}}$.

Another way of obtaining this limit is by equating the particle and the field energy density, since in the optimal case those quantities are comparable. More detailed calculations show that the field energy density is less than half of the particle energy density. This yields

$$\frac{\varepsilon_0 E^2}{2} \leq \frac{1}{2}\gamma n m_\mathrm{e} c^2 \tag{92}$$

which again reproduces (90).

Inserting this result into (87) we find a maximum coherence number of

$$\begin{aligned} N &= \sqrt{\frac{e^3 x_\mathrm{em}^3}{2\gamma^5 \Omega B_0 m_\mathrm{e} c^2 \varepsilon_0^2 \sigma_\mathrm{T}^2}} = \\ &= 3.79 \cdot 10^{15}\, \gamma^{-5/2} \left(\frac{P}{\mathrm{s}}\right)^{1/2} B_8^{-1/2} \left(\frac{x_\mathrm{em}}{50}\right)^{3/2} . \end{aligned} \tag{93}$$

Comparing the maximum coherence numbers from (89) and (93) we find that the latter is smaller whenever $\gamma \geq 1.97$. Therefore it is a good approximation to use (93) for determining the maximum coherence number.

For estimates of the radial extension of the radio emission region we take the total radio power and calculate the radiating volume necessary to reproduce the observed luminosities.

The total energy dissipation in a resistive current is given by

$$L = \int\limits_{V_\mathrm{rad}} E_\mathrm{diss} j \, \mathrm{d}V \tag{94}$$

where V_rad denotes the volume of the non-ideality.

E_diss is given by (87) and (93), $j(x) = n_\mathrm{GJ}(x) ec$, and by assuming that the non-ideality extends over the entire cross-section of open field lines; using a dipolar geometry and neglecting angular corrections to the GJ- density all quantities in (94) only depend on the radial coordinate. The volume element $\mathrm{d}V$ can be transformed to

$$\mathrm{d}V = r_\mathrm{NS} A_\mathrm{cap} x^3 \, \mathrm{d}x \, . \tag{95}$$

Here we have used (81), as the cross-section is a simple function of x. Therefore (94) reduces to a one-dimensional integral.

Inserting all the previous expressions the integral reads

$$L = \left(\frac{2\pi^2\nu^2 m_\mathrm{e}}{B_0\Omega e}\right)^{1/(2\alpha)} \sqrt{\frac{2\Omega B_0 m_\mathrm{e}c^2}{e}}\,\frac{2\Omega B_0\varepsilon_0}{e}ec \\ r_\mathrm{NS}\,\frac{\pi\Omega r_\mathrm{NS}^3}{c}\int\limits_{x_\mathrm{em}}^{x_\mathrm{em}+\tilde{l}_0} x^{3/(2\alpha)}x^{-3/2}\,\mathrm{d}x \tag{96}$$

where $\tilde{l}_0$ denotes the radial extension of the radiation region in units of r_NS, whereas x_em stands for the height of its inner edge in pulsar radii.

Evaluating the integral and inserting numbers for a frequency of $\nu = 400$ MHz we find

$$L = 5.56\cdot 10^{22}\mathrm{W}\left(\frac{P}{\mathrm{s}}\right)^{1/\alpha-5/2} B_8^{3/2-1/\alpha}F_\alpha \tag{97}$$

where

$$F_\alpha = 0.0286^{1/\alpha}\begin{cases} \tilde{l}_0 & \text{for } \alpha = 1 \\ 4\left[\left(x_\mathrm{em}+\tilde{l}_0\right)^{1/4} - x_\mathrm{em}^{1/4}\right] & \text{for } \alpha = 2 \\ \ln\frac{x_\mathrm{em}+\tilde{l}_0}{x_\mathrm{em}} & \text{for } \alpha = 3 \end{cases} \tag{98}$$

Solving this equation for $\tilde{l}_0$ in the case $\alpha = 3$ renders

$$\tilde{l}_0 = x_\mathrm{em}\left\{\exp\left[5.88\cdot 10^{-3}\left(\frac{P}{s}\right)^{13/6} B_8^{7/6}\left(\frac{L}{10^{20}\,\mathrm{W}}\right)\right] - 1\right\} \tag{99}$$

which, for typical parameters ($L = 10^{20}$ W, $P = 1$ s, $B_8 = 1$, $x_\mathrm{em} = 50$) yields $\tilde{l}_0 = 0.295$ which justifies the assumption of a narrow emission region. The dependence of $\tilde{l}_0$ and L is shown in fig. 30.

From the above result one can obtain sufficient luminosity even for slow pulsars. However, for small Ω the radial extension of the emission region increases. Especially, the corresponding electric field (87) can even exceed the vacuum field ($E_\mathrm{vac} = \Omega B_0 r_\mathrm{NS} x^{-4}$) which is not a relevant quantity in a shielded magnetosphere any more.

5.4 Micropulse flux enhancement by beaming effects

In this section we discuss anisotropy effects for pulse substructures which may enhance the observed brightness temperatures by up to several orders of magnitude. It is very unlikely that the flux enhancement only arises from

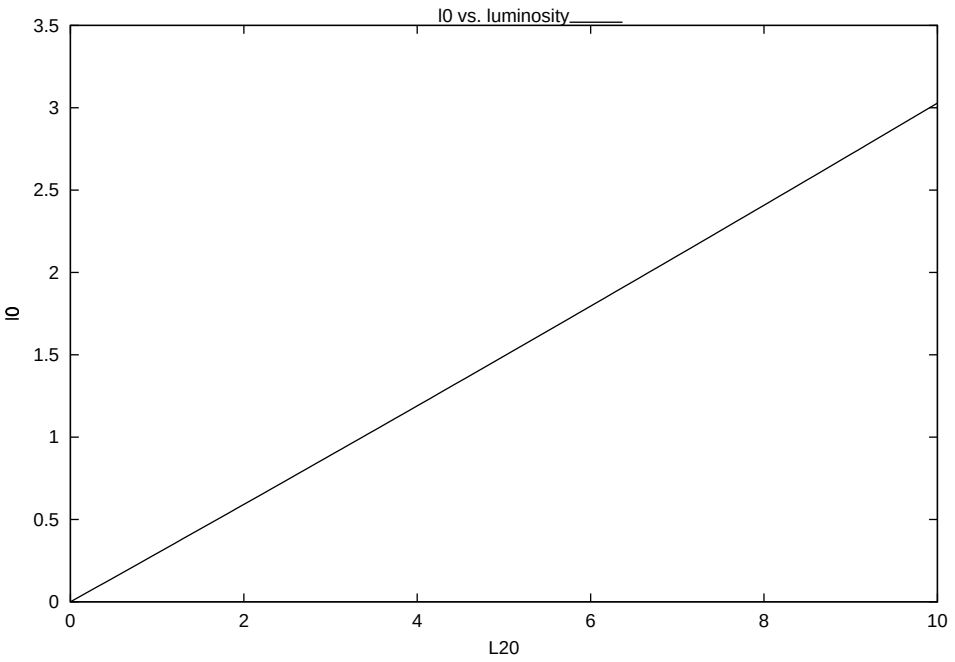

Figure 30: radial extension of the radio dissipation region versus luminosity for a standard pulsar ($P = 1$ s, $B_8 = 1$). The emission height $x_{\rm em}$ has been set to 50 pulsar radii.

a growth of the dissipation region. For the nanosecond structures of the Crab pulsar this is even impossible (if the width of the radio emission region jumped from only 0.001 (which is extremely narrow) to around 1 pulsar radius, the peak would occur on a timescale of $\tau_{\rm mic} \approx r_{\rm NS}/c \approx 3 \cdot 10^{-5}$ s. But as such small time scales also mean highly localized emission, the anisotropy of the elementary radiation process has to be considered. For an isotropic process there is a simple connection between the radiated power and the observed flux:

$$S_{\rm obs}(\nu) = \frac{1}{4\pi d^2} \frac{\partial}{\partial \nu} P_{\rm rad}(\nu) \tag{100}$$

where $P_{\rm rad}(\nu)$ is the total power emitted in frequencies below ν, whereas d denotes the transverse extension of the radiation region. For a rough quantitative estimation, we can set $P_{\rm rad}(\nu_{\rm crit}) = L$, and replace the derivative by a quotient. Thus we obtain the simpler equation

$$S_{\rm obs}(\nu_{\rm crit}) = \frac{L}{4\pi\nu_{\rm crit}d^2}\,. \tag{101}$$

This flux is drastically enhanced by two effects, producing a strongly anisotropic emission pattern. The first is the well-known relativistic lighthouse effect (Rybicki & Lightman, 1979). A relativistically moving source of isotropic radiation emits most of the power in a narrow cone with an angular opening of about $1/\gamma$ for $\gamma \gg 1$, as can easily be verified by performing the Lorentz transformation. The exact result is

$$\theta' = \arctan\left(\frac{1}{\gamma}\,\frac{\sin\theta}{(\cos\theta+\beta)}\right) \tag{102}$$

with θ being the angle between the direction of the flux and source velocity in the co-moving frame and θ' denoting this angle in the observer's system. For $\theta = 90^{\rm o}$ and $\gamma \gg 1$ the approximation $\theta' \approx 1/\gamma$ is very good. Therefore we find a flux enhancement of

$$\xi_1 = \frac{4\pi}{\pi/\gamma^2} = 4\gamma^2 \tag{103}$$

by the lighthouse effect.

Another anisotropy factor is the coherent radiation process itself, as has been shown by Kunzl *et al.* (1998b). To understand this effect, one has to recall that coherent emission requires a phase coupling of the emitting particles in one direction. For relativistic plasma emission, the preferred direction obviously is the direction of the streaming velocity (in the following called forward direction).

As long as the spatial dimension of the coherently radiating volume is small compared to the emitted wavelength, the interference is still constructive even under large angles to the forward direction. However, as soon as the extension of the coherence region becomes comparable to the wavelength, the coherent emitter can be seen as an antenna field producing intrinsically beamed emission.

For a quantitative estimation of this effect we introduce a coordinate system in which the velocity of the radiating particles in the observer's frame is in z- direction. As the situation is cylindrically symmetric, the problem can be reduced to two dimensions. As a second coordinate we use the angle α so that the (distant co-moving) observer's position is located in the direction $(\sin\alpha, 0, \cos\alpha)$. This is depicted in figs. 31 and 32.

To simplify, we assume the coherence volume to be cubic, with an edge length of

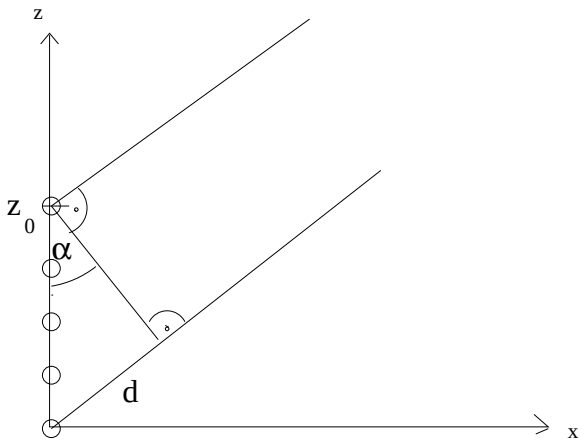

Figure 31: Phase difference for a particle shifted in z- direction relative to a reference particle at (0/0).

$$d = \left(\frac{N_{\mathrm{coh}}}{n}\right)^{1/3} \tag{104}$$

with the particle density n and under the (reasonable) assumption that all particles in the corresponding volume radiate in phase.

Now let the extension of the coherence cell be d, and the emitted wavelength λ. For an estimate of the beaming effect, we calculate the angle α_{min}, where the interference pattern has its first zero. Therefore we calculate the phase shift between the elementary waves from two particles at different positions if they show constructive interference in forward direction.

The phase difference is calculated relative to a reference particle at the lower left corner of the coherence cell (where we put the origin of our coordinate system). With $\delta(x, z)$ being the difference in the path lengths between the reference position and a particle at $(x, 0, z)$, the phase difference is

$$\Phi(x, z) = k\,[\delta(x, z) + z] \tag{105}$$

with the wave number of the emitted radiation $k = 2\pi/\lambda$. The second term in brackets guarantees constructive interference in the forward direction.

Two special cases can be treated separately:

1) $x_2 > 0$, $z_2 = 0$. From fig. 31 it can be seen that $\delta_1 = x \sin\alpha \approx x\alpha$ for small angles.

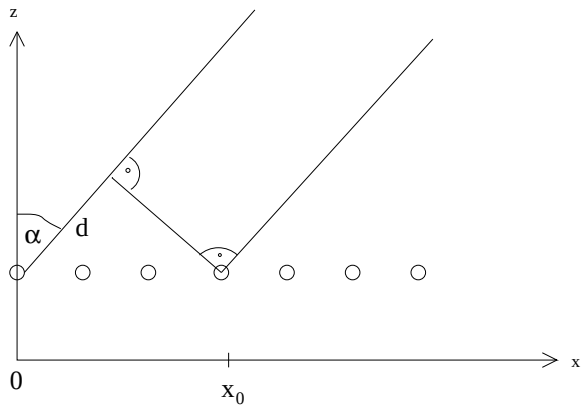

Figure 32: Phase difference for a particle shifted in x- direction relative to a reference particle at (0/0).

2) $x_2 = 0$, $z_2 = 0$. From fig. 32 we find a phase difference of $\delta_2 = -\cos\alpha \approx z(\alpha^2/2 - 1)$ for small α.

As these two phase differences are independent they can be added up. So (105) evaluates to

$$\Phi(x, z) = \frac{2\pi}{\lambda}\left(x\alpha + \frac{1}{2}z\alpha^2\right) . \tag{106}$$

The total amplitude is therefore

$$\frac{A}{A_{\mathrm{sp}}} = \sum_{i=1}^{N} \cos\Phi(x_{\mathrm{i}}, z_{\mathrm{i}}) \tag{107}$$

where A_{sp} is the single particle wave amplitude.

If $N \gg 1$ the sum can be replaced by an integral over a homogeneous density. Normalizing the integral to the interval $[0, 1]$ we find for $\alpha \ll 1$

$$\frac{A}{NA_{\mathrm{sp}}} = \int_0^1\int_0^1 \cos\left[\frac{2\pi d}{\lambda}\left(x\alpha + \frac{1}{2}z\alpha^2\right)\right] \mathrm{d}z\,\mathrm{d}x\,. \tag{108}$$

This double integral can be evaluated analytically:

$$\frac{A}{NA_{\mathrm{sp}}} = \frac{2}{T^2\alpha^3}\left(\sin a \sin b - \cos a \cos b + \cos a + \cos b - 1\right) . \tag{109}$$

Here $T := 2\pi d/\lambda$, $a := T\alpha$ and $b := T\alpha^2/2$. The first zero of (109) yields the condition $a = \pi - b$, which implies a simple quadratic equation for α. Thus we find the solution

$$\alpha_{\min} = \sqrt{1 + \frac{2\pi}{T}} - 1 \tag{110}$$

which is much smaller than unity for $T \gg 1$.

Similar to the lighthouse effect, we can use this angular extension to estimate the enhancement factor by coherence beaming. Thus the flux grows by a factor of

$$\xi_2 = \frac{4\pi}{\pi\alpha_{\min}^2} = \frac{4}{\left(\sqrt{1 + \frac{2\pi}{T}} - 1\right)^2}\,. \tag{111}$$

A more realistic treatment of the geometry uses a cylindrically symmetric soliton with a density profile proportional to $\cosh^{-2}(R_0/R)$ where $R_0 \approx \lambda_{\rm D}$ is the typical length scale. Numerical calculations for this structure show a much stronger anisotropy (Kunzl *et al.*, 1998b)

Combining the two anisotropy effects we find the total beaming factor

$$\xi := \xi_1\xi_2 = 16\gamma^2 \left(\sqrt{1 + \frac{2\pi}{T}} - 1\right)^{-2} \tag{112}$$

which, even with quite moderate parameters (like $\gamma = 10, x_{\rm em} = 50, N = 10^{13}$ for a typical pulsar), causes an enhancement of some 10^3. Therefore it can easily explain strong substructures, and micropulse brightness temperatures that are some 10^3 times above the mean value (Boriakoff, 1992).

As these beaming effects apply only to the elementary emission process, but do not enhance the mean flux significantly, it is an important check on whether the model can reproduce the observed brightness temperatures of up to 10^{31} K (Hankins, 1996) observed in *giant pulses* of the Crab pulsar (see fig. 11, chapter 2).

Therefore we take the maximum possible number of coherently radiating particles, and the corresponding beaming effects. Let A be an arbitrary cross section. Then starting with eq. (83) one can express the integrated flux $I := I_\nu\Delta\nu = L_{\rm radio,A}/A$ by the brightness temperature:

$$I := \frac{L_{\rm radio,A}}{A} = \frac{2\pi\nu^3 k_{\rm B} T_{\rm B}}{c^2}\,. \tag{113}$$

Inserting the critical frequency of the Crab pulsar $\nu = \nu_{\rm crit} = 160$ MHz and $T_{\rm B} = 10^{31}$ K, the integrated flux is

$$I = 3.95 \cdot 10^{16} \, \frac{\mathrm{W}}{\mathrm{m}^2} \, . \tag{114}$$

As this value means the beamed flux, the actual power per area is only

$$I_{\mathrm{real}} := \frac{I}{\xi} = 2.47 \cdot 10^{15} \frac{\mathrm{W}}{\mathrm{m}^2} \, \gamma^{-2} \left(\sqrt{1 + \frac{2\pi}{T}} - 1 \right)^2 \, . \tag{115}$$

Now we can compute the minimum thickness of a layer producing the power per cross-section. To obtain the lower limit we take the strongest dissipation field possible (see eq. (87)) and assume a coherence cell with a lateral extension of c/ν_{p}, so that $T = 2\pi\gamma$.

The total dissipated power from a volume with the cross-section A and the radial extension d is

$$P_{\mathrm{diss}} \stackrel{!}{=} I_{\mathrm{real}} A = E_{\mathrm{diss}} \, d \, j \, A \, . \tag{116}$$

For a relativistic Goldreich-Julian current $j = j_{\mathrm{GJ}} = n_{\mathrm{GJ}}(x) e c$ eq. (116) can be solved for d. Inserting the Crab pulsar parameters ($P = 33.4$ ms, $B = 3.8 \cdot 10^8$ T, $\nu = 160$ MHz, $x_{\mathrm{em}} = 80$) and additionally using eq. (75) we obtain

$$d = 3.85 \, \mathrm{m} \left(\frac{T_{\mathrm{B}}}{10^{31} \, \mathrm{K}} \right) \tag{117}$$

which corresponds to a time scale of

$$\tau := \frac{d}{c} = 1.28 \cdot 10^{-8} \, \mathrm{s} \left(\frac{T_{\mathrm{B}}}{10^{31} \, \mathrm{K}} \right) = 12.8 \, \mathrm{ns} \left(\frac{T_{\mathrm{B}}}{10^{31} \, \mathrm{K}} \right) \, . \tag{118}$$

Thus we can expect to see giant pulses on nanosecond timescales, with brightness temperatures above 10^{30} K, from far inside the light cylinder in the Crab pulsar, although the relative emission height will be considerably larger than for average pulsars. This idea is also supported by the observations that find a value of around 80 pulsar radii for the mean emission height.

Summarizing, we find that the current circuit description, together with a relativistic plasma emission process, can explain the observed radio luminosities, brightness temperatures and emission heights. The particles radiate in non-ideal regions, but their energy loss is balanced by a voltage drop, so that the (mean) kinetic energy remains unchanged.

The electric dissipation field is limited by the minimum conductivity in a plasma corresponding to the field strength, for which the energy densities of particles and waves are comparable. This limits the output power of a radiating sheet with a fixed radial extension, and therefore provides an estimate for the width of the dissipation region, which is needed to explain the observationally deduced luminosities.

It is found that, for young pulsars (which tend to have a very low radio efficiency), this region can be very thin, since the fields are strong enough and the cross section of the radiation zone is large. For slow pulsars (usually quite efficient radio emitters), we need a significantly thicker emission region. Though the time-averaged total radio power is not too well determined (Malov *et al.* (1994) find much larger values than Taylor *et al.* (1993)), our model predicts that the radial extension of the radiation region is small compared to the emission height in any case.

Of course, the emission zones broaden if either the radiation process is non-stationary (which is definitely the case) or coherence is less than maximum. Observational results suggest that old pulsars (showing a fairly spiky emission pattern) have a higher duty cycle (meaning each volume only radiates with a low probability at a certain time) than younger ones. For young pulsars, however, apparently coherence is lower but the temporal efficiency is large which is suggested by the smooth profiles (and also the giant pulses).

We emphasize that the model does not contradict the results of Kijak & Gil (1997, 1998), who suppose slightly higher emission distances for slower pulsars even though such a correlation would raise the extension of the radiation layer further. However, as this effect appears to be small, the corrections are not very significant.

In any case, the plasma resistivities are too small to dissipate a large fraction of the total voltage. This is because the shortcut resistance (which limits the current to a relativistic GJ current from the polar cap) is much higher than plasma-induced resistances, and is therefore responsible for the main dissipation (see next chapter).

However, different arguments are needed to explain the brightness temperatures of pulse substructures, or even giant pulses in the Crab pulsar. Here even the plasma limit fails to reproduce the observed values unless the emission region grew drastically. But for these small-scale structures the emission is definitely not isotropic. Two effects are responsible for the anisotropic emission, namely the relativistic lighthouse-effect and the beaming, due to the finite extension of the radiation region. With them the observed brightness temperatures of 10^{30} K and over on timescales of only

around 10 ns, observed in giant pulses of the Crab, can be explained. Nevertheless the emission must be produced in the higher magnetosphere, where large enough coherence numbers are allowed. But this is consistent with observational results which suggest an emission height of about 80 pulsar radii for the Crab.

For millisecond pulsars, the above considerations also apply. Since the radio luminosities of "recycled" neutron stars, and the emission heights, tend to be smaller, normally a thin radiation layer can be expected, so that no problems arise from the smaller magnetospheres.

Of course, there is a natural limit for the current-circuit description. This is the neutral surface where the "preferred" sign of charge changes, meaning that a (single-charged) current coming from one side cannot easily penetrate that surface. Processes in the vicinity of the neutral surface and beyond, as well as an idea for the global current, are discussed in the next chapter.

"You may call it 'nonsense' if you like", she said,
"but I have heard nonsense compared with which that
would be as sensible as a dictionary."
Lewis Carroll, *Through the Looking Glass*

6 Global current circuit models

In this chapter we propose a model for the global current structure in a pulsar magnetosphere. Hereby the neutral surface plays a crucial role, separating regions of positive and negative GJ charge.

In a weakly-inclined rotator there are no open field lines that cross the light cylinder in the positive region and do not intersect the neutral line (or none in the negative zone for almost antiparallel rotators). So, unless in a pulsar where the rotation and the dipole axes are almost perpendicular to each other, one sort of charge cannot flow off the surface freely. Additionally, the open field lines not crossing the neutral surface are usually curved away from the rotation axis close to the light cylinder, so that the flux of particles is reduced further.

In the following, let us consider a weakly inclined pulsar, in which the dipole and the rotational axis are almost aligned. In this case, there are only two possible ways, how positively charged particles can be transported to the outer magnetosphere. The most widely discussed idea is that a dense pair plasma flows out from an inner gap discharge; this is not affected very strongly by change of regions, as there are enough particles of both signs to shield the space charge fields effectively. The other possibility is that positive particles somehow flow across the magnetic field lines, and can therefore change from closed to open field lines without leaving the positive region. There is of course a third possibility – that there is copious pair production in an outer gap; but this also requires a procedure that transports particles to the outer regions.

As mentioned before, our findings presented in the previous sections strongly suggest that there is no pair production in the inner magnetosphere; so a mechanism of the second type is needed. The natural place for a single charge description to become invalid is the neutral surface. As the GJ density vanishes there, a pure electron current is reflected, and finally quenched by the virtual cathode, the space charge builds up, unless this is removed by another process. For inclined pulsars, we show in the following section that a particle drifting in purely toroidal direction along the neutral surface can be transported from one ("blocked") field line to another, where

it can escape freely and thus reduce the space charge on the neutral line. As a secondary effect the "free" (open) field lines are "favourably" curved in the Arons sense, and can therefore efficiently accelerate charges up to the pair cascade threshold (similar to the outer gap scenario in Cheng *et al.* (1986)). Consequently, charges of the other sign flow back towards the neutral line from outside, and thus return some particles into the inner regions. Apart from that, e.g., positive particles may drift into negative zones, to reduce the virtual cathode caused by curvature effects. Altogether, a large number of charges of both signs accumulate at the neutral surface. As will be shown later, a radial GJ outflow together with a narrow drift region requires a high particle density in a layer near the neutral line.

A similar effect applies to the "unfavourably" curved open field lines which do not intersect the neutral surface. Drift motion slowly transports particles on these field lines, and finally balance curvature effects completely so that, apart from plasma waves, a Goldreich-Julian DC current flows outwards.

It must be mentioned that the drift mechanism described here requires enough charges of both signs in the magnetosphere. Once the situation is established, the outer gap always feeds the inner regions with dense plasma but if we start with a (hypothetic) initial condition of a neutron star surrounded by vacuum, positive ions will be dragged from the surface as well as electrons and form a charge layer on the neutral surface that initiates the drift mechanism and provides particles that can be accelerated in the outer gap. In the following discussion we therefore neglect such initial effects and assume that inside the neutral surface cone there are enough charges to avoid large depletion zones.

6.1 The neutral line and drift in an inclined rotator

In contrast to the parallel rotator, a finite angle between dipole and rotation axis removes the cylindrical symmetry of the GJ solution, so that the magnetosphere must be treated fully three-dimensional. For exemplary studies of typical properties, however, it suffices to study the two-dimensional cut through the neutron star centre containing the rotational and dipole axis. In this cut the two neutral lines are not equivalent. A schematic view of this scenario is shown in fig. 33.

To compute the angles between neutral lines and rotation axis we take the dipole parameter equation

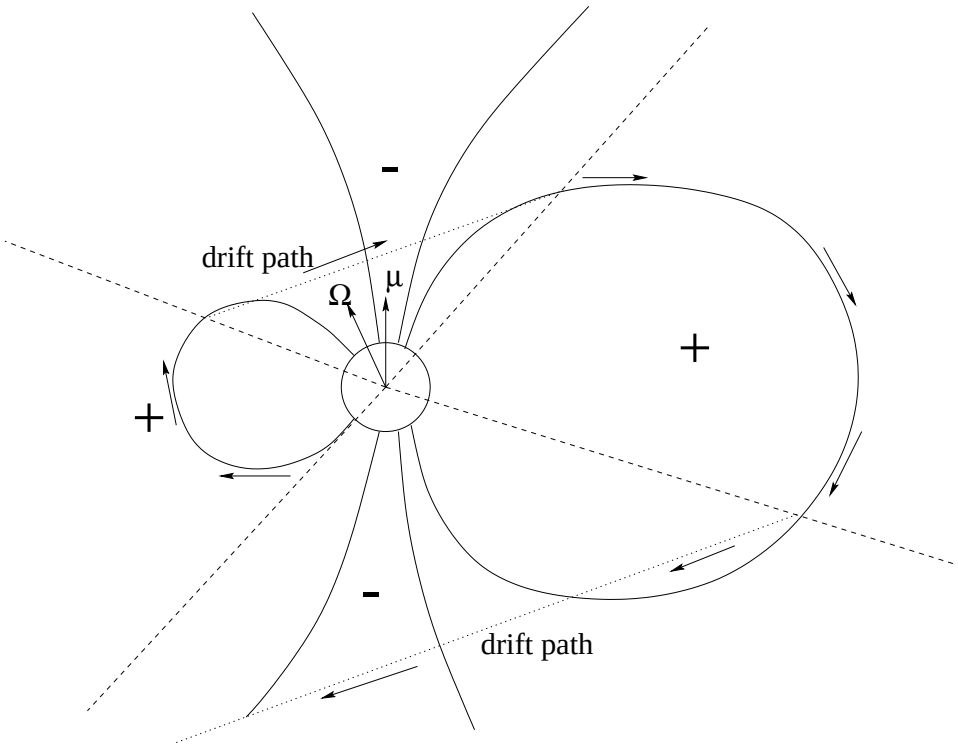

Figure 33: Dipolar geometry with the "neutral lines" in an inclined rotator. Particles are assumed to drift toroidally along the neutral cone (dotted line) and thus interchange between non-equivalent field lines (see text). The arrows mark a possible path for a positive charge flowing outwards to the light cylinder without leaving the positive region.

$$\frac{r}{r_{\rm NS}} = \frac{\sin^2\theta}{\sin^2\theta_0} \tag{119}$$

where θ and θ_0 are the polar angles of the point, and the intersection field line/neutron star surface. Here as in the following discussion $\theta = 0$ means the rotation axis.

Taking the θ- derivative of (119) we find

$$\frac{{\rm d}r}{{\rm d}\theta} = 2\sin\theta\cos\theta\frac{r_{\rm NS}}{\sin^2\theta_0} = 2\frac{r}{\tan\theta}\,. \tag{120}$$

Furthermore a geometrical analysis of the neutral line (fig. 34) renders the second condition

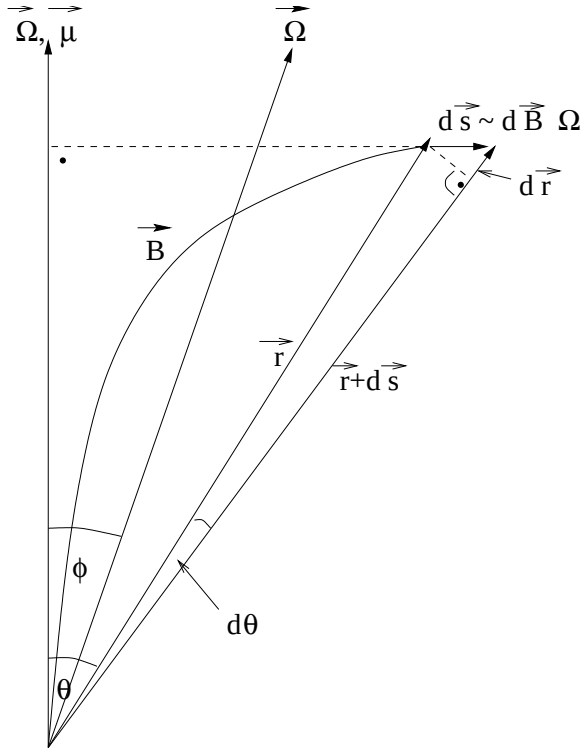

Figure 34: Dipolar geometry with the neutral line for a parallel and inclined rotator. $\mathrm{d}\vec{s}$ is an infinitesimal vector along the magnetic field line which is supposed to be orthogonal to $\vec{\Omega}$. This determines the angle of the neutral line.

$$\frac{\mathrm{d}r}{\mathrm{d}\theta} = r\,\tan\theta\,. \tag{121}$$

Combining these two equations we find the well-known result for the neutral line in the parallel rotator:

$$\tan^2\theta = 2 \Longrightarrow \cos^2\theta = \frac{1}{3}\,. \tag{122}$$

The same procedure can be applied to inclined rotators. The only difference is that (119) must be replaced by

$$\frac{r}{r_{\mathrm{NS}}} = \frac{\sin^2(\theta-\phi)}{\sin^2(\theta_0-\phi)} = \left(\frac{\sin\theta\,\cos\phi - \cos\theta\,\sin\phi}{\sin\theta_0\,\cos\phi - \cos\theta_0\,\sin\phi}\right)^2 \tag{123}$$

where ϕ is the inclination angle. Analogous to the parallel case we find

$$\begin{aligned}\frac{\mathrm{d}r}{\mathrm{d}\theta} &= \frac{2\,(\sin\theta\,\cos\phi-\cos\theta\,\sin\phi)}{(\sin\theta_0\cos\phi-\cos\theta_0\,\sin\phi)^2}\,(\cos\theta\,\cos\phi+\sin\theta\,\sin\phi)\,r_{\rm NS} = \\ &= 2\frac{r}{\tan\left(\theta-\phi\right)}\,. \end{aligned} \tag{124}$$

The second condition (121) remains the same. Combining this with the previous equation we obtain

$$\tan\theta = 2\frac{1+\tan\theta\,\tan\phi}{\tan\theta-\tan\phi} \tag{125}$$

which evaluates to a quadratic equation for $\tan\theta$:

$$\tan^2\theta - 3\tan\phi\,\tan\theta - 2 = 0\,. \tag{126}$$

Therefore the neutral lines appear under the angles

$$\theta_{\rm NL1/2} = \arctan\left(\frac{3\tan\phi \pm \sqrt{9\tan^2\phi+8}}{2}\right)\,. \tag{127}$$

The angular distance between the neutral lines and the dipole axis is given by $\left|\phi-\theta_{\rm NL1/2}\right|$. This means that the two "neutral lines" are asymmetric relative to the dipole axis. In other words, by inserting the neutral line angles into the dipole equation, the calculations presented above show that the last open field lines intersect the neutral lines at different distances.

Using these results, the path of a positive particle from the surface to the open field lines in the positive region can be described for a weakly-inclined rotator.

A particle starting at the pulsar surface on a closed field line intersecting the neutral line with a footpoint angle θ_0 reaches the neutral line at a distance of

$$\frac{r}{r_{\rm NS}} = \frac{\sin^2(\phi-\theta_{\rm NL2})}{\sin^2\theta_0} \tag{128}$$

and may drift along the neutral surface to the other side at the same radial distance. Therefore the new angle relative to the magnetic axis is only $|\phi-\theta_{\rm NL1}|$, so that the new field line has its footpoint at the smaller angle

$$\theta_1 := \arcsin\left(\sin(\phi-\theta_{\rm NL1})\frac{|\sin(\phi-\theta_{\rm NL2})|}{\sin\theta_0}\right) \tag{129}$$

relative to the dipole axis. If this field line is still closed, the particle can flow along it to the other point of intersection with the neutral surface, where the same process starts afresh. Thus, the footpoint angle of the corresponding field lines decreases, until an open field line is reached. At this point the particle is accelerated freely out towards the light cylinder. An analogous mechanism is valid for electrons. Therefore particles of both charges can be transported to the regions beyond the neutral surface, provided that the drift is efficient enough. This will be discussed in the next section.

6.2 A (semi-) quantitative description of neutral line drift

To obtain some quantitative results on charge densities, drift velocities and particle densities in the region near the neutral line, we calculate the drift field for a very simple configuration. In the following a number of simplifying assumptions are made. On the one hand we assume that all curvature effects influencing the GJ- density are balanced by particles of the other sign, drifting into regions where the opposite charge dominates. Therefore all field lines can transport a stationary relativistic GJ- current up to the neutral line. This assumption might be a little bold, but at some distance from the neutral line curvature effects must be balanced, otherwise the outflowing current on such a field line would be zero. If this balance only allowed a certain fraction of the GJ current to flow, further reasoning would not change significantly. To enable efficient drift, the neutral surface must be charged. The simplest case is an azimuthally symmetric charge configuration, with only a radial dependence. As in a weakly inclined rotator the polar cap field lines are in the electron domain, we set the sign of the neutral surface charge to a negative value. Thus the additional field is that of a (for the sake of simplicity) homogeneously positively charged inner ball, surrounded by two conal layers with negative surface charge density (as shown in fig. 35).

In this case the charge density reads

$$\rho = -\rho_0 \delta\left(\theta - \theta_0\right) \left(\frac{R}{r}\right)^3 \tag{130}$$

for the outer part and

$$\rho_{\text{inner}} = \frac{3q}{4\pi R^3} \tag{131}$$

for the positively charged inner region. Here ρ_0 denotes the (positive) charge density at the inner end of the drift region, R its distance from the

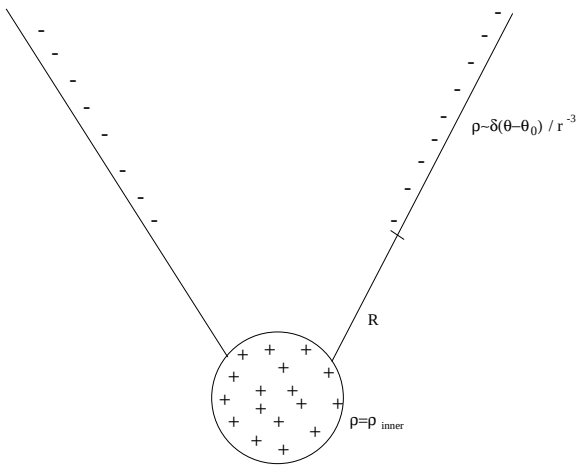

Figure 35: Assumed simplified charge distribution for a neutral line drift model. The absolute value of the charge density determines the efficiency and the width of the drift region. For details see text.

neutron star centre, θ_0 is the opening angle of the neutral surface cone, and

$$q := 2\pi\rho_0 R^3 \sin\theta_0 \ln\frac{R_{\max}}{R} \tag{132}$$

is the total (negative) charge on the neutral surface. Using Poisson's equation this yields a potential of

$$\begin{aligned}\Phi(\vec{r}) &= \Phi_0 + \vec{E}_0\cdot\vec{r} + \frac{3\sin\theta_0}{2\varepsilon_0}\rho_0 \ln\frac{R_{\max}}{R}\left(\int_0^R\int_0^{2\pi}\int_0^{\pi}\frac{r'^2\sin\theta'}{\left|\vec{r}-\vec{r'}\right|}\,\mathrm{d}\theta'\,\mathrm{d}\phi'\,\mathrm{d}r'\right.\\ &- \left.\frac{\rho_0 R^3}{\varepsilon_0}\int_R^{R_{\max}}\int_0^{2\pi}\frac{r'^2\sin\theta_0}{r'^3}\frac{1}{\left|\vec{r}-\vec{r'}\right|}\mathrm{d}\phi'\,\mathrm{d}r'\right).\end{aligned} \tag{133}$$

In spherical coordinates and for this special case we have

$$\left|\vec{r}-\vec{r'}\right| = \sqrt{r^2 + r'^2 - 2rr'\cos(\theta-\theta')\cos\phi'} \tag{134}$$

as follows from the cosine theorem for a spherical triangle.
For the positively charged inner region radial symmetry allows the assumption $\theta = 0$, whereas for the outer part we can evaluate the integral for $\phi = 0$. Therefore we find the expression

$$\Phi(\vec{r}) = \Phi_0 + \vec{E}_0 \cdot \vec{r} + \frac{3\pi\rho_0 \sin\theta_0}{\varepsilon_0} \ln\frac{R_{\max}}{R} \left[\int_0^R \int_0^\pi \frac{r' \sin\theta'}{\sqrt{r^2 + r'^2 - 2rr'\cos\theta'}} \mathrm{d}\theta' \, \mathrm{d}x \, \mathrm{d}r' - \right.$$
$$\left. - \frac{\rho_0 R^3}{\varepsilon_0} \int_R^{R_{\max}} \int_0^{2\pi} \frac{\sin\theta_0}{r'\sqrt{r^2 + r'^2 - 2rr'\cos(\theta - \theta')\cos\phi'}} \, \mathrm{d}\phi' \, \mathrm{d}r' \right] \qquad (135)$$

which, however can only be evaluated numerically. We are only interested in the electric field perpendicular to the both magnetic field line, and the rotation velocity, so that we have to take the numerical derivative of the potential in that direction. Due to the rotational symmetry of the charge distribution, the electric field does not have a ϕ- component. For a very rough estimation, we can assume the electric field to be exactly parallel to $\vec{v} \times \vec{B}$ (otherwise the result must be multiplied by a cosine factor very close to 1). We evaluate the potential for two points whose connection line is parallel to $\vec{\Omega}$ and intersects the neutral surface in the middle. An approximate value of the electric field can be obtained by dividing the potential difference by the distance between these two points.

Then the numeric value yields

$$E_{\mathrm{drift}} = 5.29 \cdot 10^9 \frac{\mathrm{V}}{\mathrm{m}} \left[\frac{\rho_0}{\rho^{\parallel}_{\mathrm{GJ}}(R)} \right] \left(\frac{d}{r_{\mathrm{NS}}} \right) \left(\frac{R}{r_{\mathrm{NL}}} \right)^{-1} \left(\frac{P}{\mathrm{s}} \right)^{-1} B_8 \, . \qquad (136)$$

Here we have considered the fact that the charge layer is not really infinitesimally thin, but has a finite width and charge density. To avoid confusion, we mention that r_{NL} means the radial distance where the last open field line intersects the neutral line in the parallel case (2/3 of the light cylinder radius). Since r_{NL} is only used as a scaling factor, it does not matter that this distance has no special meaning in the inclined case. As we see in the following, effective drift is possible for typical charge densities of the (parallel) GJ value, and a thickness of about one neutron star radius.

For a relativistic drift velocity in azimuthal direction, the condition $E \geq Bc$ must be satisfied (corresponding to $\beta(v_{\mathrm{drift}})\gamma(v_{\mathrm{drift}}) \geq 1$). As an upper limit for the inner edge of the drift region we can take the distance where the last open field line crosses the neutral surface which is about 2/3 of the light cylinder radius. Thus we find for the charge density necessary for a relativistic drift current

$$\frac{\rho_0}{\rho^{\parallel}_{\rm GJ}(R)} = 7.02 \cdot 10^{-4} \left(\frac{d}{r_{\rm NS}}\right)^{-1} \left(\frac{R}{r_{\rm NL}}\right)^{-2} \left(\frac{P}{1/2\,{\rm s}}\right) B_8\,. \qquad (137)$$

The actual charge density needed will be significantly higher as the drift region be further inside, because positive particles on closed field lines have also to drift effectively. However, even if drift already occurs deep inside the intersection of the last open field line with neutral surface, a thin drift region with a dense, almost quasineutral pair plasma produced in the outer gap is consistent with (137). But if we have an estimate of the charge density the minimum distance allowing relatvistic drift can be computed.

An additional condition to $E_{\rm drift} \geq Bc$ is that a relativistic GJ- current flows through the neutral surface. This gives another hint that we need a dense plasma with both signs of charge on the neutral surface, to obtain a thin drift region. The latter fact can be easily understood:

Consider an almost neutral plasma with a negative excess of

$$\varepsilon_- = (n_- - n_+)/(n_- + n_+)\,. \qquad (138)$$

The typical azimuthal distance, which a particle must travel to reach a free field line in the appropriate region can be estimated as almost a semicircle ($\pi r_\perp$) with a length comparable to the radial distance from the neutron star. Let the drift velocity be relativistic then the radial velocity is

$$v_{\rm rad} = \frac{d}{r}c \approx \frac{c}{x_{\rm NL}} \approx \varepsilon_- c\,. \qquad (139)$$

Here the latter approximation applies if the drift region is about one pulsar radius wide at the intersection point of the last open field line with the neutral surface. To obtain a relativistic radial GJ current from this non-relativistic particle speed, we find from (139):

$$\frac{n_- + n_+}{n^{\parallel}_{\rm GJ}} \approx \frac{r}{d} \approx x_{\rm NL}\,. \qquad (140)$$

Of course this idea still requires that the particles of the outward directed current and those carrying the inflowing current interpenetrate, but without significant interaction. This restriction, however is a very mild one, since, due to the high azimuthal speed, the particles flow almost parallel anyway. Therefore no significant streaming instabilities should occur.

Summarizing, the neutral line drift model proposes a mechanism, by means of which particles can surmount the hurdle at the neutral surface,

where a single charge current from the inner regions of the magnetosphere cannot flow further outwards along the field line. For various regions, a high number density of charges in an almost neutral plasma is necessary. On one hand, both charges have to be transported to other field lines, furthermore a relativistic GJ current in radial direction, together with a thin drift zone, requires a high number density. Apart from that, the charged neutral surface also creates an electric field *parallel* to $\vec{B}$. To prevent acceleration, a pair plasma can become polarized and thus shield parallel fields effectively, whereas the orthogonal component of $\vec{E}$ remains, because polarization of charges is not possible across the magnetic field.

Dissipation occurs because the current circuit is open, (that means, particles of both charges stream outwards through the light cylinder). In other words, the major part of the energy is not transferred to the current-carrying particles but to secondary charges forming the wind and radiating high energetic emission. Of course, a significant part of the energy may still be radiated away via direct electromagnetic emission from the winding up of the magnetic field. But all these effects can be combined so that the main dissipation occurs beyond the neutral surface, and cannot be described by a simple particle flow along a parallel electric field. Therefore, effectively, e.g. negative particles start at a field line close to the magnetic pole and return at a lower latitude and a higher potential. A global resistance picture, motivating a mildly relativistic flow in the inner magnetosphere, developed in the next section.

6.3 Resistance and its limitation for particle energies

It was shown in the previous section that drift at the neutral surface can effectively transport a full GJ current from open field lines to the last closed field line from where it can return to the neutron star. Now we assume that all curvature effects in the inner magnetosphere (meaning closed field lines and open ones inside the neutral surface) are balanced by particles of the opposite charge drifted inwards, so that the full parallel GJ-current can flow on every open field line. As discussed in the previous section this assumption is reasonable, as inside the neutral surface, every field line is "unfavourably curved" in the Arons sense. This means, every finite current density produces a virtual cathode somewhere near the neutral line.

A highly relativistic current flowing off both polar caps has the total value

$$I_{\rm total} = 2A_{\rm cap} n_{\rm GJ} ec = 2\pi \frac{\Omega}{c} r_{\rm NS}^3 \frac{2\Omega B_0 \varepsilon_0}{e} ec = 4\pi r_{\rm NS}^3 \varepsilon_0 \Omega^2 B_0 \tag{141}$$

This current faces an average voltage drop of

$$\Delta V = \frac{1}{6c} r_{\rm NS}^3 \Omega^2 B_0 \tag{142}$$

as we obtain by assuming that all electrons return at the edge of the polar cap, and averaging the voltage over that region using the small angle approximation (i.e. $\Delta V \sim (\theta_{\rm cap} - \theta)$).

Calculating the total resistance as

$$R = \frac{\Delta V}{I_{\rm total}} = \frac{1}{24\pi c \varepsilon_0} = \frac{Z_0}{24\pi} \tag{143}$$

it turns out to be completely independent of any pulsar parameter, and a fraction of the vacuum impedance Z_0. This is a clear indication that this resistance is intrinsic to the pulsar system, and has nothing to do with plasma effects. In other words, it can be identified with the outer magnetosphere dissipation region[6].

However, the above calculation of the resistance is not quite correct, as, although the particles are relativistic, their velocity is still below c. Therefore the true current is a little less, and the actual resistance larger. The ratio of the true and the ultrarelativistic resistance is about $1 + 1/(2\overline{\gamma}^2)$, where $\overline{\gamma}$ is the Lorentz factor belonging to the mean *velocity* of the particles. For $\overline{\gamma} \gg 1$ this can be transformed into

$$\varepsilon_{\rm pl} = \frac{1}{2\overline{\gamma}^2} \Longrightarrow \overline{\gamma} = (2\varepsilon_{\rm pl})^{-1/2} \tag{144}$$

with the fraction of dissipation in the inner magnetosphere $\varepsilon_{\rm pl}$, which includes radio emission and other losses there. In this framework radio emission alone (with a typical efficiency of 10^{-5}) limits the mean Lorentz factor to only 200. If even X-ray emission comes from a region close to the neutron star, the X-ray efficiency of 10^{-3} (Becker & Trümper, 1997) would

[6]Here it must be mentioned that the result will certainly have to be modified for a finite inclination, non-dipolar components or even due to angular effects producing a small period dependence. Thus the mean voltage drop and the total current might be different from the ΔV and $I_{\rm total}$ used above. The important point, however, is that as soon as the highly relativistic (=maximum) current is fixed by geometry, i.e. by period and inclination angle, the system-immanent resistance is given, and the following reasoning remains, in principle, unchanged.

even limit $\overline{\gamma}$ to 20. **This is in clear contradiction to an inner gap and ultrarelativistic particles in the inner magnetosphere.** But, even for wide radio emission regions, the plasma resistance is negligible compared with the shortcut value, which means, the particles can still be relativistic, as follows from (144). So a relativistic current is always coupled to a small radio efficiency. The argument is also valid the other way round - a small radio efficiency allows mildly relativistic particles - under the condition that no other efficient loss process occurs in the magnetosphere.

Additional losses can be caused by internal friction on the neutron star surface meaning that the polar cap is a "hot spot". For example, if a significant part of the pulsed soft X-ray emission is of thermal origin, a hot polar cap would be required and some additional power could be lost by the mild heating of the whole neutron star.

A hot polar cap with a surface temperature of $T = T_6 \cdot 10^6$ K emits the power

$$P_{\mathrm{therm}} = A_{\mathrm{cap}} \sigma_{\mathrm{SB}} T^4 = 3.73 \cdot 10^{21}\,\mathrm{W}\, T_6^4 \left(\frac{P}{\mathrm{s}}\right)^{-1} \tag{145}$$

For a temperature of several million kelvins this radiated power is compatible with a frictional re-heating of the polar cap and thus an additional dissipation.

However, such a scenario implies a slightly more efficient friction mechanism in young, quickly rotating pulsars than in slower, ones since the relativistic plasma process for the radio emission suggests slightly higher particle energies for the latter category. This might come from the surface temperature of the neutron star, which decreases with increasing age.

The most natural limit for the current is the particles' inertia. As the current-carrying particles have finite mass they also acquire kinetic energy; i. e., a (small) part of the voltage is used for particle acceleration. If the beam is monoenergetic and if inertia were the *only* energy limiting factor, the corresponding equation reads

$$1 - \beta = \frac{m_{\mathrm{e}} c^2}{e \Phi_0} \gamma \tag{146}$$

with the total potential difference Φ_0, having the approximate solution

$$\gamma = \left(\frac{e \Phi_0}{2 m_{\mathrm{e}} c^2}\right)^{1/3} \tag{147}$$

which is only about 300 for a typical pulsar. This limit is, of course,

raised for an energy distribution. For instance, taking a Jüttner distribution (Melrose & Gedalin, 1999) the inertia limit for the mean Lorentz factor is

$$\overline{\gamma} = \left(\frac{\pi e \Phi_0}{2 m_\mathrm{e} c^2} \right)^{1/2} \tag{148}$$

which is about 5000 for a standard pulsar. Nevertheless, it is important that in neither case the is energy sufficient to initiate a pair cascade. This argument is, of course, not valid if the density if far below n_GJ but is nevertheless also applicable to inner gap models as losses would strongly enhance the fraction of the dissipated power in the inner magnetosphere and reduce the total current.

Other loss mechanisms are, for example resonant inverse Compton scattering (Sturner, 1995), curvature radiation (very ineffective), centrifugal forces in non-ideality regions and so on. A detailed discussion of these effects is beyond the scope of this work.

6.4 Outer magnetosphere acceleration and high energetic radiation

A particle drifting along the neutral surface reaches a free field line at some point, whence it can travel further outwards. Since in this region the field line, is "favourably curved" in the Arons sense, there is always an underdense region on such a field line, which means that particles can be accelerated effectively. (In analogy to other outer gap models, we will also call this region "outer gap" in the following.) Therefore one can expect very high Lorentz factors close to the light cylinder. Consequently the high-energetic radiation (apart from a possible thermal or ICS X-ray component) must be produced in the outer gap region. A promising candidate for a radiation process in the outer magnetosphere is synchrotron radiation. We showed that the mechanism can produce the observed spectra in the different frequency bands by only varying the pitch angle regime (Crusius *et al.*, 2001). This is because the observed fluxes and peak frequency depend on the ratio of the pitch angle, the profile width and the emission cone by the lighthouse effect. For the Crab pulsar the model can naturally explain the high energy emission from the Crab pulsar quantitatively from the infrared to γ-rays. Our argumentation is outlined briefly:

Observations of the Crab pulsar show a steeply rising spectrum in the infrared (the spectral index is negative, around -2), which continues almost flatly in the optical range and drops with spectral indices from around 0.5 in the soft X-rays via 0.7 for the hard X-rays to 1.1 in the γ- region (Toor &

Seward, 1977, Eikenberry, 1998). The power emitted by the Crab pulsar over the whole electromagnetic spectrum is sketched in fig. 8. For other pulsars it is still not settled whether there is non-thermal pulsed emission in the infrared and optical range. The results of Nasuti *et al.* (1997) suggest non-thermal optical radiation for at least 3 pulsars (Crab, Vela and PSR 0540-69) as the flux seems to be constant over the optical range and is significantly above the thermal extension of the X-ray spectrum to low frequencies.

There are clear indications that the intrinsic radiation spectrum is not significantly modified by absorption in the wind or nebula. However, for the Vela pulsar (the weakest optical source) the optical spectrum might be thermal but modified by the pulsar's hydrogen atmosphere. Nevertheless the optical emission of the Crab pulsar cannot be explained by a thermal process.

Comparing the efficiencies of the two most likely processes in an outer gap environment, namely small angle synchrotron radiation

$$P_{\mathrm{syn}} = 1.6 \cdot 10^{-14} \mathrm{W}\, \gamma^2 \left(\frac{B}{\mathrm{T}}\right)^2 \sin^2 \Psi \,. \tag{149}$$

where Ψ is the pitch angle and curvature radiation whose power is given by (46) it turns out that for

$$\Psi \geq 1.7 \cdot 10^{-4} \left(\frac{\gamma}{10^7}\right) \left(\frac{B}{100\,\mathrm{T}}\right)^{-1} \left(\frac{R_{\mathrm{C}}}{10^6\,\mathrm{m}}\right)^{-1} \tag{150}$$

(where the small angle approximation $\sin \Psi \approx \Psi$ has been used) the first process is the dominating one. Using a purely dipolar geometry, one finds that typical curvature radii beyond the neutral surface are at least 10^6 m even for the Crab pulsar, so that $\Psi \approx 10^{-4}$ suffices to make CR losses unimportant if the Lorentz factor does not exceed 10^7.

The Lorentz factors of primary particles can be estimated by equating synchrotron losses with the gains from the outer gap electric field. Taking a typical value from the Cheng, Ho and Ruderman model (Cheng *et al.*, 1986) we obtain

$$E_{\mathrm{gap}} = Bc\delta^2 \cos\phi \tag{151}$$

with $\delta \approx 0.1$ being the ratio of the gap width to the light cylinder radius, and ϕ again denoting the inclination angle. Evaluating the expression for the Crab pulsar near the light cylinder renders

$$\gamma_{\rm syn} = 9.5 \cdot 10^6 \cos^{1/2}\alpha \left(\frac{\delta}{0.1}\right) \left(\frac{B}{100\,{\rm T}}\right)^{-1/2} \left(\frac{\Psi_{\rm p}}{10^{-3}}\right)^{-1} . \qquad (152)$$

In the following we show that a pitch angle of 10^{-3} is sufficient to explain the observed high energy luminosities, provided that the primary particles with a Lorentz factor of about $\gamma_{\rm syn}$ are efficiently converted to lower energetic pairs with a power law spectrum of spectral index 2. Such an energy distribution can be expected from numerical results but can also be understood by using a very simple argument (Crusius *et al.*, 2001):

Consider an acceleration region producing primary particles of a characteristic Lorentz factor $\gamma_{\rm p}$. In a very efficient pair cascade each primary particle decays into $M(\gamma)$ secondaries of the energy γ. The probability for a certain terminal Lorentz factor is constant over a wide range of γ. Then energy conservation leads to the obvious condition

$$M(\gamma) = \frac{\gamma_{\rm p}}{\gamma} . \qquad (153)$$

To find the distribution function we have to take the differential number density which means the number of particles per γ interval. This yields

$$N(\gamma) \sim \frac{M(\gamma)}{\gamma} = \frac{\gamma_{\rm p}}{\gamma^2} \qquad (154)$$

or a power law distribution with a spectral index of 2. The low energetic cutoff occurs at the point where cascading is no longer efficient, and therefore the argument is not applicable any more.

Due to momentum conservation it can be expected that the pairs have about the same pitch angle as the primary particles ($\Psi \approx \Psi_{\rm p} \approx 10^{-3}$).

For the small pitch angle regime (i.e. $\Psi \leq 1/\gamma$) we have to distinguish between two cases. The very small pitch angle description applies if the resolved pulse width $\Delta\Phi$ (around 10^{-2}) is much smaller than the angle of the emission cone (which is about $1/\gamma$). Then all the emission can be assumed to be perfectly in forward direction, and no angular dependence needs to be taken into account.

The emissivity of a particle at low pitch angles is given by

$$\varepsilon_\nu(\theta,\gamma) = \frac{4e^2\gamma\Psi^2\nu^3}{\nu_{\rm c} c \varepsilon_0} \left(1 - \frac{\nu}{\gamma\nu_{\rm c}} + \frac{\nu^2}{2\gamma^2\nu_{\rm c}^2}\right) \delta\left(\nu - \frac{2\gamma\nu_{\rm c}}{1+\theta^2\gamma^2}\right) \qquad (155)$$

(Epstein, 1973), where θ is the angle between the magnetic field and the direction of emission. Setting $\theta = 0$ and folding the result with a power law energy distribution $N(\gamma) \sim \gamma^{-s}$, the total spectral emissivity becomes

$$I_\nu = \int \varepsilon_\nu(0,\gamma) N(\gamma)\,\mathrm{d}\gamma = \frac{N_0 e^2 \Psi^2 \nu_\mathrm{c}^2}{\varepsilon_0 c} \left(\frac{\nu}{2\nu_\mathrm{c}}\right)^{4-s} \tag{156}$$

which yields a steeply rising spectrum with a spectral index of -2 as observed for the infrared.

The limiting frequency for this description (i.e. the frequency where $\gamma(\nu) \approx 1/\Delta\Phi$) is in the transition region between infrared and optical bands.

In the second case ($\Psi \ll 1/\gamma \ll \Delta\Phi$) we have to use the angle averaged spectrum. With these assumptions the integrated flux

$$L_\mathrm{p} = \int_0^\infty \varepsilon_\nu\,\mathrm{d}\nu = \frac{2\pi e^2 \nu_\mathrm{c}^2 \gamma^2 \Psi^2}{3\varepsilon_0 c} \tag{157}$$

is sharply peaked around $\nu = 2\gamma\nu_\mathrm{c}$ so that a monochromatic approximation can be used.

For the same particle energy distribution as above we then obtain

$$I_\nu = \int \varepsilon_\nu N(\gamma)\,\mathrm{d}\gamma = \frac{\pi e^2 N_0 \nu_\mathrm{c}^2 \Psi^2}{3\varepsilon_0 c} \left(\frac{\nu}{2\nu_\mathrm{c}}\right)^{2-s} \tag{158}$$

that means a flat spectrum for $s = 2$, consistent with the optical emission from the Crab pulsar.

To obtain even higher frequencies one must consider even larger pitch angles $\Psi \gg 1/\gamma$. For this case the typical emitted frequencies are higher, namely

$$\nu_\mathrm{cl} = \frac{3}{2}\nu_\mathrm{c}\Psi\gamma^2 \tag{159}$$

which yields a spectrum of

$$I_\nu \sim \nu^{-(s-1)/2} \tag{160}$$

that is exactly the observed value for the X-ray range if again, $s = 2$.

Besides the spectral shape our model can reproduce the observed luminosities. The total luminosity radiated via synchrotron emission in a volume V is given by

$$L = M n_\mathrm{GJ} V P_\mathrm{syn} \tag{161}$$

where

$$P_{\rm syn} = 1.6 \cdot 10^{-14}{\rm W} \left(\frac{B}{\rm T}\right) \Psi^2 \gamma^2 \tag{162}$$

and M is the pair multiplicity of the plasma in the outer magnetosphere. and can be estimated roughly by $M = \gamma_{\rm syn}/\gamma$. For the radiation region we take a spherical shell whose outer edge is at the light cylinder and whose thickness is a fraction f of $r_{\rm LC}$ (of course, $f \ll 1$). For the Crab pulsar data and the small pitch angle approximation ($\Psi \ll 1/\gamma \ll \theta$) we find the optical luminosity

$$L_{\rm opt} = 4 \cdot 10^{24}{\rm W}\, \cos^{1/2}\alpha\, \delta_{-1} f_{-1} \left(\frac{\Psi_{\rm p}}{10^{-3}}\right)^{-1} \left(\frac{\Psi_{\rm opt}}{10^{-3}}\right)^{2} \left(\frac{\nu_{\rm opt}}{10^{15}\,{\rm Hz}}\right) \tag{163}$$

which agrees strikingly well with the observationally deduced value (the index -1 means the quantity in units of 10^{-1}). It is sufficient to show that the observed fluxes are matched in the optical range because then the luminosities in the other bands are automatically correct, as the spectral shape is already reproduced by the synchrotron mechanism (see above).

Compared to that, curvature radiation alone would not suffice to explain the luminosities in the optical and X-ray range, even if the pair multiplicity was far above 10^4. Besides that, the advantage of the proposed mechanism is that the whole spectral range from infrared to X-rays can be produced with one single power law particle energy spectrum.

The γ- emission however, needs radiation from primary particles. Qualitatively, this emission can be explained by synchrotron and ICS losses of high energetic particles. But due to the pair cascade, a qualitative description would require absorption by pair production, or some other reprocessing of the energetic quanta.

It should be mentioned once more that efficient acceleration and pair production in the outer magnetosphere has another desirable effect. The inflowing positrons "feed" the neutral surface with positive charges, which can drift inwards to negative regions to balance the effects of curvature much more easily than positive ions. A mechanism like this was also assumed for the calculation of the total resistance, as we took the parallel GJ- density for computing the relativistic GJ current. For an almost aligned pulsar this assumption will still be valid, since the open field lines have their smallest angle to the dipolar axis at small distances. For higher inclinations, a significant part of the field lines is "favourably curved" near the surface and "unfavourably curved" further out, therefore some corrections may apply. Nevertheless even the assumption that the outflowing current is determined

by the "most parallel" point of each field line, does not change the fact that the total resistance is a purely geometric effect, which is not related to plasma processes. Thus a relativistic current with a density of $\zeta(\vec{r})n_{\rm GJ}^{\parallel}$ everywhere (where $\zeta(\vec{r})$ is a slowly varying scalar function with values close to 1) can flow off the polar caps. This is important to avoid particle acceleration by the mechanism of Arons type inner gap models.

In case of an incomplete shielding on the closed field lines, due to insufficient ion supply from the surface (if the binding energies are too high or the surface temperatures are small) these positrons could also be the additional positive charge needed to obtain the GJ density there. So the region inside the neutral surface will quickly reach a quasi-stationary state, with no "starved" regions anywhere, except from small-scale fluctuations in form of plasma waves.

Summarizing, we propose a modified outer gap model that uses drift on the neutral surface, caused by an accumulation of charges. This is because the neutral line is a natural border for charged particles, as the shielding charge density goes to zero when approaching that point. If particles just arrive from one side as in a dipolar geometry, such a space charge is built up very quickly. The resulting violation of ideal Ohm's law enables the particles to drift relative to the magnetic field and be transported to another field line. In the oblique geometry the new and the old field line may be not equivalent. This means that by such a process a particle can change from a closed to an open field line and be accelerated efficiently towards the light cylinder, where it produces secondary particles. This new plasma generates the softer high energetic emission from the IR to X-rays (Crusius *et al.*, 2001).

All plasma processes causing resistivity in the inner part of the magnetosphere merely present an extra resistance limiting the current to a smaller value which only means that it limits the velocity and therefore the particle energy. From typical radio efficiencies we can therefore find a rough upper limit for the particle Lorentz factors (for $\varepsilon = 10^{-5}$ we obtain $\gamma \leq 200$). An even more fundamental restriction is particle inertia which alone limits γ to a few 10^3. If other resistive processes occur in the inner magnetosphere, the limit would drop even further.

Of course, a number of assumptions have been made, which makes this model only a promising working hypothesis. Nevertheless due to the absence of an inner gap, the neutral line plays a very important role for the particle outflow, since it cannot be crossed directly. Therefore drift effects are the only way to transport particles to "free" field lines and should be considered carefully.

7 Summary and conclusions

"Never imagine yourself not to be otherwise
than what it might appear to others that what you were
or might have been was not otherwise than
what you had been would have appeared to them
to be otherwise."
Lewis Carroll, *Alice in Wonderland*

In this work we have proposed a new model for the pulsar magnetosphere with low relativistic particles of Goldreich-Julian density in the inner magnetosphere, and a modified outer gap beyond the neutral surface. In this region close to the light cylinder high energetic emission and a dense pair wind are produced, as almost all of the dissipation is supposed to occur there.

Our initial goal was to explain the most important features of pulsar radio emission. Of the two processes discussed in the literature, coherent curvature emission by bunches can be ruled out for energetic reasons as we have shown (Lesch *et al.*, 1997) and because of the lack of a suitable bunching mechanism. Therefore the second process, relativistic plasma emission is favoured.

If the emitted frequency is coupled to the plasma frequency and the energy of the radiating particles this process fails to explain the observed radiation in the low frequency radio range unless both the density and the particle energies are small. Especially, a plasma process is incompatible with a pair cascade close to the surface (Sturrock, 1971, Ruderman & Sutherland, 1975, Arons & Scharlemann, 1979) as pointed out by Kunzl *et al.* (1998a) for the example of the Crab pulsar. Additionally, von Hoensbroech *et al.* (1998), von Hoensbroech & Lesch (1999) have shown that propagation effects can explain the observed polarization features even for a mildly relativistic GJ-plasma.

To produce the high power of the radio emission, the required low kinetic energies of the particles do not suffice. The charges must therefore be reaccelerated in the radiation region. But there is another, even more convincing reason why this has to happen. A mildly relativistic particle losing energy is also slowed down considerably. This means that either the charge density grows (and therefore an electrostatic wave builds up), or the outflowing current is reduced (which has the same effect in the end). So if a particle radiates, an electrostatic field builds up, which reaccelerates it to its original energy.

Total energy loss per particle is then no longer limited by its own kinetic energy but determined only by the field strength of the electric wave integrated over the width of the radiation region. This model, as shown, predicts narrow emission regions in most cases, if we use the observationally derived values for luminosity, brightness temperature and emission heights.

A natural hurdle for a single-charge particle outflow is the neutral line, that is the point where the GJ charge changes its sign. Therefore, such a current quickly creates a huge electrostatic field there, unless the particles are carried off by some mechanism. This process is $\vec{E} \times \vec{B}$- drift. In a perfectly shielded magnetosphere the drift velocity causes exact corotation. If there is a net space charge, this allows a movement of the particles across the magnetic field lines. For an inclined rotator, particles can therefore interchange between non-equivalent field lines and thus be carried away from the neutral surface. It has been shown in this work that a dense pair plasma in a thin layer around the neutral surface can enable the particles to drift so effectively that a relativistic parallel GJ current flows out.

As the radio emission region dissipates only a tiny fraction of the total voltage, the major part of the potential difference will drop in the drift region. Energy is released in form of accelerated particles drifting to the free open field lines, where they reach ultrarelativistic energies. This causes a scenario as described in outer gap models, where an avalanche of secondary particles and all the high energetic radiation are created. Crusius *et al.* (2001) showed that the observed high-energy spectrum can be reproduced if all the high-energy radiation is due to synchrotron emission.

The described scenario is similar to a model proposed by Shibata (1991) but it does not assume an inner gap. The drift mechanism removes the necessity of two acceleration regions.

The important assumption of both models is that the system somehow fixes the current, so that changes of the GJ density must cause some reaction of the system that allows the current to be kept constant.

Altogether, the different emission processes in pulsars are closely linked and a convincing model for the radiation needs to describe the global currents, voltage drops, dissipation regions and particle energies.

Acknowledgements

First of all I want to thank Prof. Dr. Harald Lesch for supervising this thesis and giving me the possibility to work on this interesting topic. He was a great help whenever a problem occured and always provided advice and sweets when necessary. I am also grateful to Prof. Dr. Joachim Trümper for the financial support and for being the second referee.

Special thanks I owe to Dr. Axel Jessner whose profound criticism prevented me several times from over-simplifying things or ignoring important effects. Besides, many of his own ideas found their way into this work.

Furthermore I want to reciprocate Prof. Dr. Don Melrose from the University of Sydney and his colleagues Dr. Qinghuan Luo, Dr. Simon Johnston, Dr. Stephen Hardy, Dr. Lewis Ball and many others for their warm welcome and the interesting discussions we had during my time in Australia. Of course, Sam Mackinlay, who was a great help in all organizational matters, should not be forgotten either. Thanks also to the SUMSters and all the other nice people I met in Australia, especially Charlie, Lili, Ron, Vanessa, Matt, Jason, Nick, Ben, Marion, Anne and many more.

Besides, there were my colleagues Rüdiger Schopper, Christian Konz, Frank Grupp, Christoph Nodes and Markus Schmid, who made our room lively with discussions on physics, politics, chess and bughouse. Dr. Guido Birk, Dr. habil. Heinz Wiechen and Dr. André Crusius also dropped in frequently for having a chat and brewing coffee.

Concerning all matters of high energetic observations of pulsars, Dr. habil. Werner Becker and Dr. Gottfried Kanbach were important sources of information and a great help.

Furthermore I want to thank the pulsar people from the MPIfR in Bonn and the people I met there, especially Prof. Dr. Richard Wielebinski, Dr. Michael Kramer, Dr. Alexis von Hoensbroech, Dr. Nazar Ikhsanov, Dr. R.T. Gangadhara, Prof. Dr. Jan Gil and many others.

Special thanks I owe to Mrs. Phyllis Rechten for her careful cross-reading of my manuscript and changing it into "real" English where necessary.

Last, but not least, many other people contributed to this work directly or indirectly. Without listing names I nevertheless want to say thank you to everyone who supported me in these years.

8 Tabellerischer Lebenslauf

Name:	Thomas Alexander Kunzl
Geburtsdatum:	10.09. 1972
Geburtsort:	München
Familienstand:	ledig

bisheriger Bildungsweg

1979 - 83	Grundschule an der Königswieser Straße
1983 - 92	Gymnasium Fürstenried- West
Juli 1992	Abitur am Gymnasium Fürstenried West, München
November 1992	Beginn des Studiengangs Diplomphysik an der Ludwig-Maximilians- Universität München
15. April 1994	Vordiplom an der Ludwig- Maximilians- Universität München
7.8.-29.9.1995	Teilnahme am Studentenprogramm der Gesellschaft für Schwerionenforschung, Darmstadt
9. Dezember 1997	Abschluß des Studiums durch Erlangen des Diploms; Diplomarbeit am Institut für Astronomie und Astrophysik der Universität München zum Thema: Mechanismen zur Erzeugung kohären Radiostrahlung in Pulsaren
Januar- März 1998	Beschäftigung als wissenschaftl. Mitarbeiter am Institut für Astronomie und Astrophysik München
seit April 1998	Beschäftigung als wissenschaftlicher Mitarbeiter beim Max-Planck- Institut für extraterrestrische Physik, Garching
März-Juli 2000	Auslandsaufenthalt an der University of Sydney, Australien durch DAAD-Stipendium
Juni 2001	Promotion an der Ludwig-Maximilians-Universität München bei Prof. Dr. Harald Lesch, Thema: Coherent and incoherent radiation processes in pulsars

References

[Abrahams & Shapiro, 1991] Abrahams, A.M., Shapiro, S.L., 1991, ApJ, 374, 652

[Arons & Scharlemann, 1979] Arons, J., Scharlemann, E.T., 1979, ApJ, 231, 854

[Arons, 1983] Arons, J. , 1983, ApJ, 266, 215

[Arons, 2000] Arons, J., 2000 in: Pulsar Astronomy - 2000 and beyond, eds. M. Kramer, N. Wex and R. Wielebinski, IAU Colloq. **177**,p. 449

[Baade *et al.*, 1934] Baade, W., Zwicky, F., 1934, Proc. Nat. Acad. Sci., 20, 259

[Becker & Trümper, 1997] Becker, W., Trümper, J., 1997, A& A, 326, 682

[Benford & Buschauer, 1983] Benford, G., Buschauer, R., 1983, A& A 118, 358

[Beskin, 1999] Beskin, V.S., 1999, Physics-Uspekhi, 42(11), 1071

[Blaskiewicz *et al.*, 1991] Blaskiewicz, M., Cordes, J.M., Wasserman, I., 1991, ApJ 370, 643

[Boriakoff, 1992] Boriakoff, V. 1992 in *The Magnetospheric Structure and Emission Mechanisms of Radio Pulsars*, eds. Hankins, T.H., Rankin, J.M. and Gil, J.A., IAU Colloq. **128**, p. 343

[Bowyer *et al.*, 1964] Bowyer, C.S., Byram, E.T., CHubb, T.A., Friedman, H., 1964, Nature, 201, 1307

[Buschauer & Benford, 1976] Buschauer, R., Benford G., 1976, MNRAS 177, 109

[Caraveo *et al.*, 1994] Caraveo, P.A., Bignami, G.F., Mereghetti, S., Mignani, R., Gouiffes, C., 1994, AAS, 184, #21.04

[Cheng *et al.*, 1976] Cheng, A., Ruderman, M.A., Sutherland. P., 1976, 203, 209

[Cheng & Ruderman, 1977] Cheng, A.F., Ruderman, M.A., 1977, ApJ 214, 598

[Cheng *et al.*, 1986] Cheng, K.S., Ho, C., Ruderman, M.A., 1986, ApJ, 300, 500

[Chiang & Romani, 1994] Chiang, J., Romani, R., 1994, ApJ, 436, 754

[Cocke *et al.*, 1969] Cocke, W.J., Disney, M.J., Taylor, D.J., 1969, Nature, 221, 525

[Crusius *et al.*, 2001] Crusius-Wätzel, A.R., Kunzl, T., Lesch, H., 2001, ApJ, 546, 401

[Daugherty & Harding, 1982] Daugherty, J.K., Harding, A.K., 1982, ApJ, 252, 337

[Dushman, 1930] Dushman, S., 1930, Rev. Mod. Phys., 38, 626

[Edison, 1884] Edison, T.A., Engineering, 1884, 553

[Eikenberry, 1998] Eikenberry, S.S., 1998, AAS Meeting 192, #50.07

[Epstein, 1973] Epstein, R.I., 1973, ApJ, 183, 593

[Erber, 1966] Erber, T., 1966, Rev. Mod. Phys., 38, 626

[Fawley *et al.*, 1977] Fawley, W.M., Arons, J., Scharlemann, E.T., 1977, ApJ, 217, 227

[Fowler & Northeim, 1928] Fowler, R.H., Northeim, L.W., 1928, Roy. Soc. Proc., 119, 173

[Gedalin *et al.*, 1998] Gedalin, M., Melrose, D.B., Gruman, E., 1998, Phys. Rev. E, Vol. 57(3), 3399

[Gil & Kijak, 1992] Gil, J.A., Kijak, J., 1992, A&A, 256, 477

[Gil & Sendyk, 2000] Gil, J.A., Sendyk, M., 2000, ApJ, 541, 351

[Gil & Mitra, 2001] Gil, J.A., Mitra, D., 2001, ApJ, 550, *in press*

[Ginzburg & Zheleznyakov, 1970a] Ginzburg, V.L., Zheleznyakov, V.V., 1970, Comments Astrophys. Space Phys., 2 167

[Ginzburg & Zheleznyakov, 1970b] Ginzburg, V.L., Zheleznyakov, V.V., 1970, Comments Astrophys. Space Phys., 2 197

[Ginzburg & Zheleznyakov, 1975] Ginzburg, V.L., Zheleznyakov, V.V., 1975, ARAA, 13, 511

[Goldreich & Julian, 1969] Goldreich, P., Julian, W.H., 1969, ApJ 157, 869

[Gould & Lyne, 1998] Gould, D.M., Lyne, A.R., 1998, MNRAS, 301, 235

[Gunn & Ostriker, 1971] Gunn, J.E., Ostriker, J.P., 1971, ApJ 165, 523

[Gwinn *et al.*, 1997] Gwinn, C.R., Ojeda, M.J., Britton, M.C., Reynolds, J.E., Jauncey, D.L., King, E.A., McCulloch, P.M., Lovell, J.E.J., Flanagan, C.S., Smits, D.P., Preston, R.A., Jones, D.L., 1997, ApJ, 483, L53

[Hankins, 1996] Hankins, T., 1996, in *Pulsars: Problems & Progress*, eds. Johnston, S., Walker, M.A., Bailes, M., IAU Colloq. **160**, p. 197

[Hewish *et al.*, 1968] Hewish, A., Bell, J., Pilkington, J.D.M., Scott, P.F., Collins, R.A., 1968, Nature, 217, 709

[Hill, 1998] Hill, R.J., 1998, AAS Meeting 192, #50.06

[Hirotani & Shibata, 1999a] Hirotani, K., Shibata, S., 1999, MNRAS 308, 54

[Hirotani & Shibata, 1999b] Hirotani, K., Shibata, S., 1999, MNRAS 308, 67

[von Hoensbroech, 1995] von Hoensbroech, A., 1995, *diploma thesis*, University of Bonn

[von Hoensbroech *et al.*, 1998] von Hoensbroech, A., Lesch, H., Kunzl, T., 1998, A& A, 336, 209

[von Hoensbroech & Lesch, 1999] von Hoensbroech, A., Lesch, H., 1999, A&A, 342, L57

[Jessner *et al.*, 2001] Jessner, A., Lesch, H., Kunzl, T., 2001, ApJ, *in press*

[Khechinashvili *et al.*, 2000] Khechinashvili, D.G., Melikidze, G.I., Gil, J.A., 2000, ApJ, 541, 335

[Kijak & Gil, 1997] Kijak, J., Gil, J., 1997, MNRAS 288, 631

[Kijak & Gil, 1998] Kijak, J., Gil, J., 1998, MNRAS 299, 855

[Kirk, 1980] Kirk, J.G., 1980, A& A, 82, 262

[Krall & Trivelpiece, 1973] Krall, N.A., Trivelpiece, A.W., Principles of plasma physics, International Student Edition - International Series in Pure and Applied Physics, Tokyo: McGraw-Hill Kogakusha, 1973

[Kramer, 1994] Kramer, M., 1994, A&ASS, 107, 527

[Kramer, 1995] Kramer, M., 1995, *PhD thesis*, University of Bonn, Germany

[Kramer *et al.*, 1996] Kramer, M., Xilouris, K.M., Jessner, A., Wielebinski, R., Timofeev, M., 1996, A&A, 306, 867

[Kramer *et al.*, 1997] Kramer, M., Jessner, A., Doroshenko, O., Wielebinski, R., 1997, ApJ, 488, 364

[Kramer *et al.*, 1998] Kramer, M., Xilouris, K.M., Lorimer, D.R., Doroshenko, O., Jessner, A., Wielebinski, R., Wolszczan, A., Camilo, F., 1998, ApJ, 501, 270

[Krause-Polstorff & Michel, 1985a] Krause-Polstorff, J., Michel, F.C., 1985, A& A, 144, 172

[Krause-Polstorff & Michel, 1985b] Krause-Polstorff, J., Michel, F.C., 1985, MNRAS, 213, 43

[Kunzl *et al.*, 1998a] Kunzl, T., Lesch, H., Jessner, A., von Hoensbroech, A., 1998, ApJ, 505, L139

[Kunzl *et al.*, 1998b] Kunzl, T., Lesch, H., Jessner, A., 1998, A& A, 339, 917

[Kunzl *et al.*, 2001] Kunzl, T., Lesch, H., Jessner, A., 2001, A& A, *in prep.*

[Lesch *et al.*, 1998] Lesch, H., Jessner, A., Kramer, M., Kunzl, T., 1998, A&A, 322, L21

[Lesch *et al.*, 2000] Lesch, H., Kunzl. T., Jessner, A., 2000 in: Pulsar Astronomy - 2000 and beyond, eds. M. Kramer, N. Wex and R. Wielebinski, IAU Colloq. **177**, p. 381

[Lyne & Manchester, 1988] Lyne, A.G., Manchester, R., 1988, MNRAS, 234, 477

[Lyutikov *et al.*, 1999a] Lyutikov, M., Blandford, R.D., Machabeli, G., 1999, MNRAS, 305, 338

[Lyutikov *et al.*, 1999b] Lyutikov, M., Machabeli, G., Blandford, R.D., 1999, ApJ, 512, 804

[Malofeev *et al.*, 1994] Malofeev, V.M., Gil, J.A., Jessner, A., Malov, I.F., Seiradakis, J.H., Sieber, W., Wielebinski, R., 1994, A&A, 285, 201

[Malofeev, 1996] Malofeev, V.M., 1996, Pulsar Radio Spectra, in: Pulsars: Problems, ASP Conference Series, eds. Johnston, S., Walker, M.A., Bailes, M., **105**, 271

[Malov *et al.*, 1994] Malov, I.F., Malofeev, V.M., Sen'e, D.S., 1994, Astronomy Reports, 38(5), 677

[Malov, 1998] Malov, I.F., 1998, Astr. Reports, 42(2), 1998

[Mantel, 2001] Mantel, K.-H., 2001, *private communication*

[Mastichiadis *et al.*, 1986] Mastichiadis, A., Marscher, A.P. Brecher, K., 1986, ApJ, 300, 178

[Melikidze *et al.*, 2000] Melikidze, G.I., Gil, J.A., Pataraya, A.D., 2000, ApJ, 544, 1081

[Melrose, 1978] Melrose, D.B., 1978, ApJ, 225, 557

[Melrose, 1979] Melrose, D.B., Aust. Phys., 32, 61

[Melrose, 1992] Melrose, D.B., 1992 in *The Magnetospheric Structure and Emission Mechanisms of Radio Pulsars*, eds. Hankins, T.H., Rankin, J.M., Gil, J.A., IAU Colloq. **128**, p. 306

[Melrose & Gedalin, 1999] Melrose, D.B. & Gedalin, M.E., 1999, ApJ, 521, 351

[Melrose, 2000] Melrose, D.B., *private communication*

[Melrose *et al.*, 2001] Melrose, D.B., Gedalin, M.A., Kennel, C.F., Fletcher, A., 2001, submitted to ApJ

[Melrose & Stoneham, 1977] Melrose, D.B., Stoneham, R., 1977, Proc. Astr. Soc. Aust., 3 120

[Michel, 1974] Michel, F.C., 1974, ApJ, 192, 713

[Mignani *et al.*, 1999] Mignani, R.P., Caraveo, P.A., Bignami, G.F., 1999, A& A, 343, L5

[Muslimov & Tsygan, 1992] Muslimov, A.G., Tsygan, A.I., 1992, MNRAS, 255, 61

[Nasuti *et al.*, 1997] Nasuti, F.P., Mignami, R., Caraveo, P.A., Bignami, G.F., 1997, A& A, 323, 839

[Oppenheimer & Volkoff, 1939] Oppenheimer, J.R., Volkoff, G., 1939, Phys. Rev., 55, 374

[Ostriker & Gunn, 1969] Ostriker, J.P., Gunn, J.E., 1969, ApJ, 157, 1395

[Page & Sarmiento, 1996] Page, D., Sarmiento, A., 1996, ApJ, 473, 1067

[Pavlov *et al.*, 1997] Pavlov, G.G., Welty, A.D., Cordova, F.A., 1997, ApJ, 489, L75

[Pavlov *et al.*, 1999] Pavlov, G.G., Zavlin, V.E., Trümper, J., 1999, ApJ, 511, L45

[Phillips, 1992] Phillips, J.A., 1992, ApJ, 385, 282

[Radhakrishnan & Rankin, 1990] Radhakrishnan, V., Rankin, J.M., 1990, ApJ, 352, 258

[Rankin, 1983] Rankin, J.M., 1983, ApJ, 274, 333

[Rankin, 1992] Rankin, J.M., 1992 in *The Magnetospheric Structure and Emission Mechanisms of Radio Pulsars*, eds. Hankins, T.H., Rankin, J.M., Gil, J.A., IAU Colloq. **128**, p. 133

[Romani, 1996] Romani, R., 1996, ApJ, 470, 469

[Ruderman & Sutherland, 1975] Ruderman, M.A., Sutherland, P.G., 1975, ApJ, 196, 52

[Rybicki & Lightman, 1979] Rybicki, G.G., Lightman, A.P., 1979, *Radiative Processes in Astrophysics*, Wiley, New York

[Scharlemann *et al.*, 1978] Scharlemann, E.T., Fawley, W.M., Arons, J., 1978, ApJ, 231, 854

[Schopper *et al.*, 2001] Schopper, R., Kunzl, T., Ruhl, H., Lesch, H., 2001, *in prep.*

[Shibata, 1991] Shibata, S., 1991, ApJ, 378, 239

[Shibata, 1997] Shibata, S., 1997, MNRAS, 287, 262

[Shibata *et al.*, 1998] Shibata, S., Miyazaki, J., Takahara, F., 1998, MNRAS, 295, L53

[Shitov, 1983] Shitov, Y.P., 1983, Sov. Astron., 27, 314

[Smirnow, 1973] Smirnow, W.I., 1973, *Lehrgang der höheren Mathematik*, Akademie- Verlag (Berlin)

[Sturner, 1995] Sturner, S.J., 1995, ApJ, 446, 292

[Sturrock, 1971] Sturrock, P.A., 1971, ApJ, 164, 529

[Sutherland, 1979] Sutherland, P.G., 1979, Fundamentals of Cosmic Physics, Vol. 4, p. 95

[Taylor *et al.*, 1993] Taylor, J.H., Manchester, R.N., Lyne, A.G., 1993, ApJS, 88, 529

[Toor & Seward, 1977] Toor,A., Seward, F.D., 1977, ApJ, 216, 560

[Thompson, 1999] Thompson, D. J.; Bailes, M.; Bertsch, D. L.; Cordes, J.; D'Amico, N.; Esposito, J. A.; Finley, J.; Hartman, R. C.; Hermsen, W.; Kanbach, G.; Kaspi, V. M.; Kniffen, D. A.; Kuiper, L.; Lin, Y. C.; Lyne, A.; Manchester, R.; Matz, S. M.; Mayer-Hasselwander, H. A.; Michelson, P. F.; Nolan, P. L.; Ögelman, H.; Pohl, M.; Ramanamurthy, P. V.; Sreekumar, P.; Reimer, O.; Taylor, J. H.; Ulmer, M., 1999, ApJ, 516, 297

[Trümper *et al.*, 1978] Trümper, J., Pietsch, W., Reppin, C., Voges, W., Staubert, R., Kendziorra, E., 1978, ApJ, 219, L105

[Trümper, 1983] Trümper, J., 1983, Adv. Space Res., 2, 241

[Ursov & Usov, 1988] Ursov, V.N., Usov, V.V., 1988, APSS 140, 325

[Usov, 1987] Usov, V.V., 1987, ApJ ,320, 333

[Weisskopf *et al.*, 1999] Weisskopf, M.C., Marshall, H. L., Hester, J. J., Tennant, A. F., Allen, G. E., Butt, Y., Elsner, R. F., Elvis, M. S., Graessle, D. E., Kellogg, E. M., Kolodiejczak, J. J., Nichols, J. S., O'Dell, S. L., Pivovaroff, M. J., Plucinsky, P. P., Schulz, N. S., Swartz, D. A., Vrtilek, S. D., 1999, AAS Meeting 195, 112

[Woo, 1987] Wee-yong Woo, 1987, Phys. Fluids, 30(1), 239

[Xilouris *et al.*, 1998] Xilouris, K.M., Kramer, M., Jessner, A., von Hoensbroech, A., Lorimer, D.R., Wielebinski, R., Wolszczan, A., Camilo, F., 1998, ApJ 501, 286

[Yadigaroglu & Romani, 1995] Yadigaroglu, I.A., Romani, R.W., 1995, ApJ, 449, 211

[Yancopoulos *et al.*, 1994] Yancopoulos, S., Hamilton, T.T., Helfand, D.J., 1994, ApJ 429, 832

[Young *et al.*, 1999] Young, M.D., Manchester, R.N., Johnston, S., 1999, Nature, 400, 848

[Zavlin *et al.*, 1995] Zavlin, V.E., Pavlov, G.G., Shibanov, Y.A., Ventura, J., 1995, A& A, 297, 441

[Zavlin *et al.*, 2000] Zavlin, V.E., Pavlov, G.G., Sanwal, D., Trümper, J. ,2000, ApJ, 540, L25

[Zhang *et al.*, 2000] Zhang, B., Harding, A.K., Muslimov, A.G., 2000, ApJ, 531, L135